

POLITECNICO DI TORINO

FACOLTÀ DI INGEGNERIA AEROSPAZIALE



TESI DI LAUREA MAGISTRALE

**ACOUSTIC ANALYSIS OF PASSIVE METAMATERIAL PANELS
USING THE FINITE ELEMENT METHOD
AND HOMOGENIZED PROPERTIES**

GIUSEPPE D'AMICO

Supervisors:

Prof. Erasmo CARRERA

Prof. Maria CINEFRA

Ing. Matteo FILIPPI

March 2018

Acknowledgements

First of all, I am grateful to Prof. Erasmo Carrera, my supervisor at Politecnico di Torino, for the opportunities he offered me to work in a multidisciplinary topic. I would like also to express my gratitude to Prof. Maria Cinefra, my supervisor, for her support in the development of the work presented in this Thesis. I would like to thanks Sebastiano Passabi', a Master Thesis Student at Politecnico di Torino for his help in Actran learning process, Caroline Houriet visiting Student from ENSTA ParisTech for providing data of homogenized material, and Alberto Garcia De Miguel, PhD at Politecnico di Torino for providing his code for homogenization process.

Torino, March 2018

Giuseppe D'Amico

Contents

Acknowledgements	iii
List of Figures	vii
List of Tables	xi
1 The Acoustic problem	5
1.1 The Decibel scale	5
1.2 Relation between pressure,intensity and sound level	6
1.3 The mass-frequency law	8
1.4 Acoustics in aircraft fuselages	11
2 What does Metamaterial mean?	15
2.1 Examples of metamaterials	15
2.1.1 Membrane-type Acoustic Metamaterial with negative dynamic density	16
2.1.2 Dark acoustic metamaterials as super absorbers for low- frequency sound	19
2.1.3 Doubly periodic material	20
2.1.4 Omni-directional broadband acoustic absorber based on metamaterials	22
2.1.5 Honeycomb acoustic metamaterial	23
3 MSC ACTRAN description	25
3.1 Material assignment	25
3.2 Finite Fluid Component	28
3.3 Infinite Acoustic Component	29
3.4 Structural Components	32
3.5 Incident/Radiating Surface Post-Processing	33
3.6 Acoustic Sources	34
3.7 Rayleigh Surface Component	37
3.8 Acoustical and Structural Wavelength Calculation	39
3.9 Boundary Conditions	42
3.10 Input Frequency-Dependent Metamaterials in MSC Actran	42
3.11 Orthotropic material implementation	46
3.12 Evaluation of Modal Frequencies	47
3.13 Evaluation of Sound Transmission Loss with MSC Actran	49
3.14 Troubleshooting of Errors encountered	49
4 MATLAB Script to Interface MUL2-UC with ACTRAN	51

5	Choice of the Metamaterial	57
5.1	Melamine foam	57
5.2	Frequency-Dependent Engineering constants of Homogenized Metamaterial in Melamine Foam with Aluminum inclusions .	63
6	Validation of homogenization method with PVC and Melamine Foam plates	69
6.1	Mesh convergence process on a full PVC plate	70
6.2	Modal Frequencies Results	71
7	Sound Transmission Loss Results	75
7.1	PVC Perforated Plate and Homogenized material	75
7.2	Melamine Foam Metamaterial with 300 and 600 Aluminum inclusions and Homogenized metamaterial	77
7.3	Melamine Foam Metamaterial with different Inclusions Volume Fraction	79
7.4	Sound Transmission Loss of Sandwich Plates	82
	7.4.1 Nomex Core	84
	7.4.2 Effect of skin in Sound Transmission Loss	87
	7.4.3 Sandwich STL Results	88
8	Conclusions	91
8.1	Outlooks	93

List of Figures

1.1	Relation between dB and pressure ratio	6
1.2	Pressure-Intensity-Sound Level example	7
1.3	Scheme of a material interacting with acoustic waves	8
1.4	Scheme of a typical acoustic room	8
1.5	Mass-frequency law without taking into account material stiffness [32]	9
1.6	Mass-stiffness-frequency law [32]	11
1.7	An example of fuselage acoustic treatment	12
1.8	Sample of noise spectra measured in a single engine aircraft for three different engine rpm settings at a flight altitude of 1000 feet. Credits NASA 1975[23]	12
2.1	Subdivision of Materials by their dynamic density and Bulk Modulus (Li and Chan, PRE 2004)	16
2.2	Experimental STL of a membrane resonator (Yang et al.)	17
2.3	Experimental effective dynamic mass of a membrane resonator (Yang et al.)	17
2.4	Absorption coefficient and Sample A photo (Mei et al)	19
2.5	Absorption coefficient and Sample B photo (Mei et al)	20
2.6	Schematic description of a doubly periodic material, considered as a triply periodic material and finite element mesh of the unit cell. [4] [5][6]	20
2.7	Alberich anechoic layer	21
2.8	Frequency variations of the transmission coefficient of the Alberich anechoic coating	21
2.9	Photography of the structure of the metamaterial (Climente et al)[21]	22
2.10	Scheme of the multi-modal impedance chamber and the experimental setup employed in the characterization of the acoustic black-hole	22
2.11	Absorption produced by the core of the black-hole sample	23
2.12	Unit cell of the honeycomb acoustic metamaterial	24
2.13	Experimental and simulation sound transmission loss results for honeycomb structure only and the proposed metamaterial (honeycomb structure with membranes)[25]	24
3.1	Composite solid edat syntax	25
3.2	Composite solid material definition	26
3.3	Multi-layered composite material direction	27
3.4	Fluid Material definition	27

3.5	Fluid Material edat syntax	28
3.6	Model used for evaluate Sandwich Transmission Loss, with Finite fluid Acoustic Component as receiving room.	29
3.7	Infinite Domain modeled as a hollow box, without the bottom surface where the radiating surface is located.	30
3.8	An anechoic chamber [28]	30
3.9	Actran Syntax of an Infinite Domain Component	31
3.10	Infinite fluid component on Actran	31
3.11	Example of plate mesh creation using Actran Structured Mesh tool	32
3.12	Solid component in Actran graphical interface	32
3.13	Thin Shell for composite material in Actran graphical interface	33
3.14	Sound Transmission Loss Post-processing with PLT Viewer	34
3.15	Example of radiating power surfaces	37
3.16	STL using two different component: Rayleigh surface and Finite fluid volume (sandwich model with nomex core)	38
3.17	Wavelength computation for ISA Air at 1000 Hz	40
3.18	PVC wavelength computation	41
3.19	Boundary condition assignment	42
3.20	Lateral surfaces of the plate to which boundary conditions are applied	42
3.21	TABLE data block syntax	43
3.22	Example of frequency dependent properties	45
3.23	Effect of Actran linear interpolation	46
3.24	Example of User Interface of Modal Extraction Analysis	48
3.25	Example of Results from Modal Extraction Analysis	48
3.26	Example of semi-compatible mesh	49
3.27	An Interface of acoustic and structural mesh	50
4.1	Sketch of a plate with inclusions and the equivalent homogenized one [20]	51
4.2	Example of double array of unit cell with cylindrical inclusion	52
4.3	Micro-mechanics analysis using MUL2-UC [2]	54
4.4	Initializing MUL2-UC [2]	54
4.5	Introducing the material properties [2]	55
4.6	Geometry and polynomial order of the HLE [2]	55
4.7	File generated by MUL2-UC with the constitutive information [2]	55
5.1	Melamine foam structure	57
5.2	Melamine Foam Properties: $Re(E_x)$	59
5.3	Melamine Foam Properties: $Im(E_x)$	59
5.4	Melamine Foam Properties: $Re(E_y)$	60
5.5	Melamine Foam Properties: $Im(E_y)$	60
5.6	Melamine Foam Properties: $Re(E_z)$	60
5.7	Melamine Foam Properties: $Im(E_z)$	61
5.8	Melamine Foam Properties: $Re(G_{xy})$	61
5.9	Melamine Foam Properties: $Im(G_{xy})$	61

5.10	Melamine Foam Properties: $Re(G_{yz})$	62
5.11	Melamine Foam Properties: $Im(G_{xz})$	62
5.12	Melamine Foam Properties: $Re(G_{yz})$	62
5.13	Melamine Foam Properties: $Im(G_{yz})$	63
5.14	Homogenized Metamaterial Mechanical properties at different inclusion volume fraction: $Re(E_x)$	65
5.15	Homogenized Metamaterial Mechanical properties at different inclusion volume fraction: $Im(E_x)$	65
5.16	Homogenized Metamaterial Mechanical properties at different inclusion volume fraction: $Re(E_y)$	65
5.17	Homogenized Metamaterial Mechanical properties at different inclusion volume fraction: $Im(E_y)$	66
5.18	Homogenized Metamaterial Mechanical properties at different inclusion volume fraction: $Re(E_z)$	66
5.19	Homogenized Metamaterial Mechanical properties at different inclusion volume fraction: $Im(E_z)$	66
5.20	Homogenized Metamaterial Mechanical properties at different inclusion volume fraction: $Re(G_{xy})$	67
5.21	Homogenized Metamaterial Mechanical properties at different inclusion volume fraction: $Im(G_{xy})$	67
5.22	Homogenized Metamaterial Mechanical properties at different inclusion volume fraction: $Re(G_{xz})$	67
5.23	Homogenized Metamaterial Mechanical properties at different inclusion volume fraction: $Im(G_{xz})$	68
5.24	Homogenized Metamaterial Mechanical properties at different inclusion volume fraction: $Re(G_{yz})$	68
5.25	Homogenized Metamaterial Mechanical properties at different inclusion volume fraction: $Im(G_{yz})$	68
6.1	Schematic description of the three plates made of PVC	69
6.2	300 holes Perforated Plate meshed (left). Particular of meshed holes.(right).	70
6.3	Actran vs experimental error (%) of a full PVC plate, as a function of mesh configuration (first mode)	71
6.4	Actran vs experimental error (%) of a full PVC plate, as a function of mesh configuration (average of first 9 modes)	71
6.5	Modal frequencies PVC plate 300 holes	73
6.6	Modal frequencies PVC plate 600 holes	74
7.1	Boundary condition plate 309x206x20mm	75
7.2	Transmission Loss difference between 300 holes simply supported PVC plate and a full plate made of correspondent homogenized material	76
7.3	Transmission Loss difference between 600 holes simply supported PVC plate and a full plate made of correspondent homogenized material	76
7.4	309x206x20mm plate made of Melamine Foam with 300 or 600 Aluminum inclusions	77

7.5	STL of a simply supported plate, Melamine Foam and 300 Aluminum inclusions (19.2% volume fraction): comparison with equivalent homogenized material	78
7.6	STL of a simply supported plate, Melamine Foam and 600 Aluminum inclusions (58.2% volume fraction) : comparison with equivalent homogenized material	78
7.7	Sound Transmission Loss of a Melamine foam plate (simply supported)	79
7.8	Sound Transmission Loss of Metamaterial plate with different volume fraction (0.0045,0.0060,0.0075) compared with Melamine Foam plate	80
7.9	Sound Transmission Loss of Metamaterial plate with different volume fraction (0.0090,0.0105 and 0.0120) compared with Melamine Foam plate	80
7.10	Sound Transmission Loss of Metamaterial plate with 0.0150 inclusions volume fraction, compared with Melamine Foam and Nomex plates	81
7.11	STL difference between Metamaterial 0.150 and Nomex, clamped plate 309x206x20mm	82
7.12	STL of high values inclusions volume fraction (3% and 8% respect to Nomex and Melamine Foam	82
7.13	Sample A quotes (top) Sample B quotes (bottom).	83
7.14	Sandwich plate with visible boundary conditions	83
7.15	Scheme of the Sandwich plate [Costin-Ciprian Miglan (Clean-sky)]	84
7.16	Example of Aramid Honeycomb (left) and Glass Fabric Pre-impregnated Epoxy Resin [27]	85
7.17	STL comparison between Nomex, Melamine Foam and Metamaterial 0.0150: Sample A (core only) clamped plate	86
7.18	STL difference between Metamaterial 0.0150 and Nomex: Sample A (core only) clamped plate	86
7.19	Effect of skin on a Melamine foam matrix with Aluminum inclusions. (Sample A, homogenized properties)	87
7.20	Transmission Loss of sandwich plate with core in Nomex: comparison Sample A and B	88
7.21	Effect of inclusion volume fraction. Transmission Loss of sandwich plates with 2+2 plies 0/90 in Fiberglass/Epoxy resin (Sample A)	88
7.22	STL of Sample A Sandwich plate: Nomex vs Metamaterial	89
7.23	Sound Transmission Loss of a Sandwich plate with different core material (Sample B)	89
7.24	STL difference between Metamaterial 0.0150 and Nomex (Sample A)	90
7.25	STL difference between Metamaterial 0.0150 and Nomex (Sample B)	90

List of Tables

3.1	Table data block example for a frequency dependent material	45
3.2	Orthotropic solid data block syntax for an anisotropic material	47
4.1	Example of input data containing frequency-dependent mechanical properties	53
5.1	Poisson ratios of Melamine Foam	63
5.2	Metamaterial densities as a function of inclusions volume fraction	64
6.1	Engineering constants of the homogenized materials obtained by the CUF-MSG based code. [31]	72
6.2	Modal Frequency difference between a PVC plate with 300 holes (experimental) [3] and a full plate with the equivalent homogenized material.	72
6.3	Modal Frequency difference between a PVC plate with 600 holes (experimental) [3] and a full plate with the equivalent homogenized material.	73
7.1	Timings and resources comparison of the PVC perforated plate	75
7.2	Samples A and B geometries	83
7.3	Samples A and B number of mesh elements	84
7.4	Samples material properties difference: Skin plies 0/90° - Glass Fabric Pre-impregnated Epoxy Resin	85
7.5	Samples A and B material properties difference: Core - Nomex Aramid honeycomb	85
7.6	Samples A and B geometry differences	86
7.7	Weight of Sandwich plates	86

Dedicato alla mia Famiglia ed a Letizia, Novella e Daniele, senza i quali questo traguardo non sarebbe stato possibile.

Summary

The following work takes place within the frame of the CASTLE Project, which is itself a part of the Clean Sky 2 Project. Clean Sky is the largest European research program developing innovative, cutting-edge technology aimed at reducing CO₂, gas emissions and noise levels produced by aircraft, funded by the EU's Horizon 2020 program.

CASTLE Project, which stands for "*CABin Systems design Toward passenger wellbEing*" aims at improving the level of comfort of passengers of Regional jets. One of the main focus of the Project is to find better acoustic solutions for this type of plane. Indeed, these aircrafts typically have noise levels 5 dB higher than large jets. This is mainly explained by their lower operating altitude.

The approach of CASTLE is based on human factor issues regarding ergonomics, anthropometrics, as well as effects of vibration, noise on passenger. Lighter specific materials and minimum weight allocation for soundproofing are requested while providing comfort similar to that in large jets. In this framework, this work wants to investigate the soundproofing level of passive acoustic metamaterials made of Melamine Foam and cylindrical Aluminum inclusions. Latest research shows promising acoustical and optical possibility on controlling certain frequencies, varying their geometry or material configuration. Also, CUF homogenization [1] methods was applied in order to have the simplest mesh for periodical geometries (in this case, cylindrical) that reduce drastically the computation timings. MSC Actran had been used for the acoustic simulations, in particular for Sound Transmission Loss evaluation of the panels.

Description of the work

The first part of the work was a research on metamaterials to understanding the philosophy. Some meaningful examples are then described. A consistent part of the work was spent learning the basics of a Vibroacoustics dedicated software MSC ACTRAN (MSC acquired Free Field Technologies company in 2011). I was introduced in it by Sebastiano Passabi'a Post-Degree Student, which achieved experience in MSC during his Master Thesis. Hundreds of hours have been spent in order to understand ACTRAN principles, with the support of workshop useful to the purpose.

To validate the homogenization method, a modal extraction analysis was made, taking as a reference the results of the research of Langlet et al. Three models were analyzed: a full PVC plate and two perforated PVC plates with 300 and 600 holes. The good agreement of the results allowed us to evaluate the perforated plates' Sound Transmission Loss and compare it with a full plate made of an equivalent homogenized material. The assessment of this procedure has allowed us to go further and using Melamine foam, a more appropriate material for our purposes. Melamine foam frequency-dependent properties had been calculated by Caroline Houriet ([31]) a visiting student from ENSTA ParisTech, together with MUL2 Polito tutors Maria Cinefra and Alfonso Pagani. Starting from this data, a MUL2 Homogenization code [2] was fundamental to obtain the Metamaterial equivalent properties. A MATLAB script was created ad-hoc by myself to interface MUL2-UC and ACTRAN, to speed the calculation and analyze several possible configuration.

Finally, the choice of the metamaterial in terms of volume fraction of the cylindrical inclusions in order to satisfy the requirements of CASTLE project and, of course, compliance with airworthiness requirements.

The selected Metamaterial was the core of a Sandwich Plate with characteristics decided together with other CASTLE partners. The Metamaterial core was compared with Nomex, a material suggested by CASTLE partners. The tests finally showed promising acoustical performance of the Metamaterial.

Chapter 1

The Acoustic problem

Acoustics is the branch of science that studies the propagation of sound and vibrational waves. Audible acoustic waves are ubiquitous in our everyday experience: they form the basis of verbal human communication, and the combination of pitch and rhythm transforms sound vibrations into music. Waves with frequencies beyond the limit of human audibility are used in many ultrasonic imaging devices for medicine and industry. However, acoustic waves are not always easy to control. Audible sound waves spread with modest attenuation through air and are often able to penetrate thick barriers with ease. New tools to control these waves as they propagate, in the form of new artificial materials, are extremely desirable[7]

1.1 The Decibel scale

The decibel (dB) is used to measure sound level, but it is also widely used in electronics, signals and communication. The dB is a logarithmic way of describing a ratio. The ratio may be power, sound pressure, voltage or intensity or several other things.

Suppose we have two loudspeakers, the first playing a sound with power P_1 , and another playing a louder version of the same sound with power P_2 . The difference in decibels between the two is defined to be

$$10\log_{10}\left(\frac{P_2}{P_1}\right)dB \quad (1.1)$$

If the second produces twice as much power than the first, the difference in dB is

$$10\log_{10}\frac{P_2}{P_1} = 10\log_{10}2 = 3dB. \quad (1.2)$$

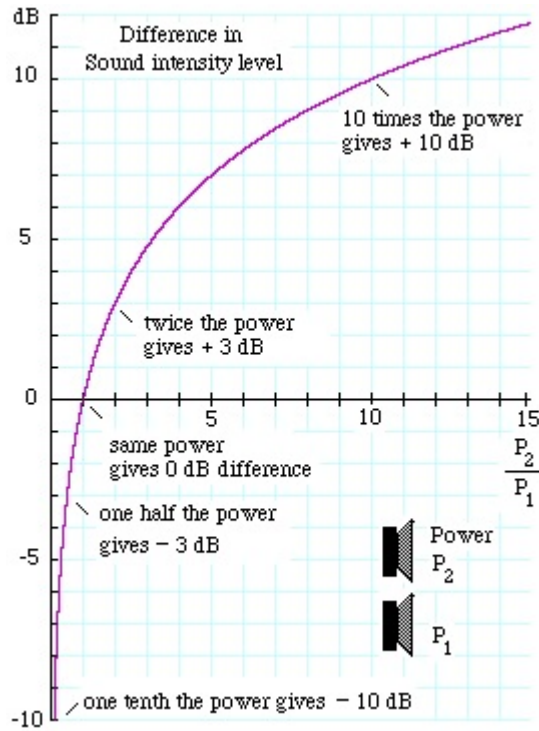


FIGURE 1.1: Relation between dB and pressure ratio

This relation is clearly shown in Fig 1.1. If the second had 10 times the power of the first, the difference in dB would be 10 dB, while if the second had a **million times** the power of the first, the difference in dB would be **60 dB**.

Decibel scales can describe very big ratios using numbers of modest size, but note that the decibel describes power ratios, not their single intensity. Sound is usually measured with microphones and they respond (approximately) proportionally to the sound pressure, p . Now the power in a sound wave, all else equal, goes as the square of the pressure. (Similarly, electrical power in a resistor goes as the square of the voltage.) The log of the square of x is just $2 \log x$, so this introduces a factor of 2 when we convert to decibels for pressures. The difference in sound pressure level between two sounds with p_1 and p_2 is therefore:

$$20 \log_{10} \frac{p_2}{p_1} \text{ dB} = 10 \log_{10} \left(\frac{p_2^2}{p_1^2} \right) \text{ dB} = 10 \log_{10} \frac{P_2}{P_1} \text{ dB} \quad (1.3)$$

1.2 Relation between pressure, intensity and sound level

If we halve the sound power,

$$10 \log_{10} \frac{1}{2} = -3 \text{ dB} \quad (1.4)$$

So, if you halve the power, you reduce the power and the sound level by 3 dB. Halve it again (down to 1/4 of the original power) and you reduce the level by another 3 dB. If you keep on halving the power, you have these ratios.

Pressure	$\frac{p}{\sqrt{2}}$	$\frac{p}{2}$	$\frac{p}{2\sqrt{2}}$	$\frac{p}{4}$	$\frac{p}{4\sqrt{2}}$	$\frac{p}{8}$	$\frac{p}{8\sqrt{2}}$
Intensity	$\frac{I}{2}$	$\frac{I}{4}$	$\frac{I}{8}$	$\frac{I}{16}$	$\frac{I}{32}$	$\frac{I}{64}$	$\frac{I}{128}$
Sound Level	L-3dB	L-6dB	L-9dB	L-12dB	L-15dB	L-18dB	L-21dB

Human ear doesn't respond equally for all the audible frequencies, but there's a curve called **equal-loudness contour** that ties up sound pressure levels having equal loudness as a function of frequency. Two of the most famous sets of equal-loudness contours are presented by Fletcher-Munson [35] in 1933, even though in 1956 the re-determination made by Robinson and Dadson [34] are the basis of the new standards, ISO 226:2003. The contours shows the large difference in the low-frequency region: to obtain the same loudness (expressed in phon) it takes more dB of Sound Pressure Level for high frequencies than low. Because our interest is for frequencies up to 500 Hz (near those emitted by a Turboprop), every dB reduced by the structure is a great achievement for human acoustic comfort.

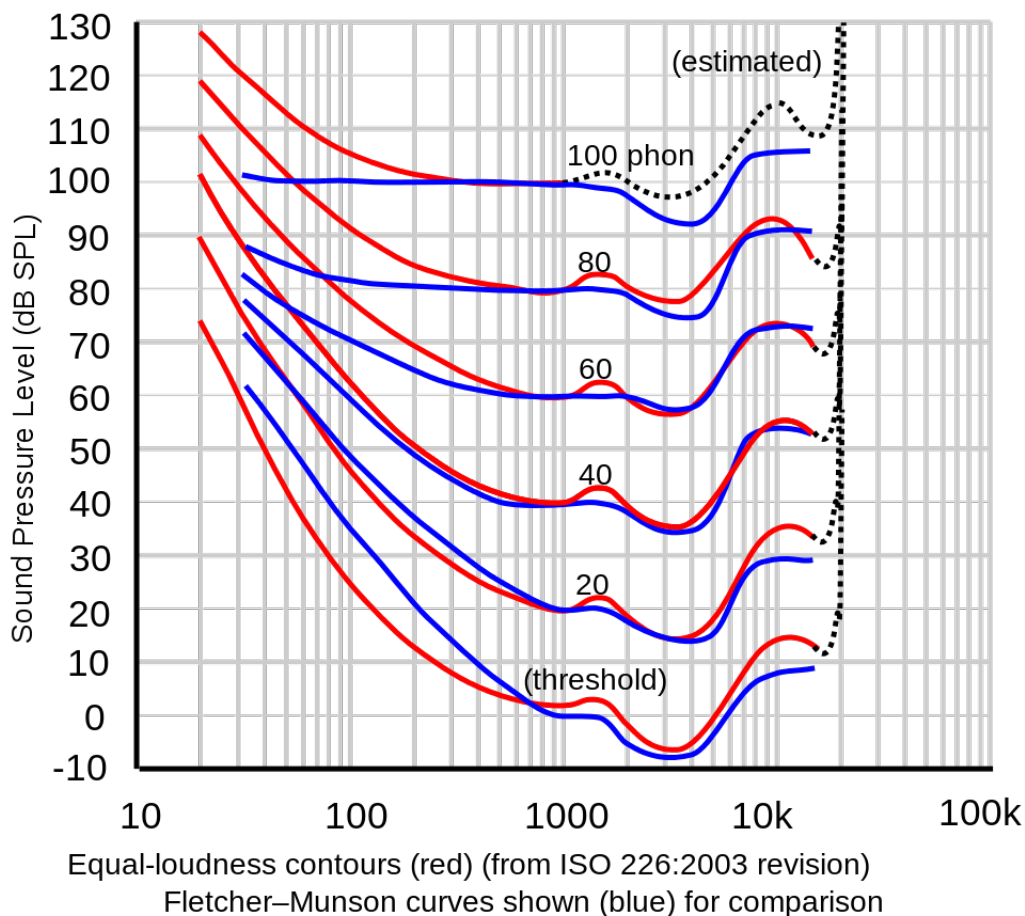


FIGURE 1.2: Pressure-Intensity-Sound Level example

1.3 The mass-frequency law

In order to read the results in this work, it is necessary to briefly introduce some notions of acoustic physics. In the figure below, a wall is reached by an incident acoustic wave. Because of their non-infinite material stiffness, proportional to its acoustic impedance Z ¹, the wall transmit some of the incident power, adsorb some power while a reflected wave returns back.

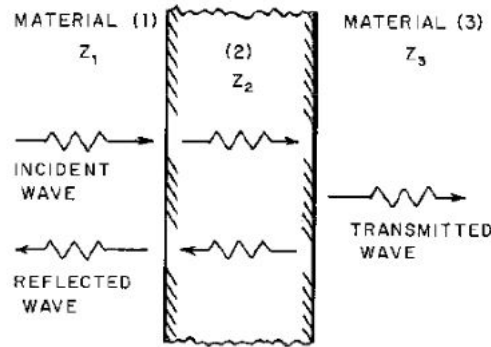


FIGURE 1.3: Scheme of a material interacting with acoustic waves

1

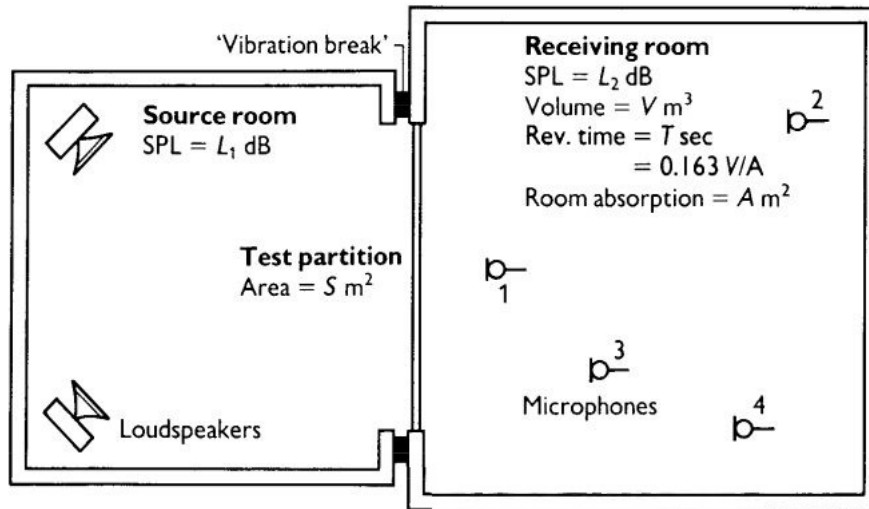


FIGURE 1.4: Scheme of a typical acoustic room

From Newton second law:

$$m \frac{dU_i}{dt} = \Delta p S = (2p_i - p_d) S \approx 2p_i S \quad (1.5)$$

¹Specific Acoustic Impedance is the ratio of acoustic pressure p to acoustic velocity flow u , and is an intrinsic property of a medium. Usually, it varies strongly when the frequency changes. [33]

then $p_i = P_i \cos(\omega t)$ is the incident pressure. The Incident velocity

$$U_i = \frac{2S}{m\omega} P_i \sin(\omega t) \quad (1.6)$$

because $U_i = U_d$.

$$p_d = \frac{\rho c}{S} U_d = \frac{\rho c}{S} \frac{2S}{m\omega} P_i \sin(\omega t) \quad (1.7)$$

The acoustic power ratio τ is then:

$$\tau = \frac{P_i}{P_d} = \frac{m\omega}{2\rho c} \quad (1.8)$$

where c is the speed of sound, ρ is the density of the fluid and $\omega = 2\pi f$.

Sound Transmission Loss (also called Noise Reduction Index) is then

$$STL = 10 \log_{10} \frac{I_i}{I_d} = 10 \log_{10} \frac{P_i^2}{P_d^2} = 20 \log_{10} \frac{P_i}{P_d} = 20 \log_{10} \frac{m\pi f}{\rho c} [dB] \quad (1.9)$$

STL for different materials is shown in Fig 1.5.

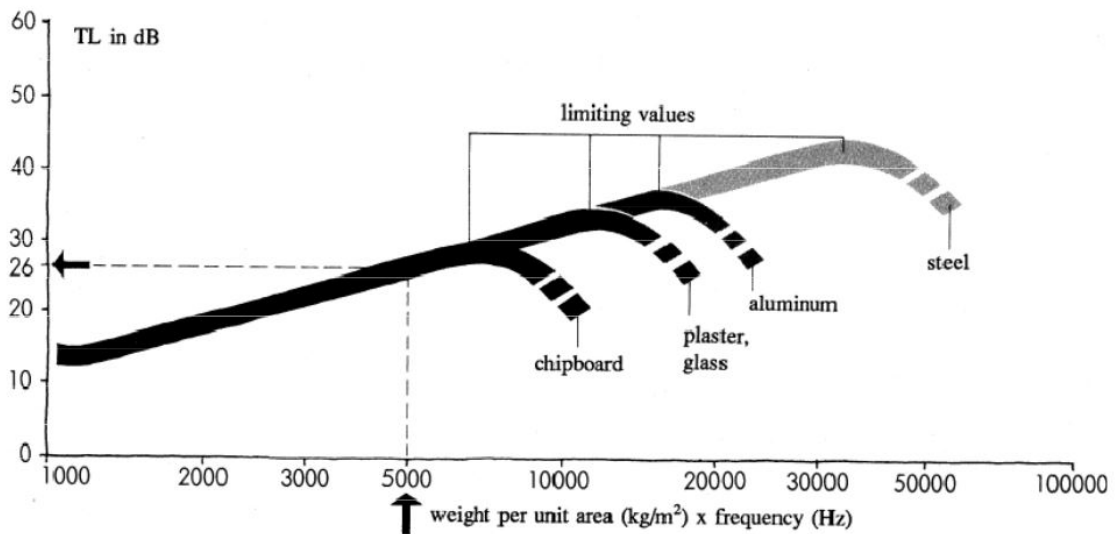


FIGURE 1.5: Mass-frequency law **without** taking into account material stiffness [32]

As expected, the greater the mass of the material, the higher is the sound energy required to set the medium in motion. The mass law applies strictly to limp, non-rigid partitions. However, most materials used in buildings possess some rigidity or stiffness. This means that other factors must really be considered, and that the mass law should only be taken as an approximate guide to the amount of attenuation obtainable. Taking into account the

material **stiffness**

$$p_d = \frac{\rho c}{S} U_d = \frac{\rho c}{S} \frac{2S}{m\omega i + k} P_i \sin(\omega t) \quad (1.10)$$

$$\tau = \frac{P_i}{P_d} = \frac{i(m\omega - \frac{k}{\omega})}{2\rho c} \quad (1.11)$$

The transmitted power P_d become now more complex:

$$P_d = \frac{2P_i}{\frac{i(\omega m - \frac{k}{\omega})}{\rho_2 c_2} + \frac{d}{\rho_2 c_2} + \frac{\rho_1 c_1}{\rho_2 c_2} + 1} \quad (1.12)$$

Using these equation, one can plot the Sound Reduction Index R. Sound Reduction Index is a laboratory-only measurement, and takes to account the size of the test rooms to produce accurate and repeatable measurement. The term "Sound Transmission Loss" is also used.

$$\begin{aligned} \omega \ll \omega_0 &= \sqrt{\frac{k}{m}} & \tau &\approx \left(\frac{2\rho c \omega}{k}\right)^2 & R &= 20 \log k - 20 \log f - 20 \log(4\pi\rho c) \\ \omega \gg \omega_0 &= \sqrt{\frac{k}{m}} & \tau &\approx \left(\frac{2\rho c}{\omega m}\right)^2 & R &= 20 \log m + 20 \log f - 20 \log\left(\frac{\rho c}{\pi}\right) \\ \omega \approx \omega_0 &= \sqrt{\frac{k}{m}} & \tau &\approx \frac{4n}{\left(\frac{d}{\rho_2 c_2} + n + 1\right)^2} \approx 1 & R &= 0 \end{aligned}$$

with

$$n = \frac{\rho_1 c_1}{\rho_2 c_2}$$

Lowest frequencies are stiffness-controlled, then resonance peaks zone, and mass-controlled central zone. Near the critical frequencies $R=0$ means a low peak visible in Fig 1.6. Also, damping effects lead to higher R near critical frequencies.

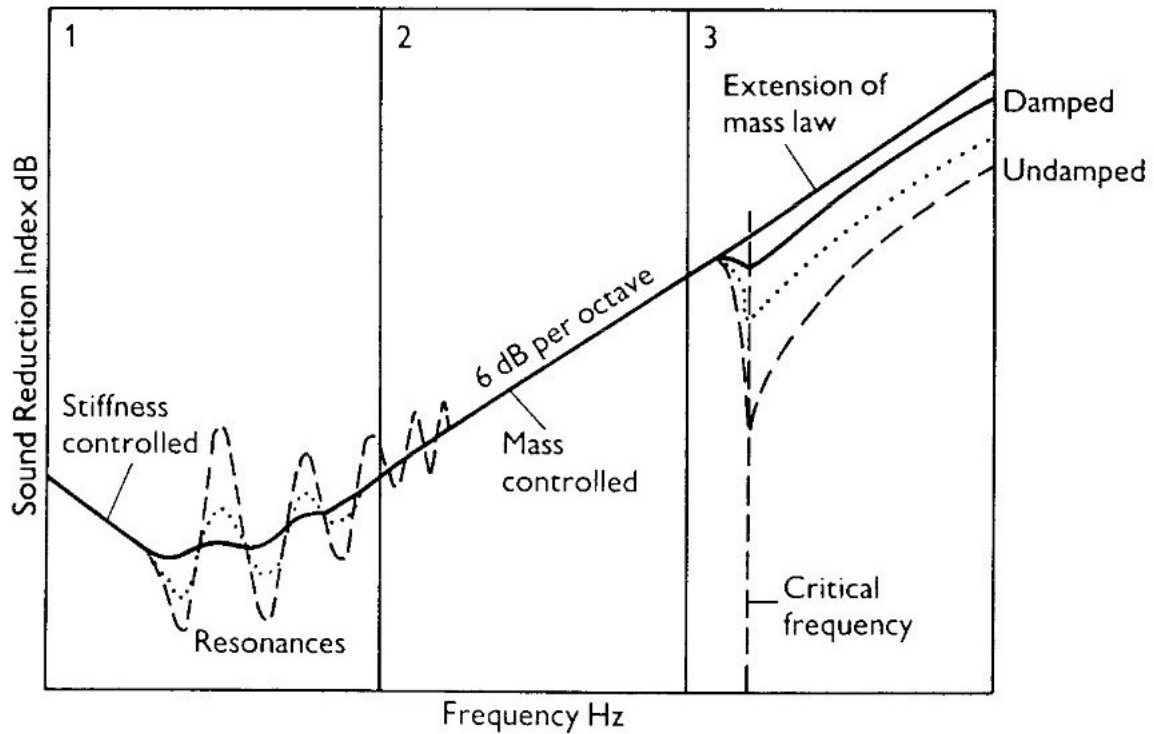


FIGURE 1.6: Mass-stiffness-frequency law [32]

1.4 Acoustics in aircraft fuselages

One critical shortcoming of Aircraft materials is their suboptimal acoustical performance: they allow sound to pass through rather easily and therefore yield a low sound transmission loss. This phenomenon can be in part explained by the mass-frequency law. Low frequencies are also an issue because there's an order of magnitude between their wavelengths (1 meter) and a typical thickness of damping materials in aircraft fuselages for space constraints.

Typical configuration for a fuselage are **skin-stiffened Aluminum panels** with damping materials like polyamide foams or melamine foams.

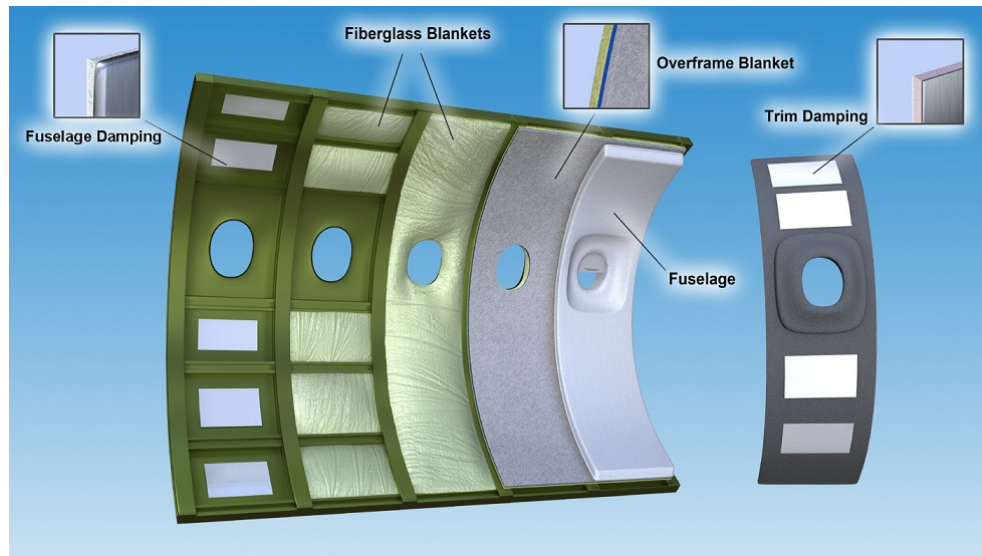


FIGURE 1.7: An example of fuselage acoustic treatment: From Aeero Technologies LLC, <https://earglobal.com/en/aircraft/applications/fuselage>

Interior noise levels of light propeller-driven aircraft have been measured (NASA report, 1975[23]) between 84 and 104 dB on the A-weighted scale.

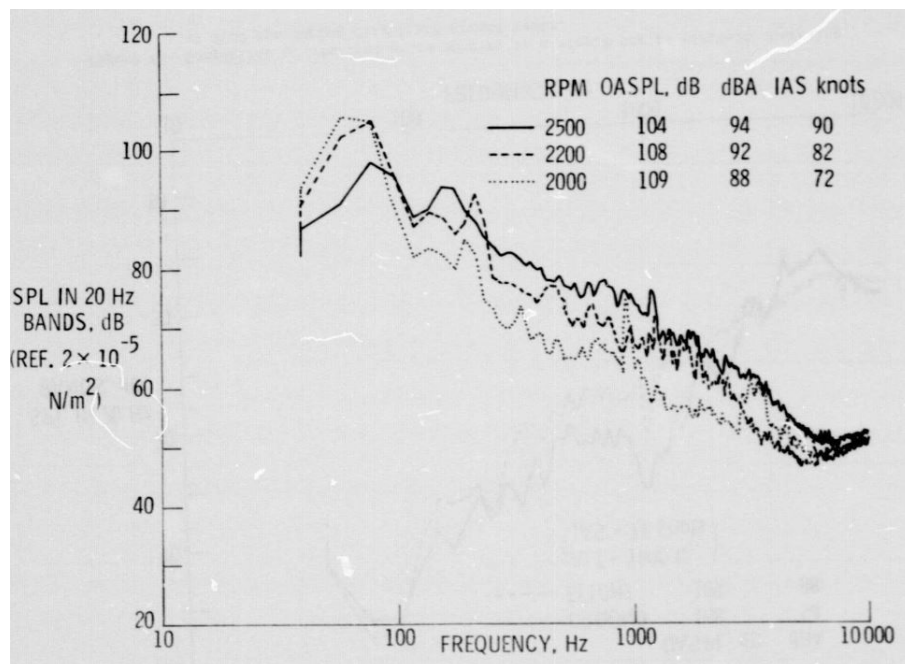


FIGURE 1.8: Sample of noise spectra measured in a single engine aircraft for three different engine rpm settings at a flight altitude of 1000 feet. Credits NASA 1975[23]

These noise levels are substantially higher than the levels for other types of aircraft with conventional take-off and landing and for ground transportation vehicles. Limited exposure to these noise levels can cause a temporary shift in the hearing threshold of the listener, and prolonged exposure could result in permanent hearing damage. The distinguishing characteristic of

interior noise for propeller-driven aircraft is the low-frequency tonal nature of the noise. The noise is caused primarily by the first few harmonics of the propeller blade-passage frequency and by the engine firing harmonics (if the aircraft is equipped with reciprocating engines). Maximum sound pressure levels typically occur in the frequency range from 80 to 200 Hz on the A-weighted scale [23]. This low-frequency character of the noise handicaps efforts to diagnose the path of the noise, and, because of weight considerations, renders many conventional noise control treatments impracticable. Some information that is either necessary or desirable for designing an aircraft with quieter interior noise levels is as follows:

- 1. Transmission loss of the fuselage walls
- 2. Relative importance of structural and acoustic paths of the noise
- 3. Critical noise paths of the fuselage
- 4. Relative effectiveness of various add-on noise control treatments[24]

Typically, there are mainly 4 different noise sources critical to cabin noise:

- auxiliary power unit (APU) noise;
- environment control system (ECS) noise;
- engine noise and turbulent boundary layer (TBL) noise.

Because of the different acoustic characteristic and transmission path for each resource, their impacts to cabin noise level are not the similar. A vibration and noise test under ground and flight status of an in-service civil aircraft was conducted. Based on the test results, comparing the data under different test status, the acoustic characteristic and transmission path are analyzed for the 4 noise resources in this paper, including distribution characteristic, spectrum characteristic and transmission path. APU noise mainly affects the rear fuselage, ECS noise transmits by ducts, engine noise and TBL noise transmit through side panel. [22]

Chapter 2

What does Metamaterial mean?

Cummer et al, in "Controlling sound with acoustic" published by Nature in 2016 [7], describe metamaterials as follow: Metamaterials are artificial structures, typically periodic (but not necessarily so), composed of small meta-atoms that, in the bulk, behave like a continuous material with unconventional effective properties. Research in this area rapidly expanded with the understanding that relatively simple, but sub-wavelength, building blocks can be assembled into structures that are similar to continuous materials, yet have unusual wave properties that differ substantially from those of conventional media.

The term *Metamaterial* is not very precisely defined, but a good working definition is: a material with 'on-demand' effective properties, without the constraints imposed by what nature provides.

For acoustic metamaterials, the goal is to create a structural building block that, when assembled into a larger sample, exhibits the desired values of the key effective parameters (mass density and the bulk modulus). The most common approach to constructing acoustic metamaterials is based on the use of structures whose interaction with acoustic waves is dominated by the internal behavior of a single unit cell of a periodic structure, often referred to as a *meta-atom*. To make this internal meta-atom response dominant, the size of the meta-atom generally needs to be much smaller (about ten or more times smaller) than the smallest acoustic wavelength that is being manipulated.

This sub-wavelength constraint ensures that the metamaterial behaves like a real material in the sense that the material response is not affected by the shape or boundaries of the sample.

Acoustic Metamaterials (AMs) composed of sub-wavelength artificial resonant micro-structures can exhibit negative mass density, negative modulus or double-negative characteristics. The development of AMs has presented some anomalous properties for the manipulation of acoustic waves such as flat focusing effect [8], super-lens [9][10][11], reversed Doppler Effect [12], acoustic cloaking [13] [14][15],etc.

2.1 Examples of metamaterials

Metamaterial structures like the ones described here are potentially applicable as acoustic invisibility devices based on total absorption as well as practical structures to attenuate environmental noise.

In a *Review on acoustic metamaterials of Jose' Sanchez-Dehesa* these materials are divided in 4 categories identified by 2 parameters: Bulk modulus and mass density, as in Figure 2.1.

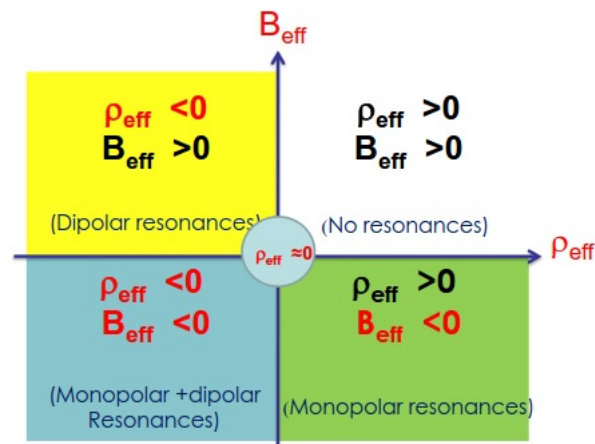


FIGURE 2.1: Subdivision of Materials by their dynamic density and Bulk Modulus (Li and Chan, PRE 2004)

2.1.1 Membrane-type Acoustic Metamaterial with negative dynamic density

Yang et al.[29] presented in 2008 the experimental realization of a membrane-type acoustic metamaterial with very simple construct, capable of breaking the mass density law of sound attenuation in the 100-1000 Hz regime by a significant margin (200 times). Owing to the membrane's weak elastic moduli, there can be low-frequency oscillation patterns even in a small elastic film with fixed boundaries defined by a rigid grid. They can tune vibrational eigenfrequencies by placing a small mass at the center of the membrane sample. Near-total reflection is achieved at a frequency between two eigenmodes where the in-plane average of normal displacement is zero. By using finite element simulations, negative dynamic mass is explicitly demonstrated at frequencies around the total reflection frequency. Excellent agreement between theory and experiment is obtained.

The basic unit of this metamaterial consists of a circular elastic membrane (20 mm in diameter and 0.28 mm thick) with fixed boundary, imposed by a relatively rigid grid, with a small weight attached to the center. Acoustic waves are incident perpendicular to the membrane plane. The central mass is a hard disk 6.0 mm in diameter.

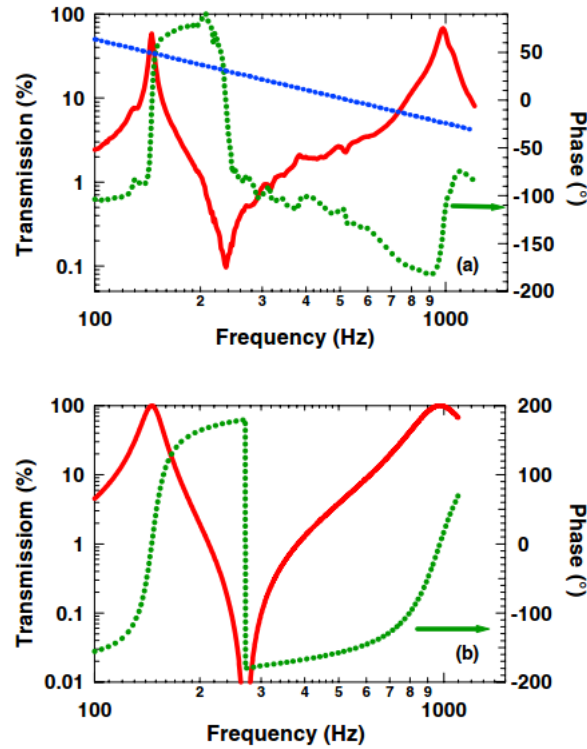


FIGURE 2.2: (a) Experimental transmission amplitude (solid red curve) and phase (dotted green curve) of the membrane resonator. The blue dashed line indicates the transmission amplitude predicted by the mass density law with the same average area mass density as the resonator. (b) Theoretical transmission amplitude (solid red curve) and phase (dotted green curve) of the membrane resonator.[29]

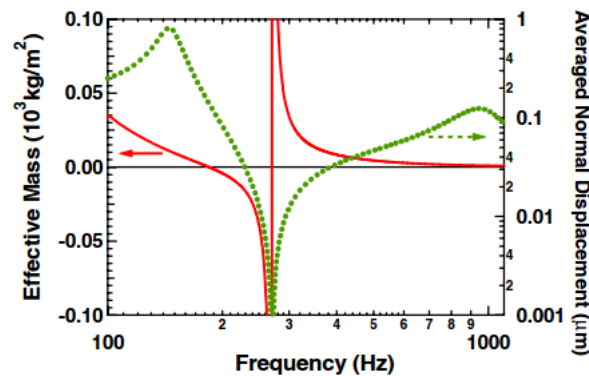


FIGURE 2.3: The calculated effective dynamic mass of the resonator (red solid curve, left axis) as defined in the text, together with the in-plane averaged normal vibration amplitude (green dotted curve, right axis), evaluated with an incident wave with pressure modulation amplitude of 10^3 Pa . It is seen that in our system, negative dynamic mass and $|u_z| \sim 0$ coincide, and they constitute the basic mechanism for near-total reflection of low-frequency acoustic waves.[29]

Figure 2.2(a) shows the measured transmission amplitude (solid red curve) and phase (dotted green curve) spectra. The blue dashed line indicates the mass density law that is pertinent to our sample density of 0.1 Kg/m^2 . There

are two peaks at 145 and 984 Hz. But perhaps the most surprising is the dip at 237 Hz that breaks the mass density law by a factor of 200, implying near-total reflection by such a flimsy membrane. They found that this phenomenon arises directly from the negative dynamic mass at this frequency, and it is an inevitable consequence of multiple low-frequency vibrational eigenmodes of the system. Fig. 2.2(b) show the calculated transmittance amplitude (solid red curve) and phase (dotted green curve) of a circular thin rubber membrane. The edge of the circular membrane was fixed, with a 6.0 mm diameter circular steel disk of 300 mg fixed at the center. In their calculation, the mass density, Young's modulus, and the Poisson ratio for the rubber membrane are 980 kg/m^3 , $2 * 10^5 \text{ Pa}$, and 0.49, respectively. While Young's modulus and Poisson's ratio for the disk are $2 * 10^{11} \text{ Pa}$ and 0.29, respectively. Standard values for air, i.e., 1.29 kg/m^3 , ambient pressure of 1 atm, and speed of sound in air of c 340 m/s were used. It can be seen that there are two transmission peaks at 146 and 974 Hz, with a dip at 272 Hz. These features do not depend on the incidence angle of the sound waves, owing to the orders of magnitude difference between the wavelength of sound in air and the sample size. It is seen that the theoretical predictions agree very well with the experiments under normal incidence.

The effective dynamic mass of the system may be obtained by dividing the averaged stress by the averaged acceleration, i.e., $\rho_{eff} = \langle \sigma_{zz} \rangle / \langle a_z \rangle$, with $\langle \rangle$ denoting volume average over the whole membrane structure (membrane plus the weight), while σ_{zz} and a_z are the stress and acceleration normal to the membrane plane at rest, respectively. Figure 2.3 shows the results of such calculations. Close to the transmission dip frequency, the effective dynamic mass turns from positive to negative. It then jumps to positive at the dip frequency and then approaches the actual value of the system (0.1 Kg/m^2) at high frequencies. Also plotted in Fig. 2.3 is the in-plane averaged normal displacement (the dotted green curve), which peaks at the two eigenmodes and goes through zero at the frequency where the transmission is at a minimum. As shown below, there is a link between the two phenomena. Their calculations also show that the first low-frequency transmission peak is due to the eigenmode in which the membrane and the weight vibrate in unison, while the second transmission peak at high frequency is due to the eigenmode in which the membrane vibrates while the central weight remains almost motionless. As a result, the first peak frequency should depend strongly on the mass of the central weight, while the second peak frequency should have a very weak dependence on the central mass. The experimental transmission spectra for different masses show the same feature of twin peak with a dip in between. The first transmission peak and the dip shift significantly to higher frequencies with the reduction of the mass, while the second transmission peak shifts only by a very small amount.

2.1.2 Dark acoustic metamaterials as super absorbers for low-frequency sound

Mei et al.[30] focus on a relatively simple, proof-of-principle structure, denoted Sample A. Fig.2.4a, show a photo of the unit cell used in the experiment, comprising a rectangular elastic membrane that is 31 mm by 15 mm and 0.2 mm thick. The elastic membrane was fixed by a relatively rigid grid, decorated with two semi-circular iron platelets with a radius of 6 mm and thickness of 1 mm. The iron platelets are purposely made to be asymmetrical so as to induce flapping motion, as seen below. Here the sample lies in the x - y plane, with the two platelets separated along the x axis. Acoustic waves are incident along the z direction. This simple cell is used to understand the relevant mechanism and to compare with theoretical predictions.

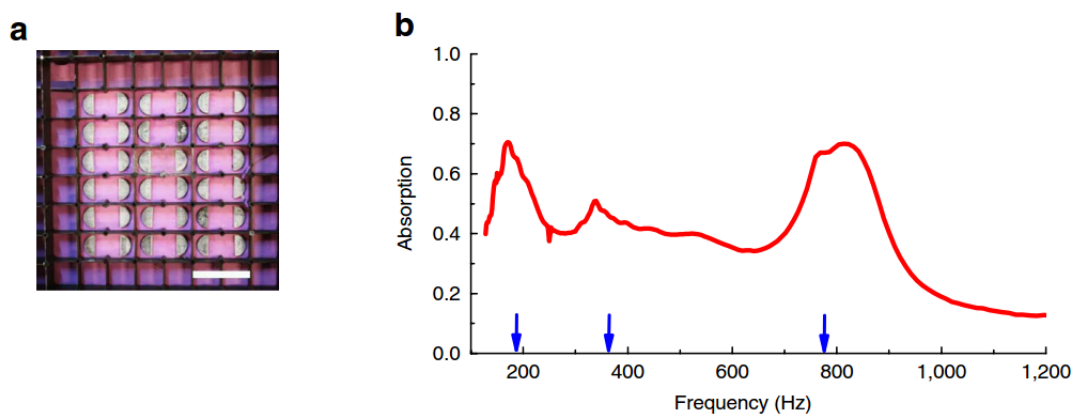


FIGURE 2.4: Absorption coefficient and displacement profiles of sample A. (a) Photo of sample A. The scale bar is 30 mm. (b) The measured absorption coefficient (red curve) and the positions of the absorption peak frequencies predicted by finite-element simulations (blue arrows). There are three absorption peaks located at 172, 340 and 813 Hz. [30]

Another type of unit cell, denoted Sample B (Fig.2.5), is 159 mm by 15 mm and comprises 8 identical platelets decorated symmetrically as two 4-platelet arrays (with 15 mm separation between the neighboring platelets) facing each other with a central gap of 32 mm. Sample B is used to attain near-unity absorption of the low-frequency sound at multiple frequencies.

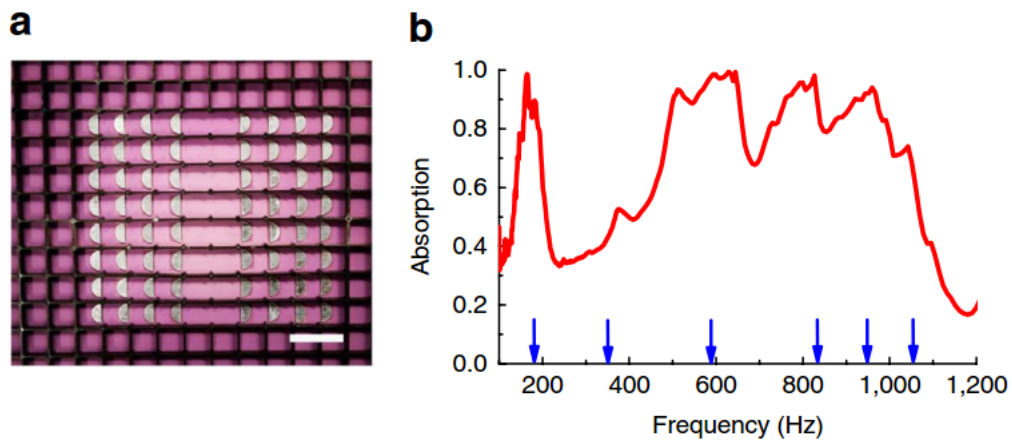


FIGURE 2.5: Absorption coefficient of sample B. (a) Photo of sample B. The scale bar is 30 mm. (b) The red curve indicates the experimentally measured absorption coefficient for two layers of sample B with an aluminum reflector placed 28 mm behind the second layer. The distance between the first and second layers is also 28 mm. The absorption peaks are located at 164, 376, 511, 645, 827 and 960 Hz. Blue arrows indicate the positions of the absorption peak frequencies predicted by finite-element simulations.[30]

2.1.3 Doubly periodic material

Langlet, Hladky-Hennion and Decarpigny [4] [5][6] (1995) worked on periodic materials, such as porous or fibrous materials and composites, that have arisen a great deal of interest and are now widely used in underwater acoustics, signal processing, as well as for medical imaging applications. Particularly, in order to explain their physical behavior, they studied the propagation of harmonic elastic waves through periodic materials.

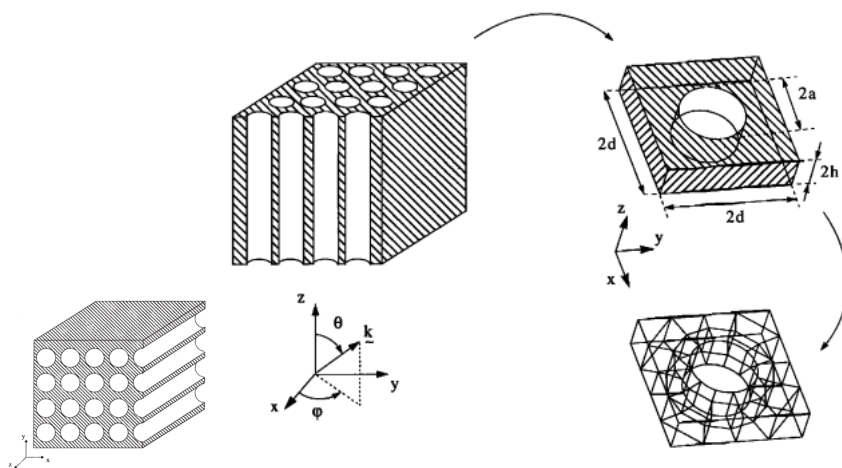


FIGURE 2.6: Schematic description of a doubly periodic material, considered as a triply periodic material and finite element mesh of the unit cell. [4] [5][6]

The periodic material (Fig 2.6) is supposed to be periodic in one, two, or three space directions, finite or infinite in the others. Within this cell, a phase relation is applied on nodes separated by one period, defining boundary conditions between adjacent cells. The phase relation is related to the wave number of the incident wave in the periodic material. The dispersion curves present the variations of the eigenfrequencies versus the wave number, and they provide phase velocity and group velocity for each propagation mode, stop-bands, pass-bands, etc.

The the material is excited by a plane, monochromatic wave, the direction of incidence of which is marked by an angle θ with respect to the positive y axis. The incident wave is characterized by a real wave vector k , the modulus of which is called the wave number and is denoted k .

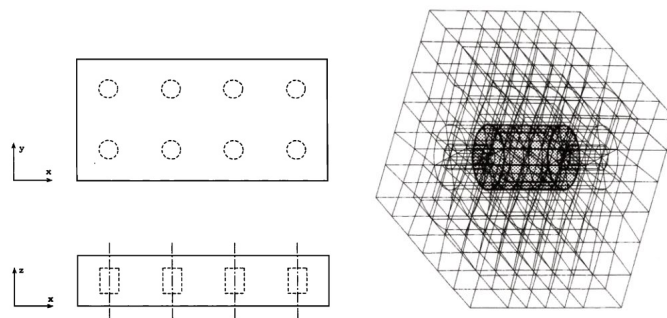


FIGURE 2.7: (left) Cross-section and top views of the reference Alberich anechoic layer.(right) FE mesh of the elementary cell for the Alberich anechoic coating. The dotted domain is the air cavity (air not modeled). [4] [5][6]

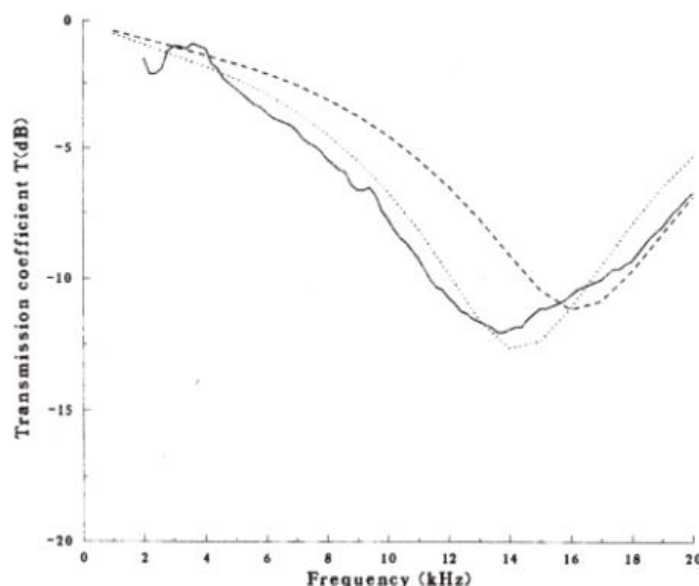


FIGURE 2.8: Frequency variations of the transmission coefficient of the Alberich anechoic coating, made of polyurethane: full line: measurements; dashed line: FEM; dotted line: FEM with adjusted properties. [4] [5][6]

2.1.4 Omni-directional broadband acoustic absorber based on metamaterials

Climente, Torrent and Sanchez-Dehesa [21] studied this metamaterial (Fig 2.9) based on a cylindrical symmetry and made of two parts, a shell that bends the sound towards the center and a core that dissipates its energy. The outer shell is made of cylinders whose diameters increase with decreasing distance to the center. The inner core is made of identical cylinders in a hexagonal lattice with about 84 percent of filling fraction, that perfectly matches the acoustic impedance of air and behaves like a gradient index lens. The inset shows the ray trajectories of the sound traveling within the outer shell. Their experimental data obtained in a multi-modal impedance (Fig 2.10) chamber demonstrate that the proposed acoustic black-hole acts like an omni-directional broadband absorber with strong absorbing efficiency.

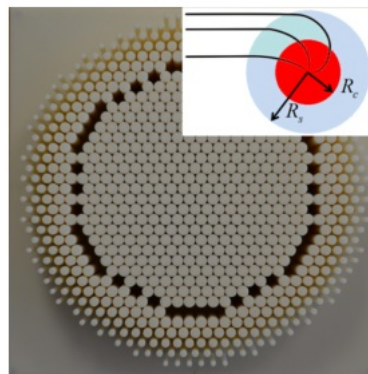


FIGURE 2.9: Photograph of the structure of the metamaterial (Climente et al)[21]

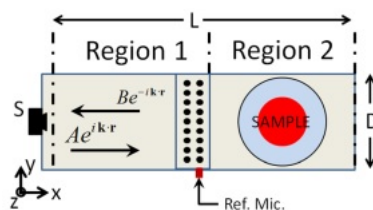


FIGURE 2.10: Scheme of the multi-modal impedance chamber and the experimental setup employed in the characterization of the acoustic black-hole. The chamber has a width $D = 30$ cm, a length $L = 150$ cm, and height $h = 5$ cm. The speaker (S) at the left excites an acoustic flow represented by coefficients A , while the backscattered flow is given by coefficients B . Black dots define the 9 pairs of microphones used to record the signal. Another microphone (Ref. Mic.) is employed as the reference. The sample is placed in the right hand side region, which is accessible by a removable tap.[21]

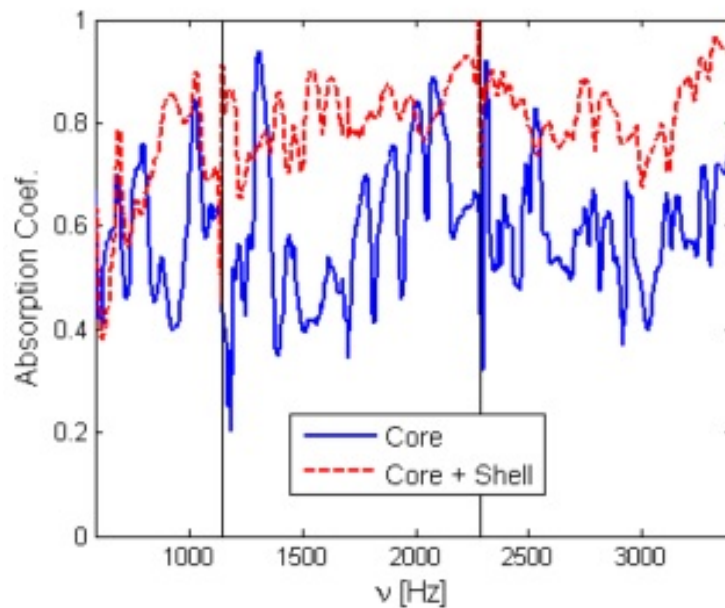


FIGURE 2.11: Absorption produced by the core of the black-hole sample (continuous line) and by the complete black-hole (dashed line).[21]

The sample constructed acts like a broadband omni-directional acoustic absorber where a 80 percent of the impinging acoustic energy is dissipated (Fig 2.11). This structure has been designed by considering an outer shell that guides the sound energy to the core center and a core that dissipates the incoming energy by friction.

2.1.5 Honeycomb acoustic metamaterial

The honeycomb structures are typically bonded to high-modulus laminate face sheets to form honeycomb sandwich panels. However, the sandwich panels are notorious for their poor acoustic performance at low frequencies due to the high stiffness and lightweight.

Sui et al. [25] studied an honeycomb acoustic metamaterial. Figure 2.12 and 2.13 shows its unit cell, where an isotropic membrane is adhered on the top of the honeycomb structure. This material is termed as a lightweight yet sound-proof acoustic metamaterial. Such a material can be readily implemented as the honeycomb core material and thus can potentially make honeycomb sandwiched structures possess simultaneously strong, lightweight, and sound-proof properties.

It is here reported that the proposed metamaterial having a remarkably small mass per unit area at $1.3 \text{ Kg}/\text{m}^2$ can achieve low frequency ($<500 \text{ Hz}$) sound transmission loss (STL) consistently greater than 45 dB. Furthermore, the sandwich panel which incorporates the honeycomb metamaterial as the core material yields a STL that is consistently greater than 50 dB at low frequencies. This metamaterial is promising for constructing structures that are simultaneously strong, lightweight, and sound-proof.

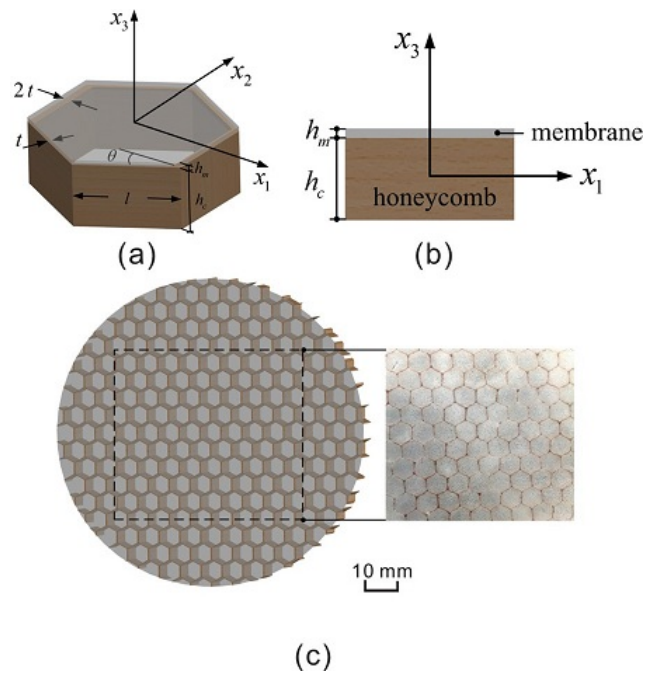


FIGURE 2.12: (a) Unit cell of the honeycomb acoustic metamaterial. The honeycomb core was made from aramid fiber sheets with $t=0.07$ mm, $l=3.65$ mm, $h_c=25$ mm, and $\Theta = 30$. The membrane material was latex rubber with a thickness $h_m=0.25$ mm. Two side walls (one marked in the figure and the opposing one) had a thickness of $2t$. The other side walls had a thickness of t . This is common and is a result of the traditional honeycomb production method. (b) Side view of the acoustic metamaterial. (c) The metamaterial prototype used for the acoustical test.[25]

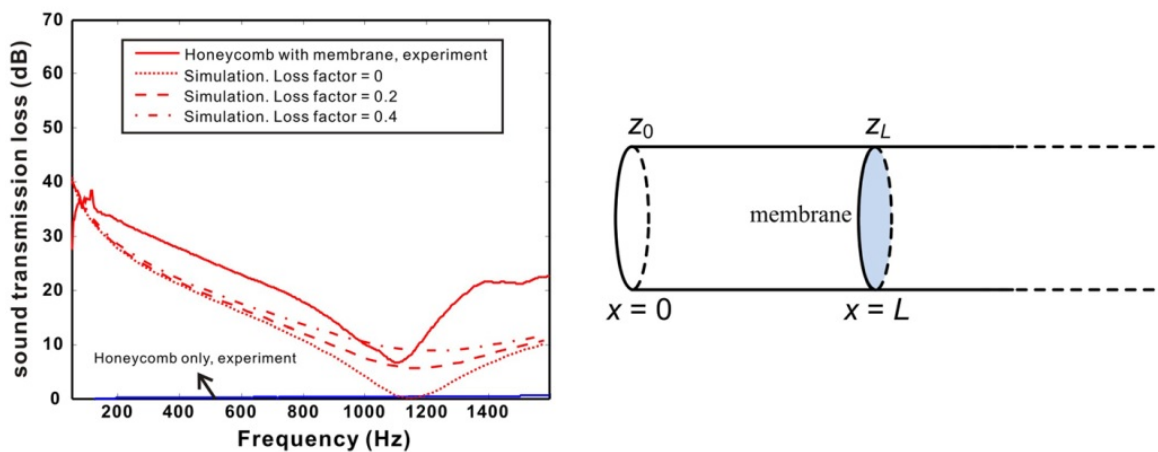


FIGURE 2.13: Experimental and simulation sound transmission loss results for honeycomb structure only and the proposed metamaterial (honeycomb structure with membranes)[25]

Chapter 3

MSC ACTRAN description

MSC ACTRAN is a powerful tool that allow us to calculate the Transmission Loss of a specific sample with different geometries and materials, even those materials having frequency dependent mechanical properties, both for real and imaginary part, like in our case. The samples have been created and discretized with the version 17.1 of Actran with the integrated meshing tools. For more complexes geometries an external program (MSC PATRAN, APEX) had been used.

Analyses can be imported, created and saved in DAT or EDAT formats, once they are specified, using the command “export analysis”. Analyses are subdivided in eight fields: components, boundary conditions, load-cases, post processing options, solvers, field data, user function and local systems and transformations. The analysis properties window also includes some analysis parameters which can be added, as the frequency range.

3.1 Material assignment

Here’s a description of the materials used in this work: solids, fluids, composites. A Composite solid material allows to model a multilayered composite material using homogenized material properties, computed by Actran. This material can be referenced by a shell or dshell component using the mandatory material keyword.

```

for each composite material
  BEGIN MATERIAL material_id
    [NAME material_name]
    COMPOSITE_SOLID
    for each layer
      LAYER layer_id MATERIAL mat_id ...
      ... THICKNESS thick_value or FIELD id ...
      ... ANGLE alpha or FIELD id
    end for
    [HOMOGENIZATION_OPTION homogeni_value]
    [GLOBAL_DAMPING damping_value or TABLE table_id]
  END MATERIAL material_id
end for

```

FIGURE 3.1: Composite solid edat syntax

where:

- **material_name** is the optional label assigned to the material. Each line defines one ply of the layered composite:
 - **mat_id** refers either to a valid isotropic solid, transverse isotropic solid or orthotropic solid material;
 - **thick_value** is equal to the thickness of the considered ply and can be spatially varying using the field;
 - **alpha** describes the angle (expressed in degrees) between the axis 1 of the ply coordinate system and the x0 axis of the local reference material coordinate system x_0, y_0, z_0), and can be spatially varying using the field.
- The keyword *HOMOGENIZATION_OPTION* selects the homogenization procedure to be applied to the laminate structure. Please refer to Chapter 33 of [18] for more details.
- The keyword *GLOBAL_DAMPING* can be used to apply a constant damping factor to the entire laminate structure. This damping can be constant or frequency dependent through the usage of a table. If not specified, Actran uses the damping of each ply individually. If specified, it replaces all provided damping factors within each ply.

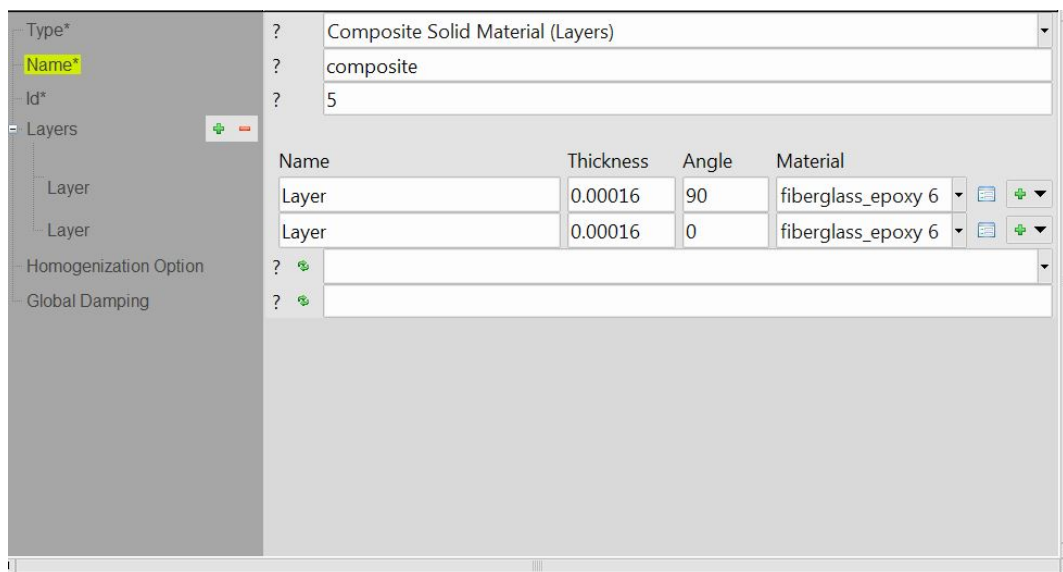


FIGURE 3.2: Composite solid material definition

The geometry of considered composite materials is described by a sequence of N layers. Layer i (where $1 \leq i \leq N$) is defined by its thickness h_i (Figure 3.3). The material of layer i can be orthotropic, transverse isotropic or isotropic. The related material properties are defined in a particular (local for each layer) coordinate system $(1, 2, 3)$ where axis 1 and 2 are contained in the layer plane while axis 3 is normal to the layer.

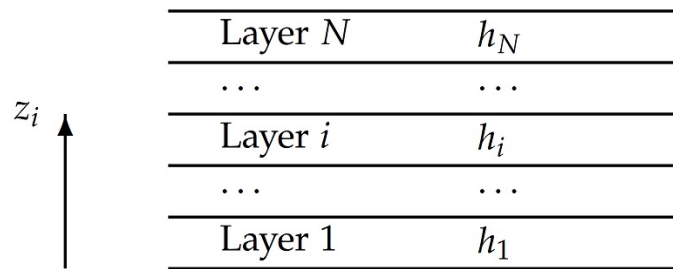


FIGURE 3.3: Multi-layered composite material direction

Fluid Material A fluid material is the standard material defining both viscous and non viscous fluids related to an acoustic medium.

Type*	? Fluid Material
Name*	? Air
Id*	? 3
Sound Speed	? Value 340
Fluid Density	? Value 1.225
Specific Heat (Constant Pressure)	? Value
Specific Heat (Constant Volume)	? Value
Advanced	

FIGURE 3.4: Fluid Material definition

```
for each fluid material
  BEGIN MATERIAL material_id
    [NAME material_name]
    FLUID
    [SOUND_SPEED sound_speed or TABLE table_id]...
      [or FIELD field_id]
    [FLUID_DENSITY fluid_density or TABLE table_id]...
      [or FIELD field_id]
    [VISCOSITY viscosity or TABLE table_id]...
      [or FIELD field_id]
    [THERMAL_CONDUCTIVITY thermal_conductivity]...
      [or TABLE table_id or FIELD field_id]

    [CP cp]
    [CV cv]
    [REFERENCE_FLOW flow]
  END MATERIAL material_id
end for
```

FIGURE 3.5: Fluid Material edat syntax

where:

- material_name is the optional label assigned to the material;
- All material properties having default values (air at 15C and 1 atm), none is mandatory;
- The definition of sound speed and fluid density depend on the flow type acting with the concerned component:

3.2 Finite Fluid Component

The Finite Fluid component is used for modeling all type of finite acoustic media (including heavy fluids media such water). The Unknown variable here is the fluid pressure, which mean only 1 DOF (degree of freedom) for each node.

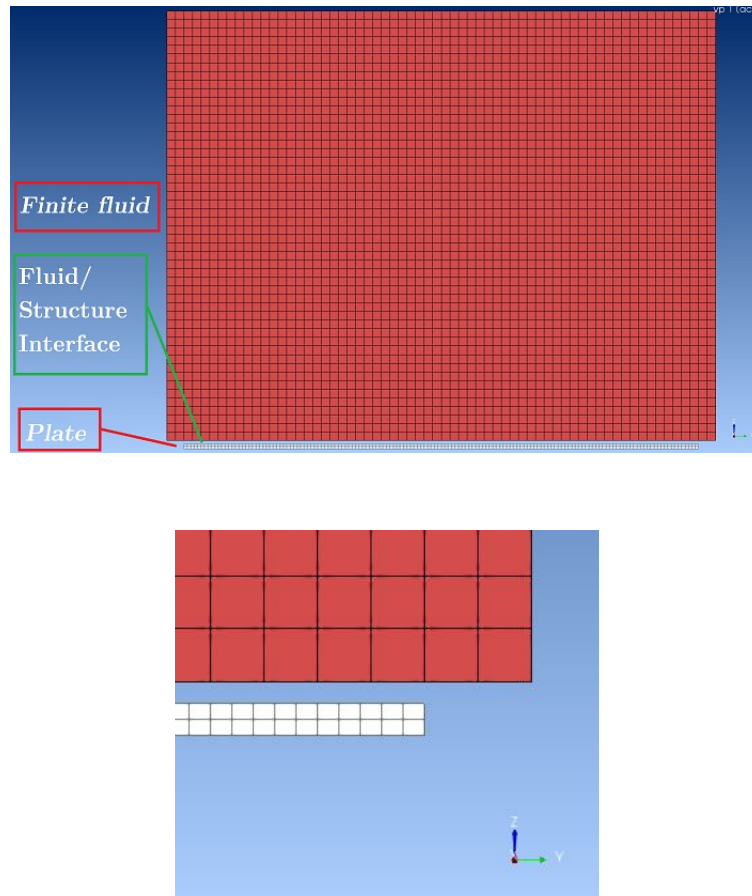


FIGURE 3.6: Model used for evaluate Sandwich Transmission Loss, with Finite fluid Acoustic Component as receiving room.

The default boundary condition on free faces of Finite Fluid component is a rigid wall. The normal velocity is considered equal to 0 and the acoustic wave is perfectly reflected. In order to model a Free Field condition (no reflected waves) an Infinite Fluid component is mandatory(see subsection 3.3). The space between fluid and solid component is necessary to avoid mesh congruence errors in the interface component: even with full compatible meshes (node-to-node matching) there was no radiated power. This solution was taken according to FFT Technical Support suggestion.

3.3 Infinite Acoustic Component

When modeling free field radiation problems, the acoustic field near the source is modeled with acoustic finite elements but the entire unbounded acoustic domain cannot be discretized for obvious reasons. Actran uses Infinite Elements to model the unbounded acoustic domain. The Infinite Elements are represented by 2D elements applied to the exterior boundary of the finite element domain. The objectives of the Infinite Elements are to act as a non reflective boundary condition and to compute the sound pressure levels (SPL) in far field.

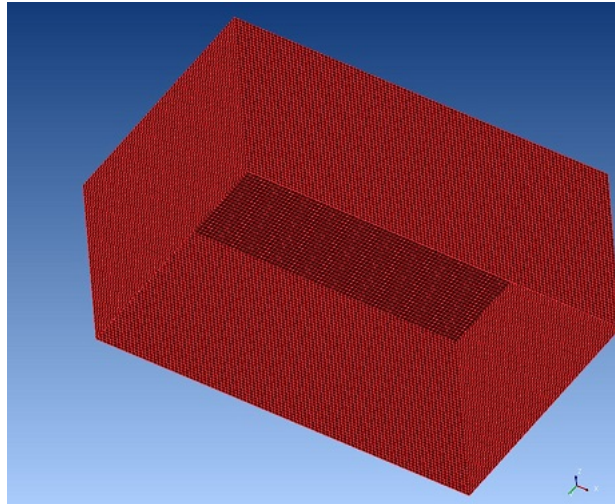


FIGURE 3.7: Infinite Domain modeled as a hollow box, without the bottom surface where the radiating surface is located.



FIGURE 3.8: An anechoic chamber [28]

The Infinite Fluid COMPONENT is the component for modeling unbounded acoustic media, and it is assigned to a fluid material. Mandatory attributes to be given in the analysis file are:

- Material ID
- Order of interpolation (default value is 5)
- axes of the reference coordinate system
- Origin of the reference coordinate system

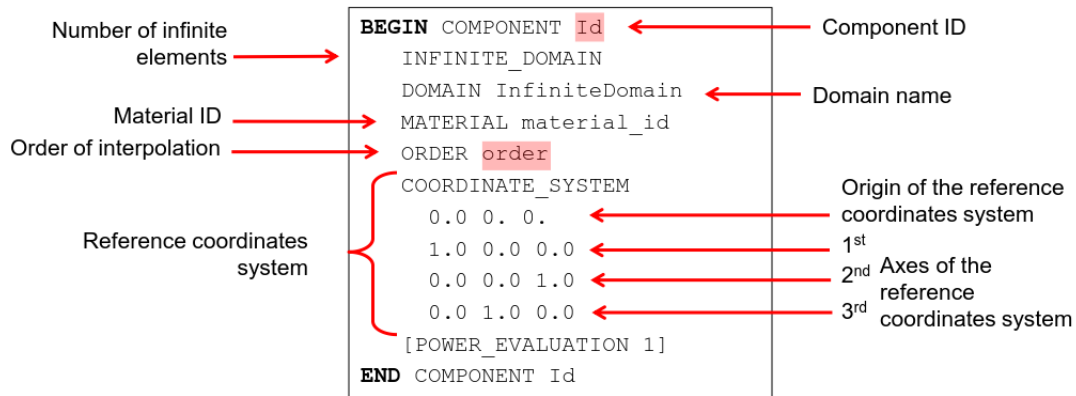


FIGURE 3.9: Actran Syntax of an Infinite Domain Component

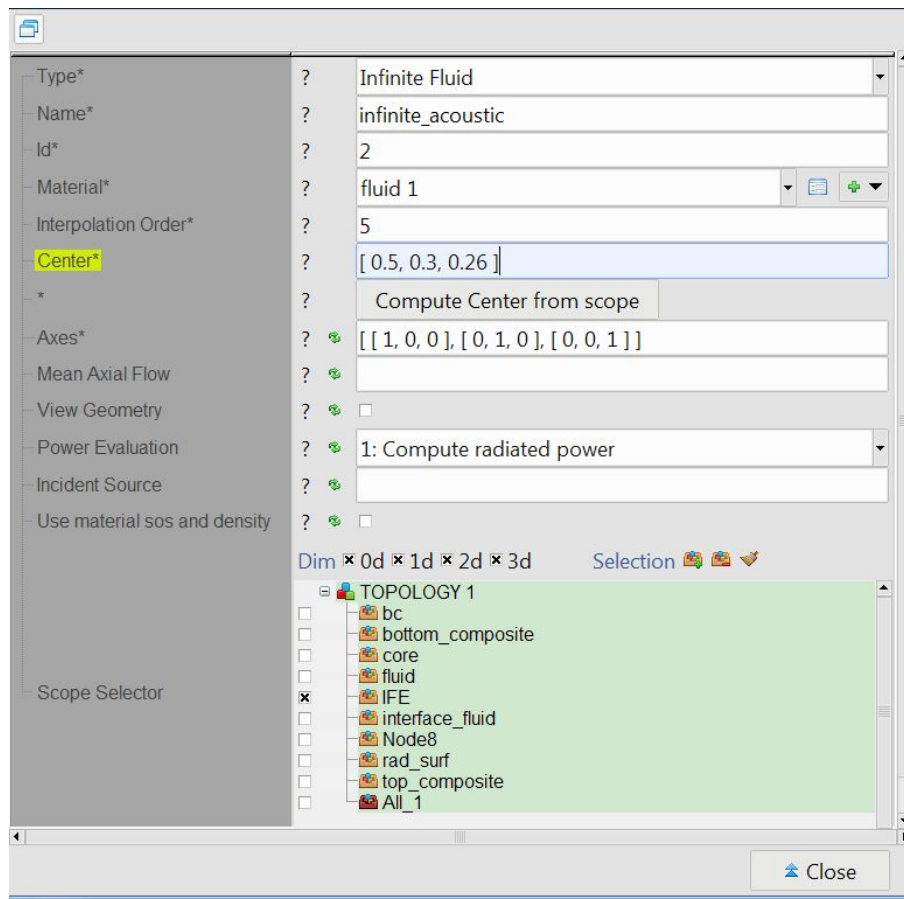


FIGURE 3.10: Infinite fluid component on Actran

An Infinite Fluid COMPONENT is applied to a domain that is made of free faces of finite elements (doesn't have to touch any structural element, see section 3.14 for the error that Actran gives for this action). The unknown variable here is the fluid pressure, so 1 DOF/node on the surface where is applied.

3.4 Structural Components

The plates were created using the internal meshing tool "Structured Mesh", that need the origin coordinates, size and the number of finite element for each direction.

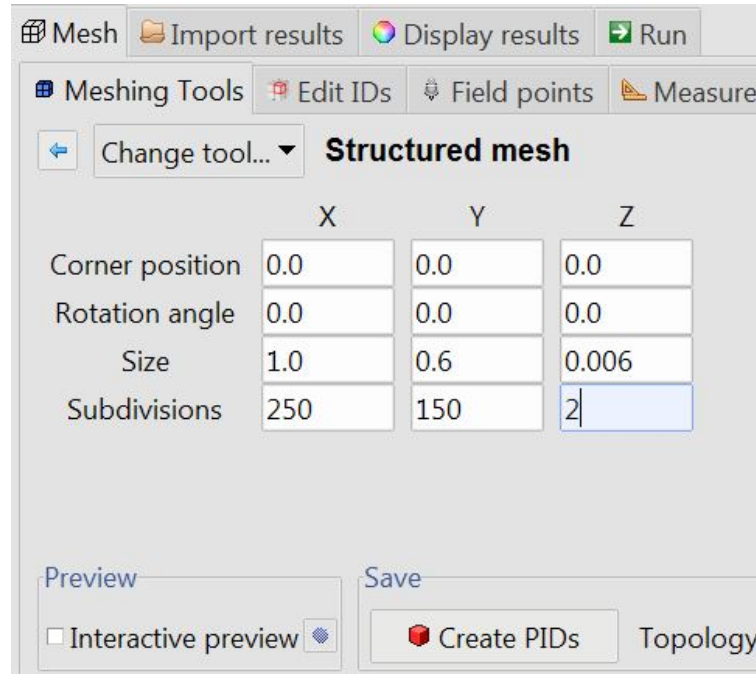


FIGURE 3.11: Example of plate mesh creation using Actran Structured Mesh tool

The 309x206x20mm plate, and the 1000x600 mm Sandwich plate cores had been assigned to a *Solid* component.

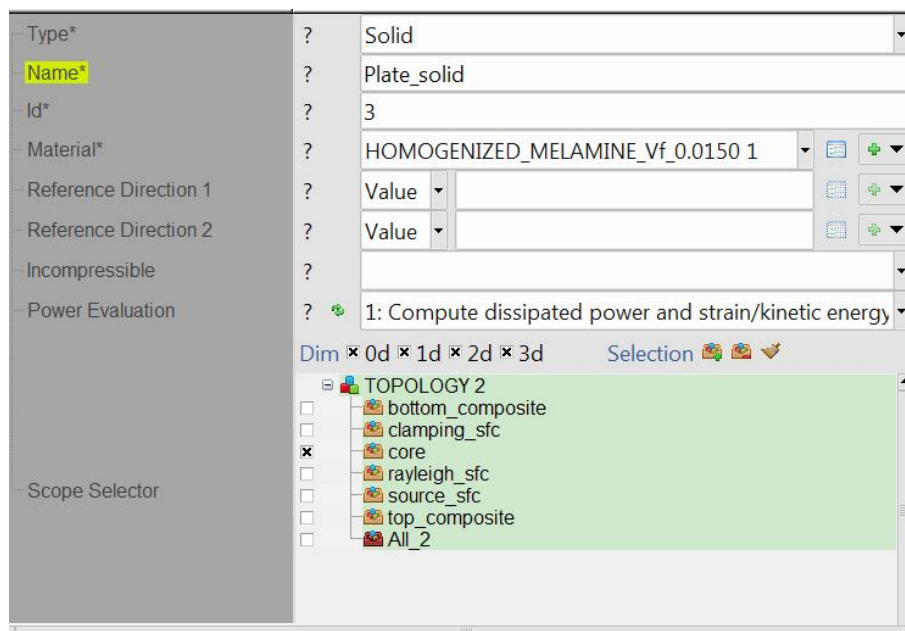


FIGURE 3.12: Solid component in Actran graphical interface

The Sandwich plate skins had be assigned to a *Thin Shell* component, and the material assigned to the Thin Shell component is a composite material.

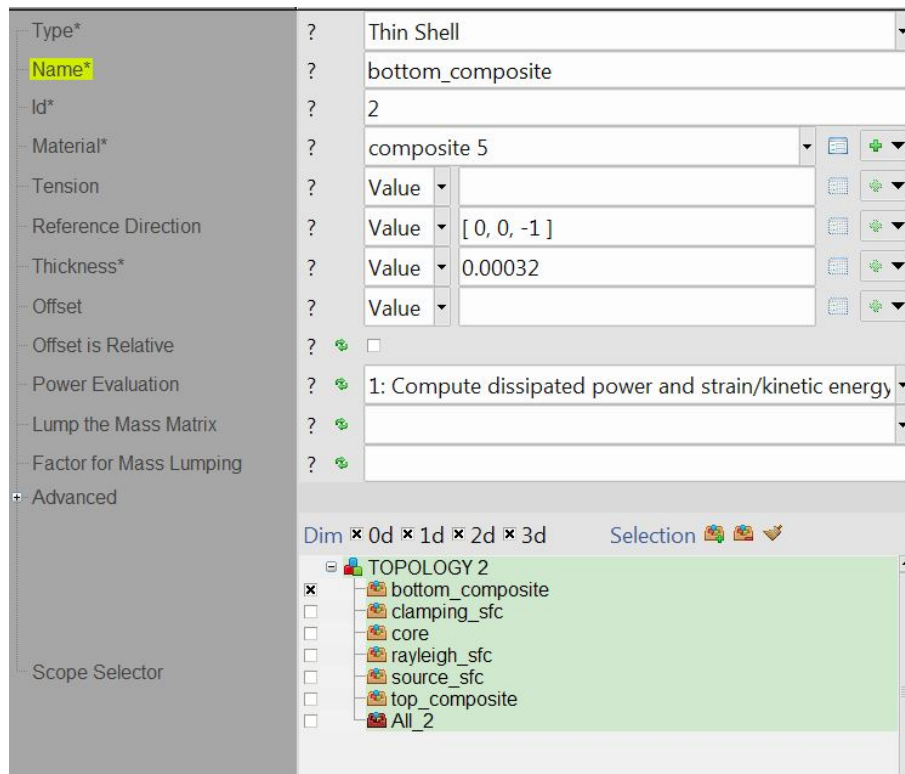


FIGURE 3.13: Thin Shell for composite material in Actran graphical interface

3.5 Incident/Radiating Surface Post-Processing

Fig 3.14 shows the post-processing for Sound Transmission Loss evaluation. Input are frequency at which the results are requested, the incident power of the incident surface (the source itself provide this) and the radiated power of the radiating surface (either a Rayleigh surface or a radiating surface if using a finite fluid component).

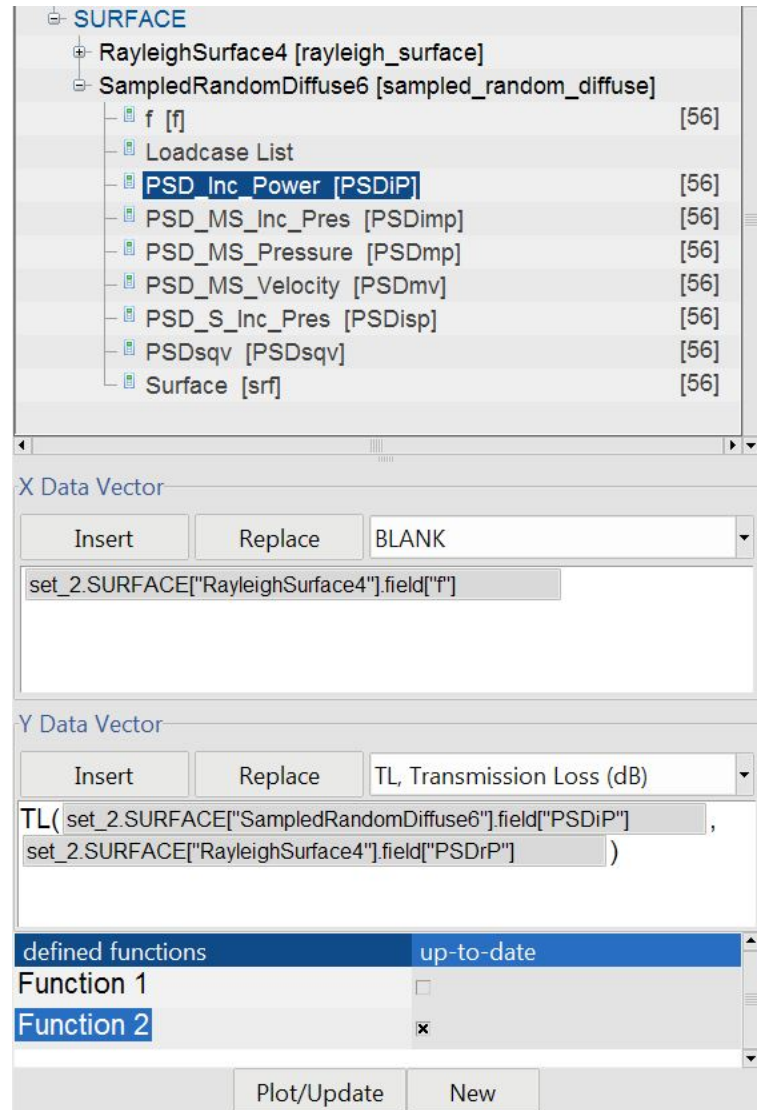


FIGURE 3.14: Sound Transmission Loss Post-processing with PLT Viewer

3.6 Acoustic Sources

There's a variety of available acoustic sources in MSC Actran: from acceleration to different source shape (spherical, planar, cylindrical) and a series of sampled random excitations. Since our purpose is to calculate Sound Transmission Loss of a rectangular panel, and we don't want to model an excitation room, the best choice is a **Sample Random Diffuse Field**.

The Institute of Noise Control Engineering (INCE-USA) proposes the following definition for a diffuse field: *"sound field in which the time average of the mean-square sound pressure is everywhere the same and the flow of acoustic energy in all directions is equally probable"*.

Diffuse fields are produced experimentally by activating strong acoustic sources in a reverberant chamber, the multiple reflections along the boundary walls leading to a "diffuse" field. A diffuse field excitation can be applied to the element faces of a structure or an infinite domain component. It should

be stressed that the standard use of this capability is related to acoustic transmission studies of (baffled) plane (or nearly plane) structures subjected to a diffuse field excitation. The Actran Syntax is as follows:

```
BEGIN DIFFUSE_FIELD diffuse_field_id
  [NAME boundary_condition_name]
  DOMAIN domain_name_list
  SOUND_SPEED speed_of_sound
  FLUID_DENSITY fluid_density
  REFERENCE_PSD reference_psd_value or ...
    TABLE table_id or FIELD field_id
  [MAXIMUM_INCIDENCE angle]
  [SURFACE_FILE filename list_of_PID]
  either
    NUMBER_SAMPLES number_samples
    [RADIUS radius]
    [ORIGIN o1 o2 o3]
    [POLE_DIRECTION d1 d2 d3]
    [NUMBER_PARALLELS number_parallels]
    [MULTISAMPLE_UNIQUE or MULTISAMPLE_ALL
    or MONOSAMPLE]
  or
    nothing
  end either
  [POWER_EVALUATION 0 or 1]
END DIFFUSE_FIELD diffuse_field_id
```

where:

- *boundary_condition_name* is the optional label assigned to the boundary condition.
- *domain_name_list* determines the list of domains (defined in the topology data block) to which the boundary condition is applied. If the domain is also linked to an *INFINITE_DOMAIN*, *APML* or *PML* component, the diffuse sound field must be applied using a planes waves sampling.
- *speed_of_sound* and *fluid_density* correspond to the speed of sound and fluid density of the fluid in which the diffuse field is defined;
- *reference_psd_value* is the value of the reference power spectral density injected (this can be a real value, a reference to a field block or a real frequency table);
- The keyword *maximum_incidence* is used to eliminate grazing incidences of a diffuse sound field. The value angle (in degrees) defines the angle β with respect to the normal, for which the waves are accounted for. By default no incidence is eliminated and $\beta = 180deg$

A sampling strategy is selected through the keyword *NUMBER_SAMPLES*. Two sampling methods are available for a diffused field.

1) The first sampling method is based on a superposition of a large number of plane waves. The presence of the NUMBER_PARALLELS parameter in the data block automatically activates this method. The reference sphere used to support the plane waves can be either automatically generated from the structure dimensions or controlled by the combination of *radius*, *origin* and *pole_direction* parameters. The three previous parameters must be explicitly specified. If one of them is missing, the user's sphere definition is skipped and the automatic process is executed.

- POLE_DIRECTION defines the north pole of the reference sphere. At least one plane wave will be generated along this direction. If the keyword MAXIMUM_INCIDENCE is specified, the POLE_DIRECTION is automatically defined as normal to the loaded surface. If the keyword is not specified, the POLE_DIRECTION is taken normal to the loaded surface.
- ORIGIN defines the center of the reference sphere. When the origin is not specified, it is automatically defined at the geometric center of the loaded structure;
- RADIUS is the radius of the reference sphere. If the keyword is not specified, the radius of the sphere is taken as 50 times the half-dimension of the loaded surface.
- NUMBER_PARALLELS drives the number of generated plane waves. The sphere is divided in slices normally to the pole direction. The thickness of each slice is defined so that the angle intercepting each slice is constant. The surface of each slice is divided in subsurfaces, each carrying a plane wave. The area of each sub-surface is equal to the area of the cap. The plane waves generated can be visualized in ActranVI by loading the file *plane_waves.dat* located in the report directory. In addition, the different samples can be found in the file *loadcase.dat* located in the report directory and be used in an equivalent computation, involving scattering effects for instance.

2) The second sampling method is based on a Cholesky decomposition of the cross PSD matrix. This method is activated when none of the NUMBER_PARALLELS, RADIUS, ORIGIN and POLE_DIRECTION keywords is present in the data block. The method is driven by *number_samples*, which defines the number of realizations that are treated. - In the case of a sampling method, different sampling options are available, controlled by the optional keywords MULTISAMPLE_UNIQUE or MULTISAMPLE_ALL (default) or MONOSAMPLE:

- MULTISAMPLE_UNIQUE initializes the random generator of phases at the first frequency and samples the phases at each frequency;
- MULTISAMPLE_ALL (default) initializes the random generator of phases and samples the phases at each frequency;

- MONOSAMPLE initializes the random generator of phases and samples the phases only once, at the first frequency of computation. This means that the same phases are used over the whole frequency range.

These two parameters of the sampling method can be either defined directly within the DIFFUSE_FIELD data block, either in the related LOADCASE data block. Using the LOADCASE data block allows defining different stochastic excitations or varying the parameters of a single excitation in the same run.

The optional keyword POWER_EVALUATION (default = 0) set to 1 activates the computation of the power injected by the boundary condition.

```
BEGIN DIFFUSE_FIELD 4
REFERENCE_PSD 1
SOUND_SPEED 340
FLUID_DENSITY 1.2
NUMBER_SAMPLES 100
MULTISAMPLE_ALL
DOMAIN diffuse_field
END DIFFUSE_FIELD 4
```

will prompt Actran to excite the structure on domain diffuse_field with a diffuse field of reference PSD amplitude defined by the FIELD 2 using a sampling method based on a Cholesky decomposition. 100 samples will be successively computed.

In the proposed Thesis, 10 Samples had been used, with MULTISAMPLE_ALL method.

3.7 Rayleigh Surface Component

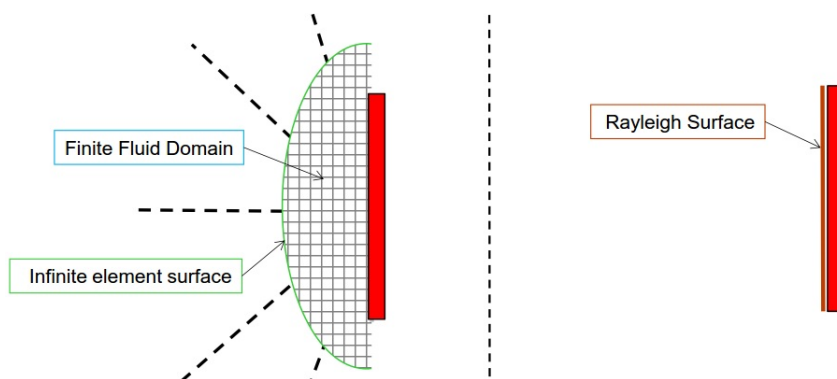


FIGURE 3.15: Example of radiating power surfaces

A **Rayleigh Surface** component is an interface between a plane or a nearly plane baffled structure and a semi infinite acoustic fluid. The sound field in the acoustic fluid is modeled by a Rayleigh integral. The feature can be used to:

- model the effect of a semi infinite fluid on the structure
- compute the power radiated by the structure (except for a time domain analysis)
- compute acoustic results at field points located in the far field (this is only possible with a direct frequency response)

Each node carries one single degree of freedom: the normal displacement u_n , which is aliased on the structural component displacements. The domain supporting the Rayleigh surface should be in contact with a valid structural component:

- shell, dshell or solid in a direct frequency response
- modal elastic in a modal frequency response

This contact can be congruent or incongruent. The coupling in this case should be insured using an interface between the structural component and the Rayleigh surface. A Rayleigh surface cannot be used when:

- it is specified on a modal elastic component in a direct frequency response, unless used through a staggered solver;
- the analysis is 2d or axi-symmetric

The Rayleigh Surface, unfortunately, use more RAM than other components because of the high density of the impedance matrix. In order to calculate the Sound Transmission Loss at higher frequency for a given geometry and material, this component show its limitations, so a new model with fluid volumes for the acoustic room was necessary.

For a sufficient level of accuracy, 8 elements/wavelength are required. Here's an example of the results obtained with a Rayleigh surface valid up to 500 Hz forcedly extended to 1000 Hz, compared with a finite fluid model and a finer mesh valid up to 1000 Hz.

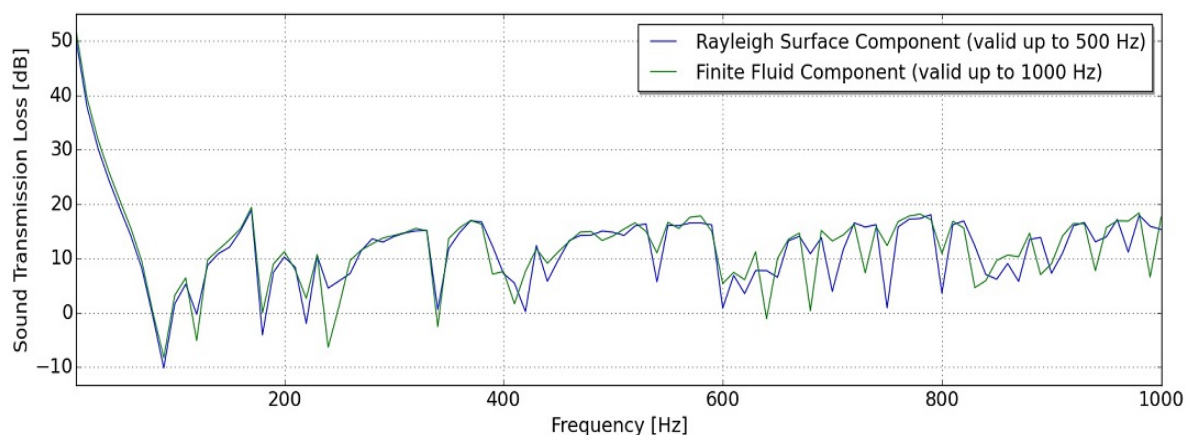


FIGURE 3.16: STL using two different component: Rayleigh surface and Finite fluid volume (sandwich model with nomex core)

The results shows good agreement up to 800 Hz, except for a slightly different resonance peak around 410 Hz. Over 800 Hz a mesh with less than 8 elms/wavelength is no more reliable. Using a Finite fluid component and a more complex model with coupling surfaces and interfaces, about 20 GB of RAM had been requested, against the over 64 GB of Rayleigh(not enough for the current capacity of the available server).

3.8 Acoustical and Structural Wavelength Calculation

This calculation need to comply the minimum requirement of 8 elements for structural or acoustic wavelength, depending on the component to which is applied.

For an acoustic fluid the wavelength depends on its speed of sound c and its density. In order to have a sufficient level of accuracy, if no flow condition is assumed it needs 8 to 10 linear elements per wavelength, or 4 to 6 for quadratic element interpolation.

$$h = \frac{\lambda_{min}}{4} = \frac{c}{4f_{max}} \quad (3.1)$$

for International Standard Air (ISA), $c=340$ m/s, if $f_{max} = 1000$ Hz and choosing for 8 linear elements/wavelength, then

$$h=0.0425\text{m} = 42.5\text{mm}$$

has to be the minimum length of the acoustic mesh elements. We can demonstrate that using Actran internal tool to calculate this value, the result is the same (see Fig.3.17

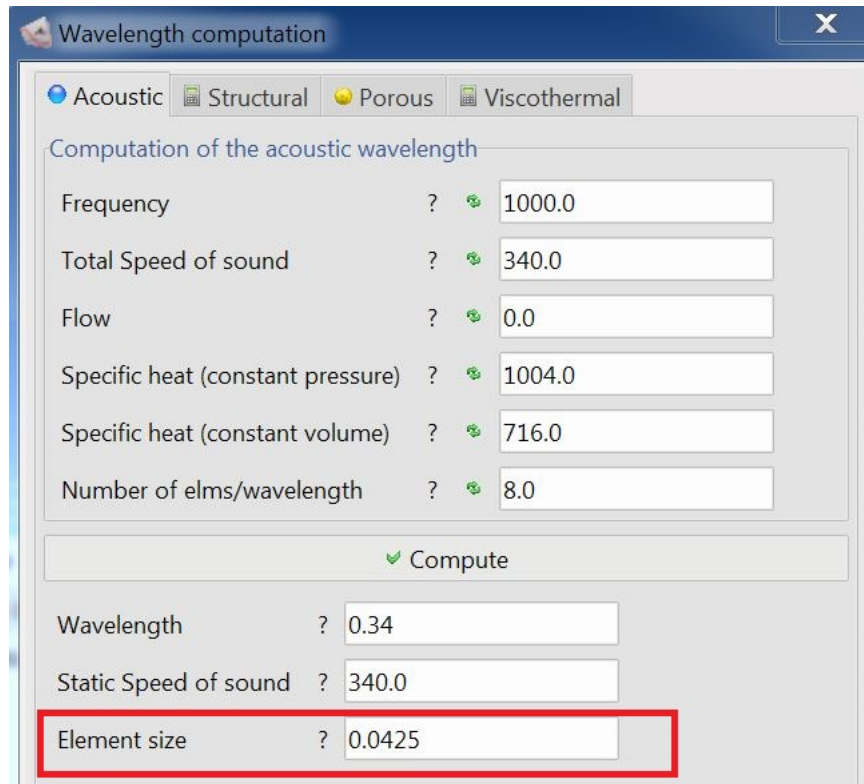


FIGURE 3.17: Wavelength computation for ISA Air at 1000 Hz

For an isotropic solid material:

$$\lambda = \sqrt{\frac{\pi \sqrt{\frac{E}{\rho}} h}{\sqrt{3} f \sqrt{1 - \nu^2}}} \quad (3.2)$$

The Equation (3.2) is used in the internal tool of Actran

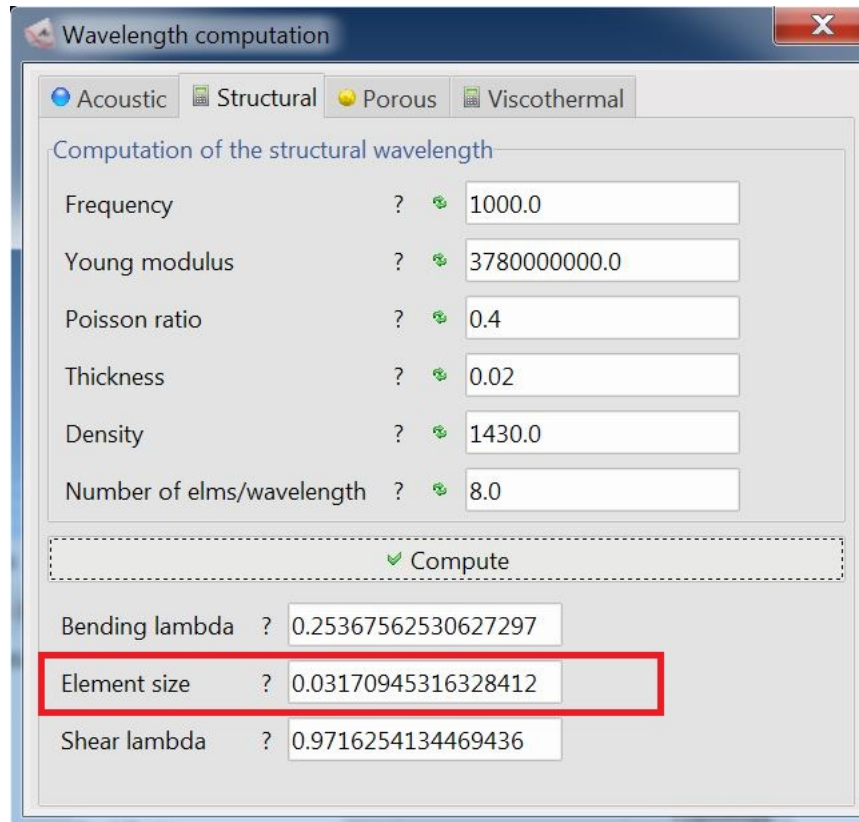


FIGURE 3.18: PVC wavelength computation

For an Orthotropic material, the equation (3.2) is no more reliable, but is based on the minimum wavelength over the 3 directions of **shear waves**:

$$c = \sqrt{\frac{G_{ij}}{2\rho}} \quad (3.3)$$

where

- c is the speed of sound in the considered medium
- G_{ij} is the Shear Modulus over one of the 3 directions

Example: for Nomex, $G_{xy}=100000$ Pa, density = $48 \text{ Kg}/\text{m}^3$ so the speed of sound inside Nomex is equal to **32.275 m**. Using equation 3.1 but with 8 linear structural elements instead of 4 (which is valid for fluid elements), Shear Wave Wavelength at a frequency of 1000 Hz is equal to:

$$h = \frac{\lambda_{min}}{8} = \frac{c_{nomex}}{8f_{max}} = 4.034mm \quad (3.4)$$

3.9 Boundary Conditions

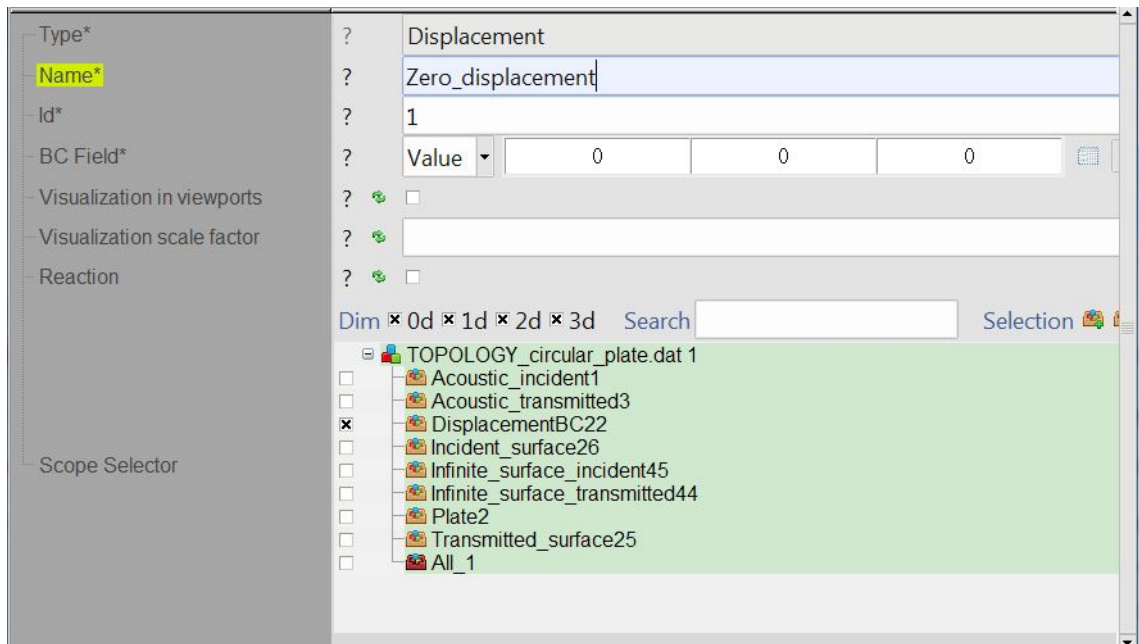


FIGURE 3.19: Boundary condition assignment

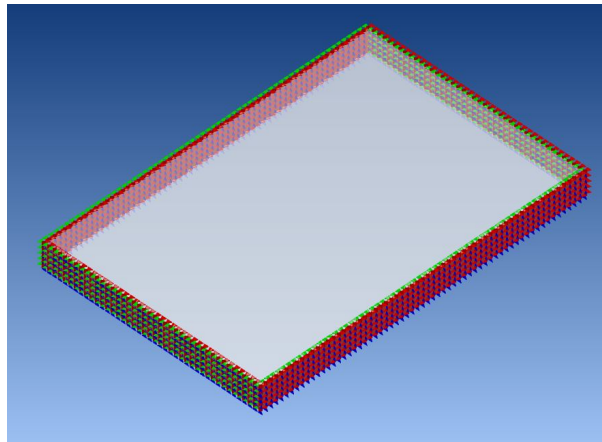


FIGURE 3.20: Lateral surfaces of the plate to which boundary conditions are applied

3.10 Input Frequency-Dependent Metamaterials in MSC Actran

TABLE data blocks defines tables of frequency (or time) dependent quantities. Using a table data block we can implement a frequency-dependent material in terms of 9 mechanical properties, each for real and imaginary part.

The syntax of each table is as follows:

```
for each table
  BEGIN TABLE table_id
    [NAME table_name]
    [none or OCTAVE or THIRD_OCTAVE]
    [BAND_NORMALIZATION 0 or 1]
    [REF_DB ref_pres]
    [CONVENTION LINEAR or QUADRATIC]
    [THERMAL_TRANSLATION real translation_factor]
    either
      table_type, table_size
      for each table entry
        real frequency, complex data_value
      end for
    or
      FILE external_file
      FORMAT TXT or CSV
      table_type, table_size
    END TABLE table_id
end for
```

FIGURE 3.21: TABLE data block syntax

where:

- table name is the optional label assigned to the table
- table type defines the type of interpolation when the frequency of computation is not listed in the table (see below). The table type can be:
 - * table type is 1: Frequency table using Real-Imaginary interpolation between the frequencies: it is the only one used in this work
 - * table type is -1: Frequency table using Amplitude-Phase interpolation between the frequencies
 - * table type is 2: Time table using Real-Imaginary interpolation between the time steps
 - * table type is -2: Time table using Amplitude-Phase interpolation between the time steps
 - * table type is 3: Frequency table using constant frequency bands interpolation
 - * table type is 4: WLF table no interpolating between the orders, for missing orders the value of the superior order is taken

For a full explanation of Table syntax see page 587 of [19].

When performing a computation for frequency, time or order value that is not in the table, Actran will use:

- * The first value of the table if the frequency or time is lower than all the table entries;
- * The last value of the table if the frequency or time is higher than all the table entries;
- * A linear interpolation between the two closest table entries in other cases if the table type is not 3. The interpolation will be performed on Real-Imaginary parts for table of type 1 and 2, and on Amplitude- Phase parts for table of type -1 and -2.
- * For a table type of type 3, the value is assumed constant within the provided octave (or third octave) band. By default, it will be constant in the octave bands, and is activated for each individual third octave band if the keyword THIRD OCTAVE is selected. If no value is provided in the current band, the value is set to 0. If several values are provided for a unique band, the last one is used.
- * For a WLF table, the value of the superior order is taken in case of missing orders.
- * table size is the number of records;
- * The values of the table can either be provided directly within the input file or referred to from an external txt or csv file. The different values must be provided in increasing order of frequency or time.

Here's an example:

```

BEGIN TABLE 1
NAME E11
1 15
0 {1540461.586 0}
5 {1553673.228 1948.219}
10 {1557043.139 2428.2201}
20 {1561252.456 3018.3503}
35 {1565397.021 3589.2324}
50 {1568446.271 4002.8831}
60 {1570141.369 4230.5113}
80 {1573019.081 4613.1912}
100 {1575434.14 4930.6981}
120 {1577533.688 5204.068}
196 {1583797.098 6004.8644}
272 {1588524.634 6594.9271}
348 {1592394.198 7068.7756}
424 {1595703.983 7467.6574}
500 {1598615.547 7813.648}
END TABLE 1
BEGIN TABLE 2
.....
END TABLE 9

```

TABLE 3.1: Table data block example for a frequency dependent material

NOTE: inside the parenthesis the first values are the real part.

An important consideration on the possibility of analyze the Transmission Loss at frequencies not included in the table data blocks. In this case Actran will perform a linear interpolation of the table entries between the two closest frequencies. This could be acceptable when the variation of the frequency-dependent properties is smooth, as is shown in figure 3.22.

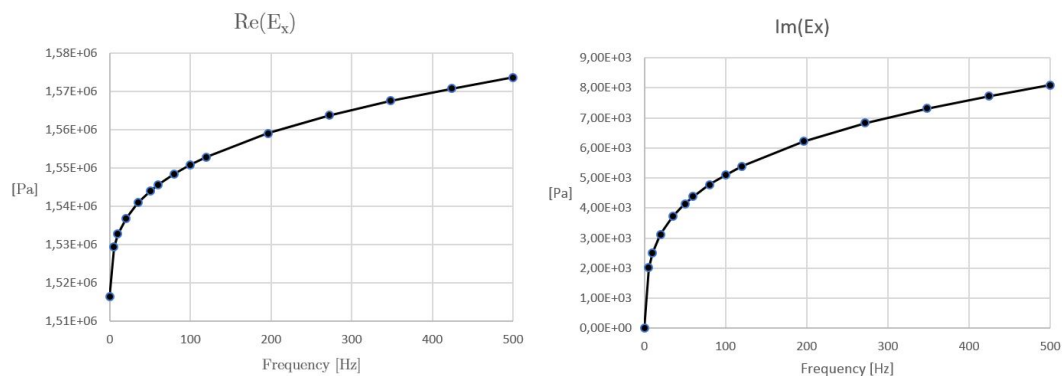


FIGURE 3.22: Example of frequency dependent properties (Homogenized Melamine foam with Aluminum inclusions at 1.95% volume fraction)

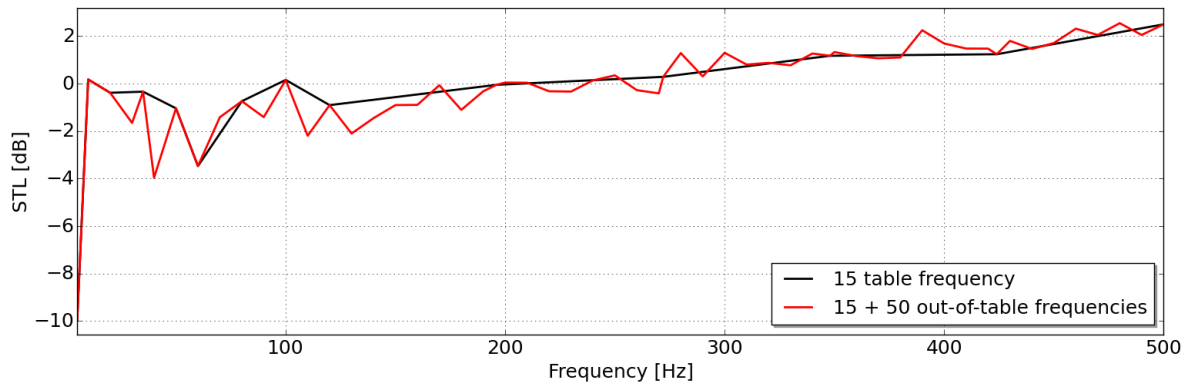


FIGURE 3.23: Effect of Actran linear interpolation of material properties at frequencies out of table data block: Example of a plate in Homogenized Melamine foam with $V_f=0.0195$ Aluminum inclusions

3.11 Orthotropic material implementation

The Material data block "Orthotropic solid" allows to specify a material with mechanical properties that are different along the directions of each of the axes. The syntax is the following:

```

BEGIN MATERIAL material_id
NAME material name
ORTHOTROPIC_SOLID
SOLID_DENSITY solid_density or TABLE table_id or FIELD field_id
YOUNG_1 young_1 or TABLE table_id
YOUNG_2 young_2 or TABLE table_id
YOUNG_3 young_3 or TABLE table_id
POISSON_12 poisson_12 or TABLE table_id
POISSON_13 poisson_13 or TABLE table_id
POISSON_23 poisson_23 or TABLE table_id
...
END MATERIAL material_id

```

where "*id*" are integers. For example:

```
BEGIN MATERIAL 1
NAME HOMOGENIZED_MELAMINE_Vf_0.03
ORTHOTROPIC_SOLID
YOUNG_1 TABLE 1
YOUNG_2 TABLE 2
YOUNG_3 TABLE 3
POISSON_12 TABLE 7
POISSON_13 TABLE 8
POISSON_23 TABLE 9
SHEAR_12 TABLE 4
SHEAR_13 TABLE 5
SHEAR_23 TABLE 6
SOLID_DENSITY { 88.76, 0}
END MATERIAL 1
```

TABLE 3.2: Orthotropic solid data block syntax for an anisotropic material

3.12 Evaluation of Modal Frequencies

Modal Extraction Analysis computes the modes of an uncoupled and closed acoustic or undamped structural model. The procedure consists in solving the eigenvalue problem:

$$K = \omega^2 M \quad (3.5)$$

with K the stiffness matrix and M the mass matrix. Both matrices are real symmetric, and M is positive-definite. The eigenvectors are scaled so that their M norms are equal to one (unit modal mass). Modal extraction works only for real problems (never damped ones). The problem is purely acoustic or purely structural. For coupled systems, frequency response analysis should rather be used.

Modal Extraction Analysis need a frequency range definition to work properly.

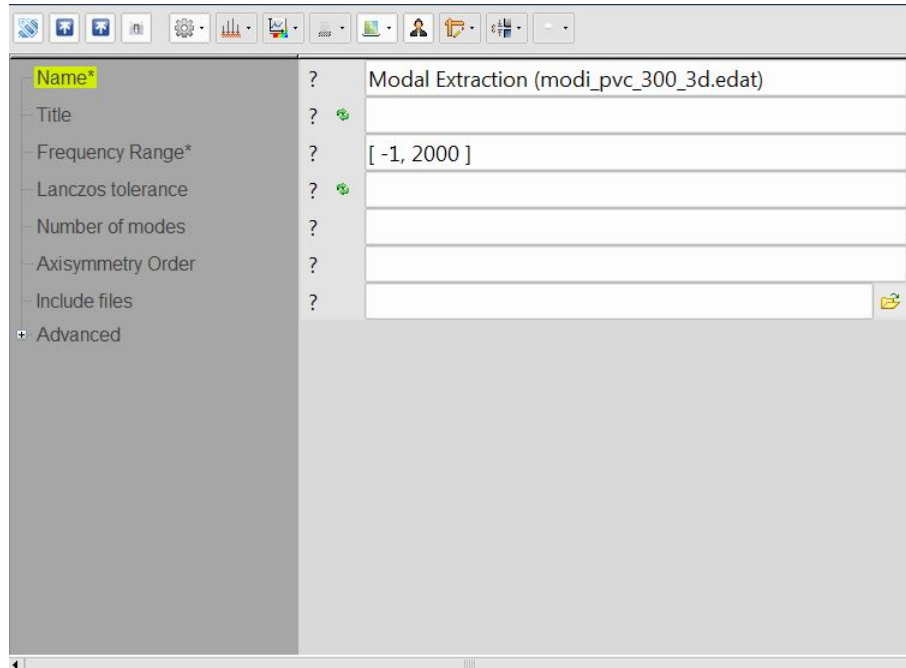


FIGURE 3.24: Example of User Interface of Modal Extraction Analysis

The output results are contained in a .plt file, as in figure below:

```

1 BEGIN LOADCASE_INDEX
2   1 0
3 END LOADCASE_INDEX
4 BEGIN OUTPUT_FRF
5 BEGIN TITLE
6 Actran Analysis
7 END TITLE
8 BEGIN DOMAIN Solid1 "solid"
9   /*      NFreq      NLdCase
10  |      |
11  |      19          1
12  /*      Freq
13  1.7133543380534e-04
14  2.1545392308793e-04
15  2.7587625269936e-04
16  3.4298551385348e-04
17  3.4475216643779e-04
18  4.8277552890410e-04
19  2.8387655785868e+02
20  3.0500558622961e+02
21  6.4601898314547e+02
22  7.1863275155946e+02
23  7.9275420884048e+02
24  9.6159418645421e+02
25  1.1726996203893e+03
26  1.3385830045478e+03
27  1.6520045818897e+03
28  1.7137743599369e+03
29  1.8086256498948e+03
30  1.9573485340772e+03
31  1.9786489882467e+03
32 END DOMAIN Solid1
33 END OUTPUT_FRF

```

FIGURE 3.25: Example of Results from Modal Extraction Analysis

Here the first 6 results are too small to be considered. This happens when selecting "-1" in the frequency range, as suggested in the dedicated Actran Workshop "Plate Modal Extraction".

3.13 Evaluation of Sound Transmission Loss with MSC Actran

Sound Transmission Loss, as already explained in dedicated chapter, had been evaluated by Actran and plotted with *PltViewer* from the Acoustic Incident and Transmitted power.

PltViewer is an internal Actran tool and it is used to plot the results with *.plt or *.txt extension. The Incident power is evaluated by the diffuse sound field source while the Transmitted power is contained either in a Rayleigh surface component or in a Radiating Surface. Rayleigh surface had been used for the majority of the time, because of its simple implementation, while for the last sandwich plate (named Sample B) a new model with finite fluid volume and interfaces with structural elements, leading to a lower memory consumption and a higher frequency limit.

3.14 Troubleshooting of Errors encountered

THE COUPLING_SURFACE 1 AND 2 HAVE A COMPATIBLE INTERFACE AND CAN THEREFORE NOT BE REFERENCED IN THE INTERFACE 1 BLOCK.

This error means that apparently we are using a compatible interface (node-to-node sharing) and then it is not necessary an interface component. This error was given using a mesh configuration as below:

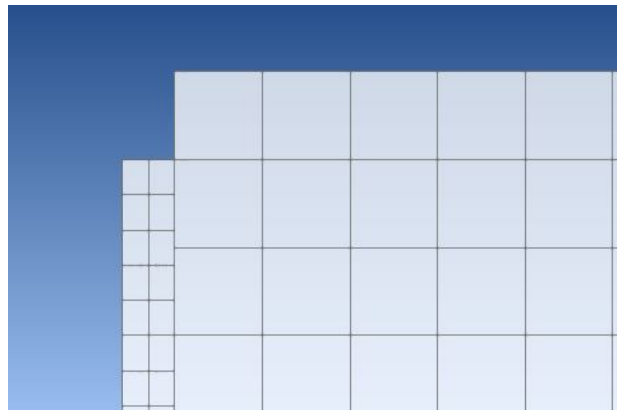


FIGURE 3.26: Example of semi-compatible mesh

As you can see, only some nodes are shared. This is called a semi-compatible mesh, and had been recognized by Actran during its execution as a compatible mesh. Thanks to the help of FFT Support Team I have solved this problem by using an incompatible mesh with a void gap as in Figure 3.27 and 3.6.

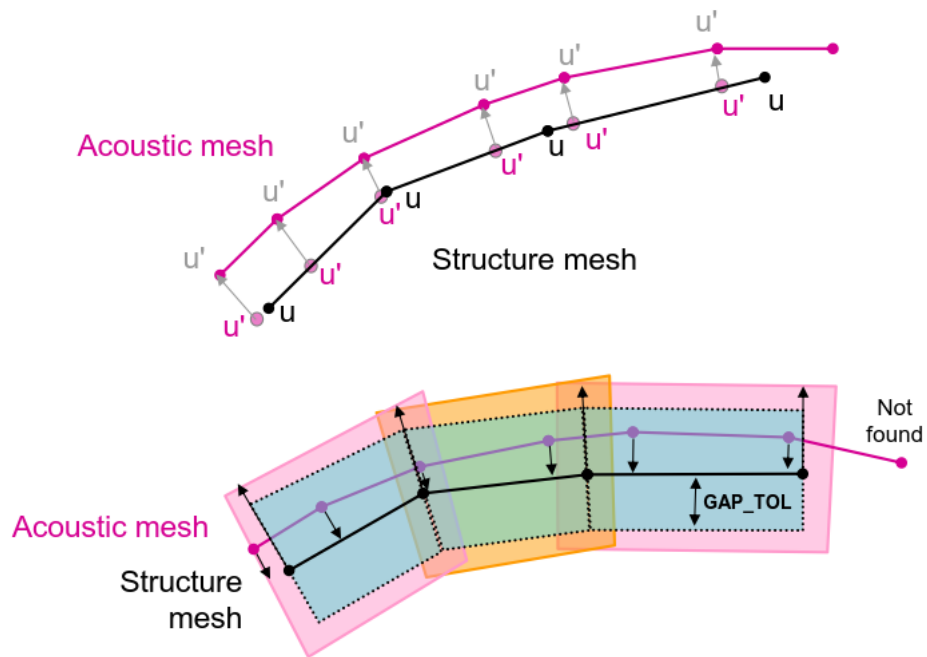


FIGURE 3.27: An Interface of acoustic and structural mesh

INFINITE SURFACE ERROR:

It's important to do not connect any structural component (solids, shells) to an infinite fluid component, otherwise the analysis could not be executed, or the output radiated power will be zero. Only fluids component can touch this component.

Chapter 4

MATLAB Script to Interface MUL2-UC with ACTRAN

An homogenization process has to be made because the Finite Element Method would have been too computationally expensive due to the geometrical shape and the number of inclusions.

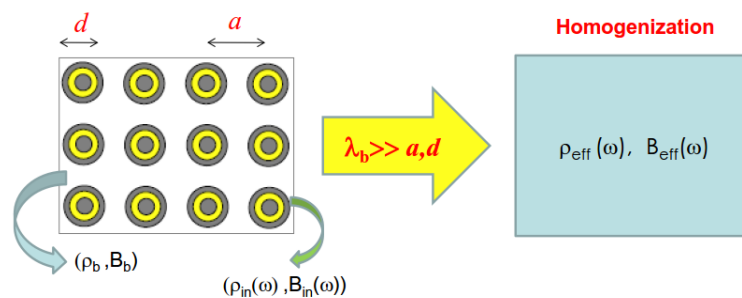


FIGURE 4.1: Sketch of a plate with inclusions and the equivalent homogenized one [20]

This method is based on higher-order Layer-Wise beam theories in the framework of Carrera Unified Formulation (CUF)[1] that is more accurate than classical 2D theories and less expensive than 3D solid finite elements. It is able to homogenize the material by only knowing the unit cell geometry and the material properties of its components. The method lays on the Mechanics of Structure Genome (MSG) which is identical to the concept of Unit Cells as the smaller mathematical building block of the structure. MSG is also based on the Variational Asymptotic Method (VAM) to minimize the loss of information between the heterogeneous cell and the equivalent homogeneous body.

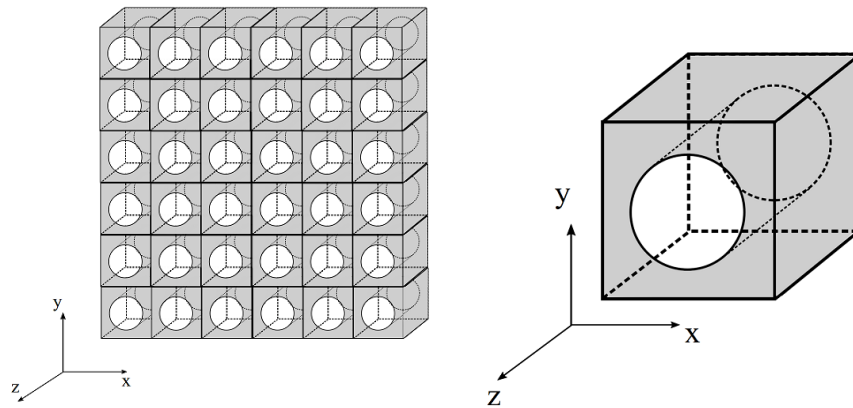


FIGURE 4.2: Example of double array of unit cell with cylindrical inclusion

The material homogenization of periodically heterogeneous composites material was achieved using a MUL2-UC Micro-mechanics code (see [2]) beam modeling for UC (Unit Cell). MATLAB script has been created ad-hoc in order to interface the big amount of data to be homogenized (for each frequency, Real part and Imaginary part separately calculated). For each Volume Fraction, the iterations are 28 (2x14 frequencies calculated by [17]) that, multiplied by 18 Volume fractions (from 0.0045 to 0.03) are 504 iterations! This could have caused potential typing errors, together with useless waste of time.

For this reason, an interface between original data of raw materials and the resultant homogenized material in the exact Actran syntax was mandatory. The timings of each iteration was approximately 0.5s. This period is the forced pause between each iteration, to avoid read and write errors on the .dat files. For 504 iterations the total computational was about 252 s.

This interface script has been written in Matlab 2017b, and it's composed of four main parts:

1. read a DATA.DAT file with this syntax:

```

FREQUENCY1
Re( $E_x$ ) [Pa]
Im( $E_x$ ) [Pa]
Re( $E_y$ ) [Pa]
Im( $E_y$ ) [Pa]
Re( $E_z$ ) [Pa]
Im( $E_z$ ) [Pa]
Re( $G_{xy}$ ) [Pa]
Im( $G_{xy}$ ) [Pa]
Re( $G_{xz}$ ) [Pa]
Im( $G_{xz}$ ) [Pa]
Re( $G_{yz}$ ) [Pa]
Im( $G_{yz}$ ) [Pa]
 $\nu_{xy}$ 
 $\nu_{xz}$ 
 $\nu_{yz}$ 
FREQUENCY2
....

```

TABLE 4.1: Example of input data containing frequency-dependent mechanical properties

2. For every Volume fraction, and for every frequency: the code runs MUL2-UC for Real and Imaginary part (in 2 different runs) of mechanical properties of fiber (Aluminum) and matrix (raw Melamine Foam from experimental results [16][17])
 - A square pack unit cell model corresponds to the typical square pack illustrated in Figure 4.3. The dimensions of the Unit Cell are $1 \times 1 \times 1$ and the volume fiber is introduced by the user during the analysis. Due to the unidirectional arrangement of the constituents, only one section is enough to represent the micro-structure. The curvature of the fiber section is directly mapped into the cross-section of the model, enabling to use only one domain for the fiber, being a total of 5 the number of sub-domains employed for the cross-section expansion.[2]
 - Once selected the cell geometry, material properties of fiber and matrix are requested.
 - Volume Fraction input (relative to the fiber).
 - Last step needed is the polynomial order of expansions: since this analysis is relatively fast (approx 0.3 s), maximum value (8th order) is selected.

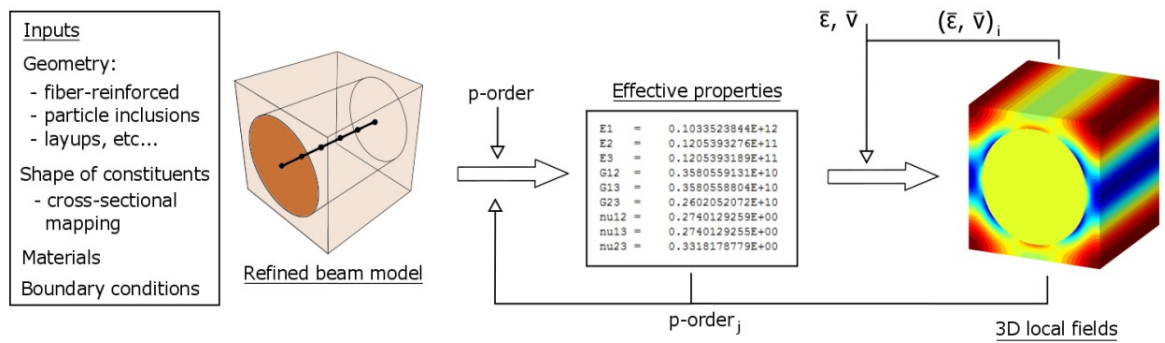


FIGURE 4.3: Micro-mechanics analysis using MUL2-UC [2]

```

Mul2, Politecnico di Torino

Welcome to MUL2-UC!

The micromechanics tool for the beam modeling of
composite materials

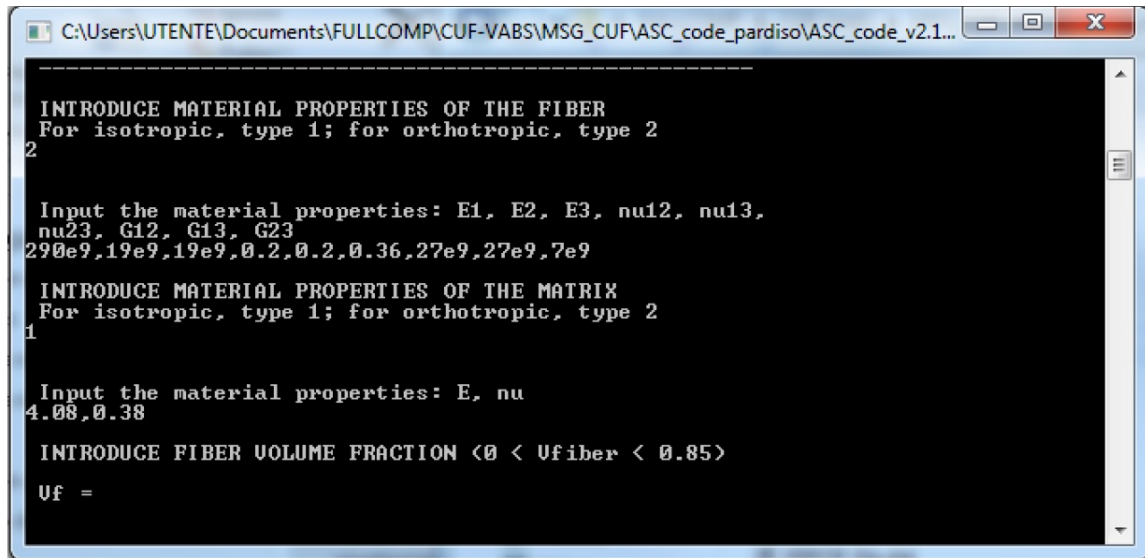
-----

Please, introduce the microstructure type:

- square-pack = 1
- hexagonal-pack = 2
- rectangular inclusion = 3
- cylindrical inclusion = 4

* For free modeling, introduce 5 (input files required).
2
  
```

FIGURE 4.4: Initializing MUL2-UC [2]



```

C:\Users\UTENTE\Documents\FULLCOMP\CUF-VABS\MSG_CUF\ASC_code_pardiso\ASC_code_v2.1...
-----
INTRODUCE MATERIAL PROPERTIES OF THE FIBER
For isotropic, type 1; for orthotropic, type 2
2

Input the material properties: E1, E2, E3, nu12, nu13,
nu23, G12, G13, G23
2.90e9, 1.9e9, 1.9e9, 0.2, 0.2, 0.36, 2.7e9, 2.7e9, 7e9

INTRODUCE MATERIAL PROPERTIES OF THE MATRIX
For isotropic, type 1; for orthotropic, type 2
1

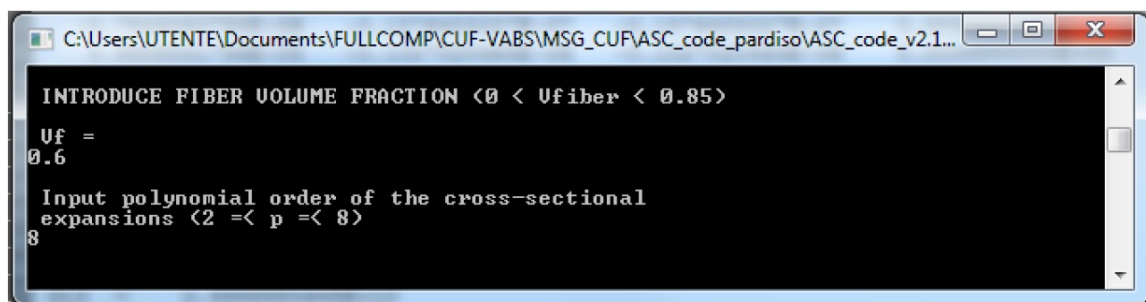
Input the material properties: E, nu
4.08, 0.38

INTRODUCE FIBER VOLUME FRACTION (0 < Ufiber < 0.85)

Uf =

```

FIGURE 4.5: Introducing the material properties [2]



```

C:\Users\UTENTE\Documents\FULLCOMP\CUF-VABS\MSG_CUF\ASC_code_pardiso\ASC_code_v2.1...
-----
INTRODUCE FIBER VOLUME FRACTION (0 < Ufiber < 0.85)

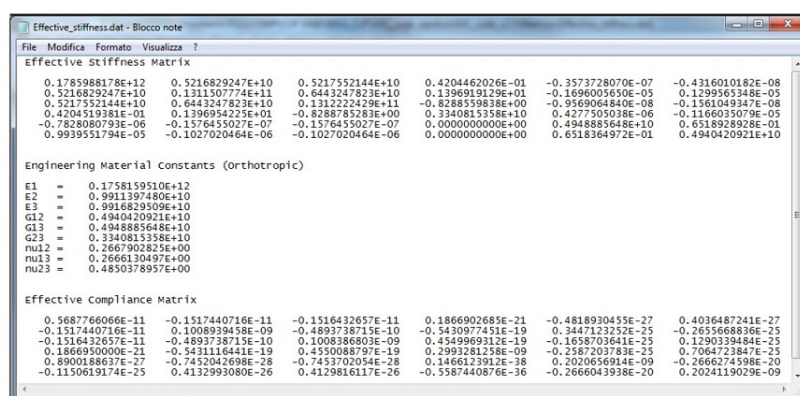
Uf =
0.6

Input polynomial order of the cross-sectional
expansions (2 =< p =< 8)
8

```

FIGURE 4.6: Geometry and polynomial order of the HLE [2]

3. Reading the Effective Mechanical properties (Real or Imaginary part) of the homogenized material resulting after the computation.



```

Effective_stiffness.dat - Blocco note
File Modifica Formato Visualizza ?
Effective Stiffness Matrix
0.1785988178e+12 0.5216829247e+10 0.5217552144e+10 0.4204462026e-01 -0.3573728070e-07 -0.4316010182e-08
0.5216829247e+10 0.1311507774e+11 0.6443247823e+10 0.1386919129e+01 -0.1696005830e-05 0.1229565348e-05
0.5217552144e+10 0.6443247823e+10 0.1312222429e+11 -0.8288559838e+00 -0.9569064840e-08 -0.1561049347e-08
0.4204462026e-01 0.1386919129e+01 -0.8288559838e+00 0.3340815358e+10 0.4277505038e-06 -0.1166035079e-05
-0.3573728070e-07 -0.1696005830e-05 -0.9569064840e-08 0.3340815358e+10 0.4277505038e-06 -0.1166035079e-05
-0.4316010182e-08 -0.1229565348e-05 -0.1561049347e-08 -0.1166035079e-05 0.4277505038e-06 -0.1166035079e-05
0.9939551794e-05 -0.1027020464e-06 -0.1027020464e-06 0.0000000000e+00 0.6518364972e-01 0.4940420921e+10

Engineering Material Constants (Orthotropic)
E1 = 0.1758159510e+12
E2 = 0.9911397480e+10
E3 = 0.9916829509e+10
G12 = 0.4940420921e+10
G13 = 0.4948885648e+10
G23 = 0.3340815358e+10
nu12 = 0.2667902825e+00
nu13 = 0.2666130497e+00
nu23 = 0.4890378957e+00

Effective Compliance Matrix
0.5687766066e-11 -0.1517440716e-11 -0.1516432657e-11 0.1866902685e-21 -0.4818930455e-27 0.4036487241e-27
-0.1517440716e-11 0.1008939458e-09 -0.4893738715e-10 -0.5430977451e-19 0.3447123252e-25 -0.265566836e-25
-0.1516432657e-11 -0.4893738715e-10 0.1008386803e-09 0.4549969312e-19 -0.1638703641e-25 0.1290339484e-25
0.1866902685e-21 -0.5430977451e-19 0.4549969312e-19 0.2993281238e-09 -0.2587203783e-25 0.7064723847e-25
0.8900188637e-27 -0.7452042698e-28 -0.7453702054e-28 0.1466123912e-38 0.2020656914e-09 -0.2666274598e-20
-0.1150619174e-25 0.4132993080e-26 0.4129816117e-26 -0.5587440876e-36 -0.2666043938e-20 0.2024119029e-09

```

FIGURE 4.7: File generated by MUL2-UC with the constitutive information [2]

4. Creation of a Table data block compatible with Actran syntax (see Table 4.1).

Chapter 5

Choice of the Metamaterial

Metamaterials for aeronautical uses should have:

- excellent sound-transmission loss properties in the widest range possible
- light
- fire-repellent according to aviation standards
- good stiffness and compressive strength
- easy to manufacture
- already produced in sufficiently large scale for cost effectiveness

Poro-elastic materials (Polyurethane, Polyamide or Melamine Foam have good fire repellent properties) have good acoustic properties in the high-frequency domain, together with aluminum cylinders (chosen for their good stiffness and lightness) in order to increase the damping properties in the low-frequency range.

5.1 Melamine foam

Melamine foam is a flexible, open-cell foam made material consisting of formaldehyde-melamine-sodium bi-sulfite copolymer melamine. It has a three-dimensional network structure consisting of slender and thus easily flexed filaments.

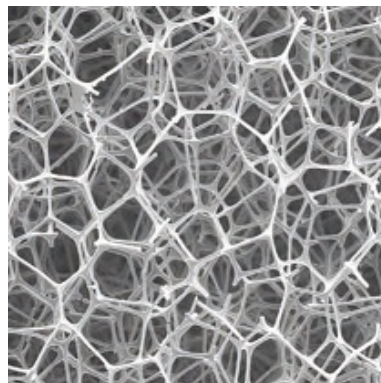
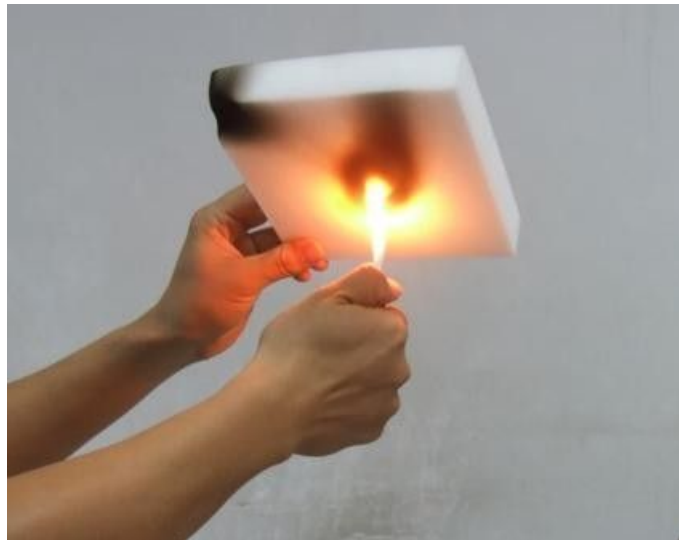


FIGURE 5.1: Melamine foam structure

A supplier is BASF with Basotect[®] and it is used, for example, as sound absorber or thermal insulation in buildings, cars and trains.



- Flame resistance (without the addition of flame retardants)
- Application temperature up to 240°C
- Constant physical properties over a wide temperature range



Furthermore, resulting from the open-cell foam structure:

- High sound absorption capacity
- Low weight
- Good thermal insulation properties
- Flexibility at very low temperature

Basotect[®] in construction and industrial applications

Its high sound absorption capacity and safe fire characteristics make Basotect[®] G, G+ and UF ideal for use as sound absorption in buildings. Decoratively designed acoustic panels, suspended baffles and metal ceiling panels backed with Basotect[®] significantly and measurably improve the acoustics. In industrial applications such as solar collectors or heating systems, Basotect[®] can serve as thermal insulation

due to its heat resistance while maintaining good thermal insulation properties.

Basotect[®] can ideally fulfill the rising demand for soundproofing in the field of transportation. Thanks to its good sound absorption, very low weight and high heat resistance Basotect[®] offers a wide variety of applications ranging from automotive construction to aerospace.

Melamine foam properties have been evaluated experimentally by Jaouen [16] and adapted for our purposes by [31] using the method proposed by Cuenca [17].

Aluminum was chosen for its relatively high Young Modulus-Specific weight ratio, which could lead to good acoustical properties accordingly with the mass-frequency law, complying with the weight constraints.

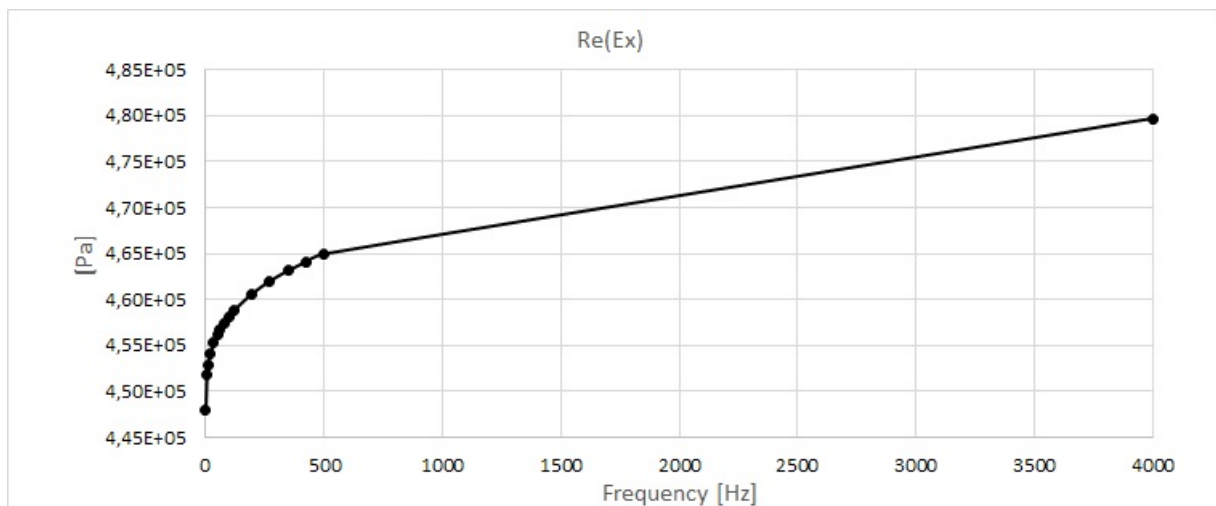


FIGURE 5.2: Melamine Foam Properties: $Re(E_x)$

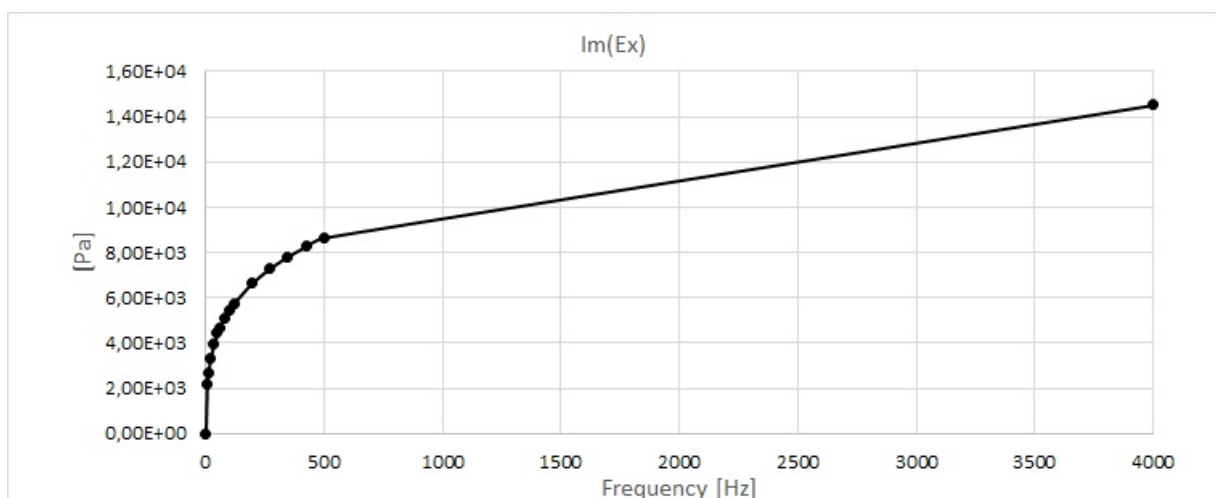
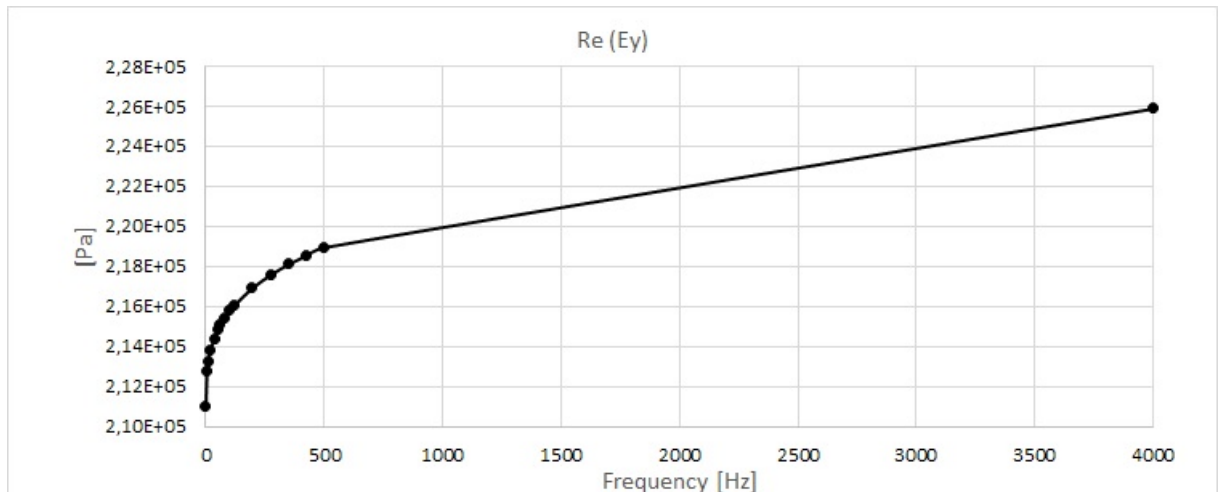
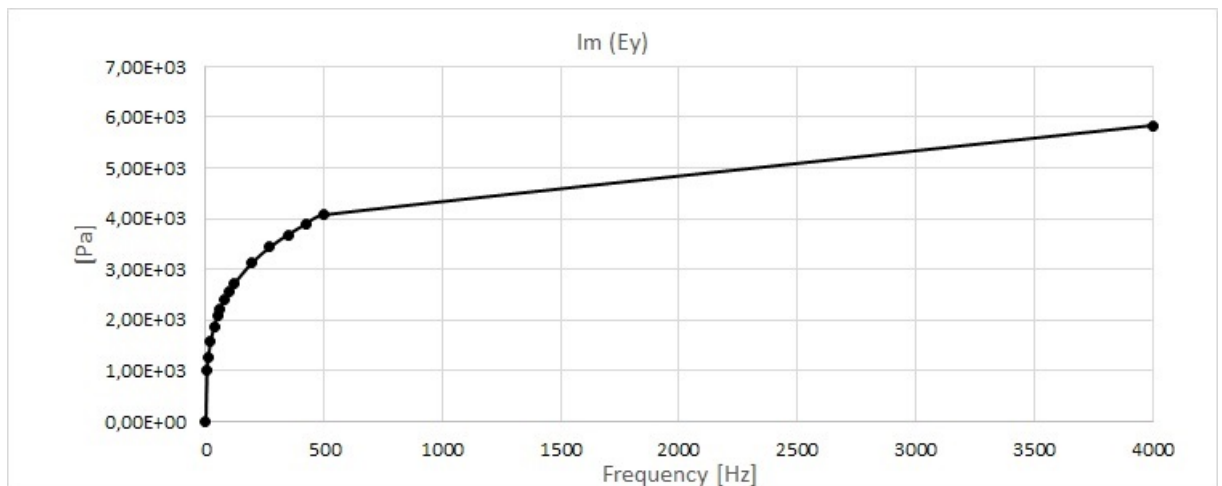
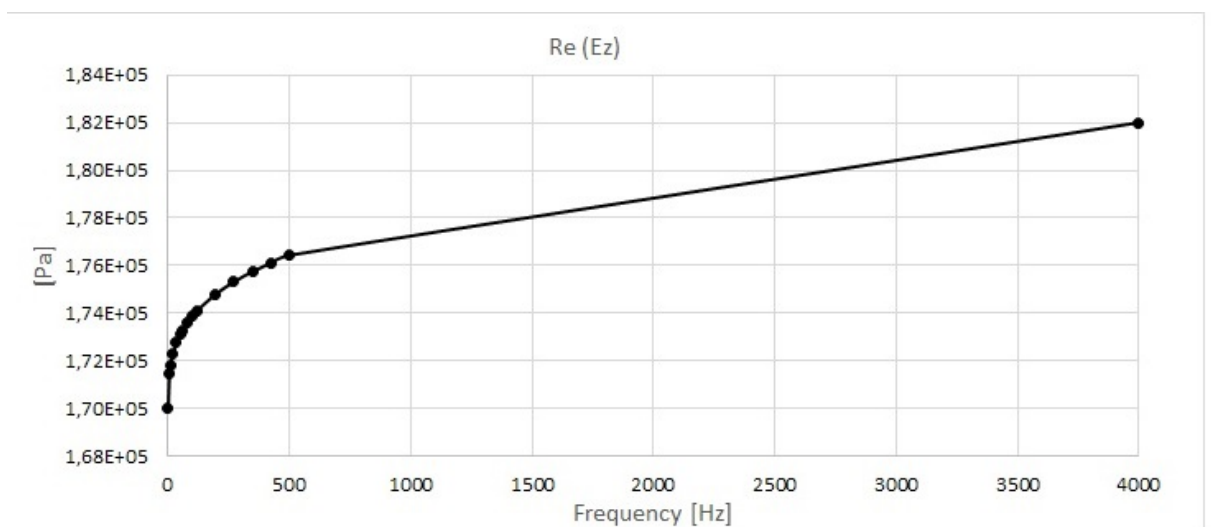
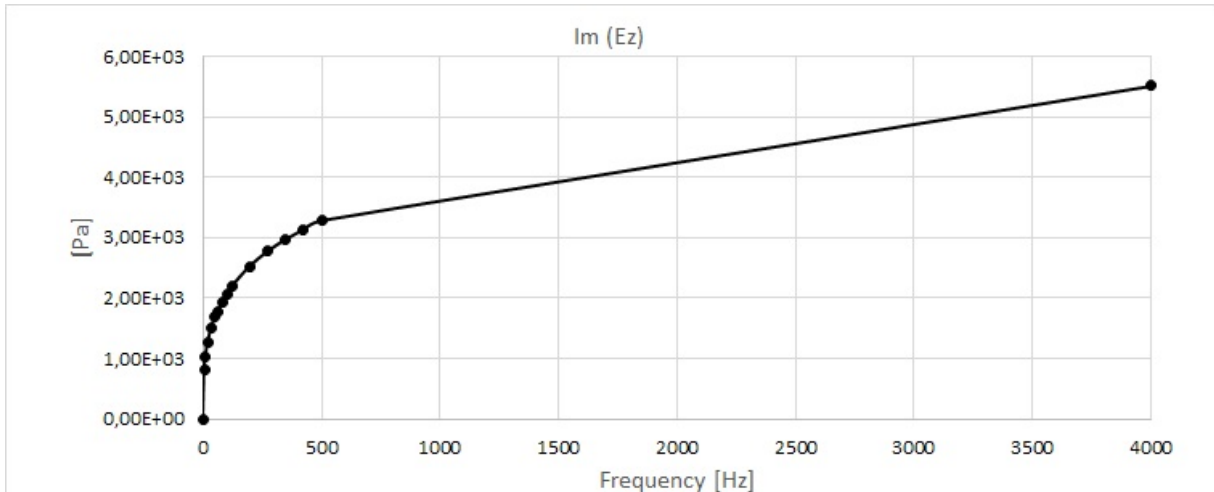
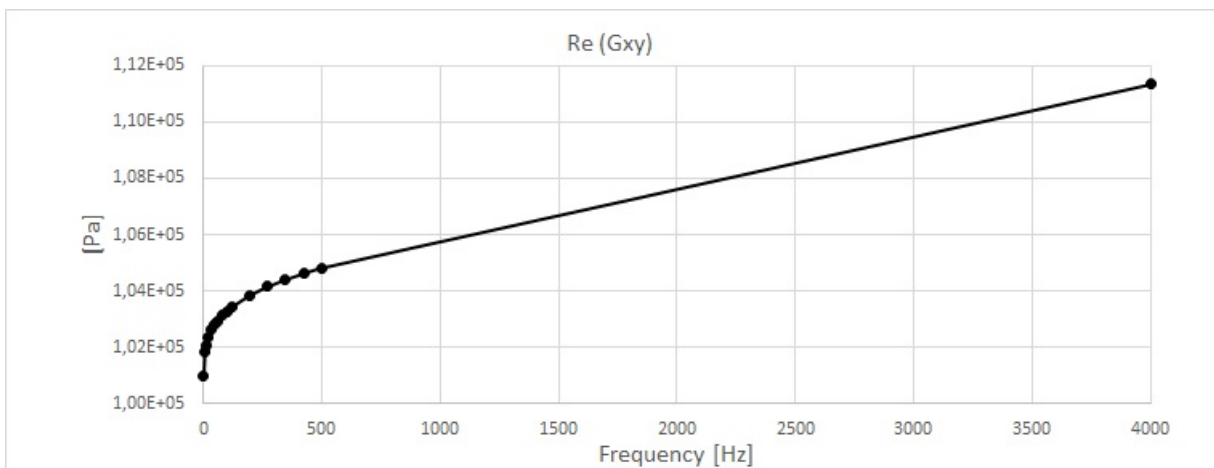
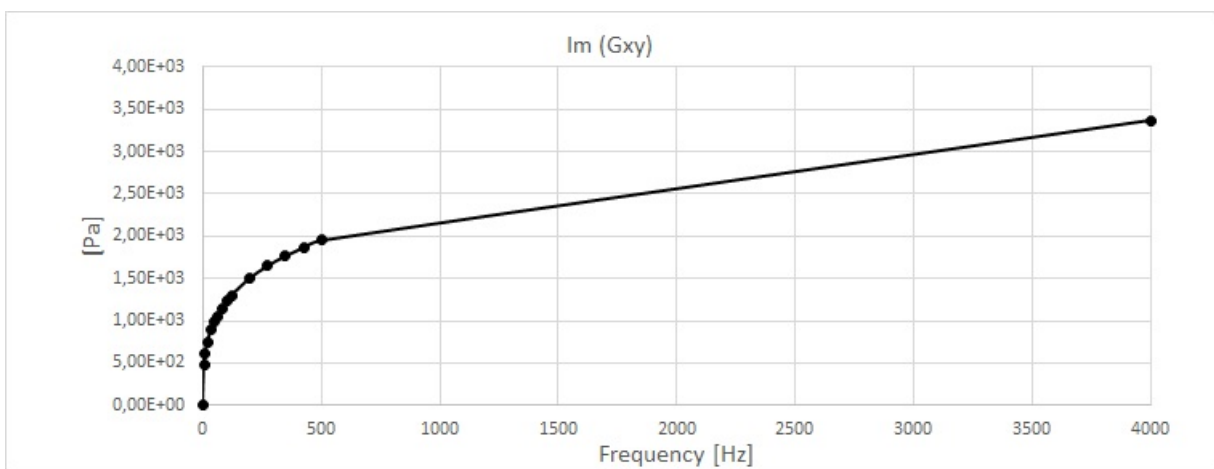
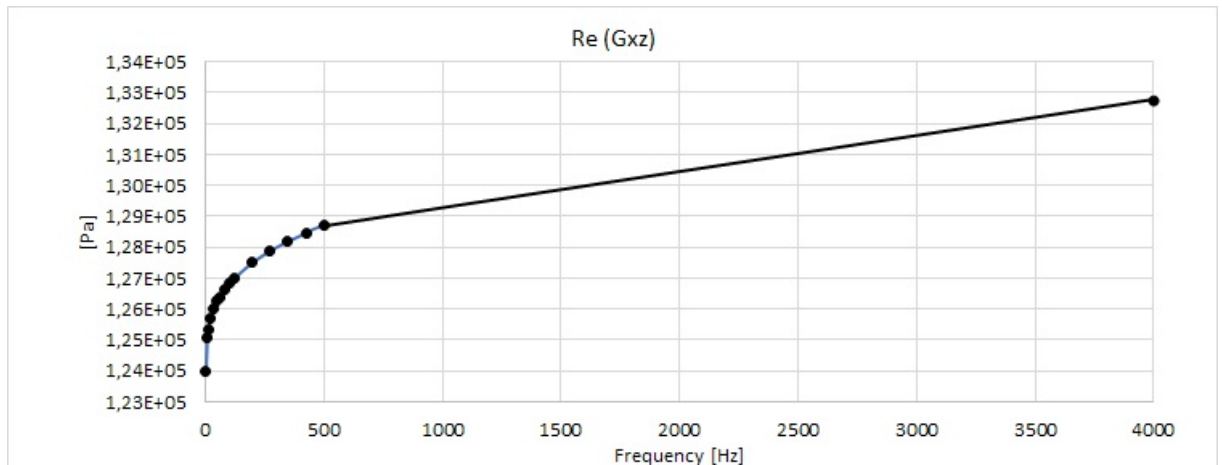
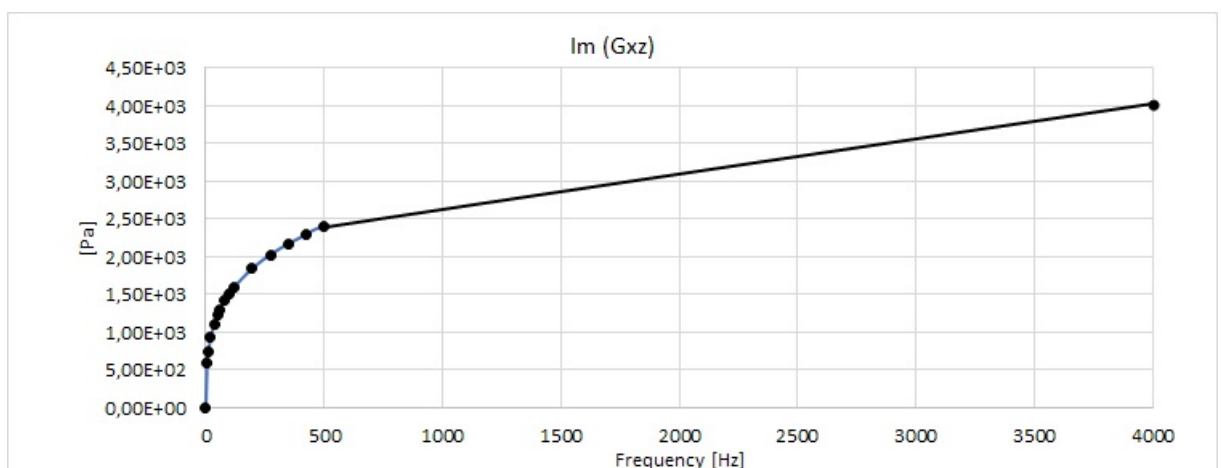
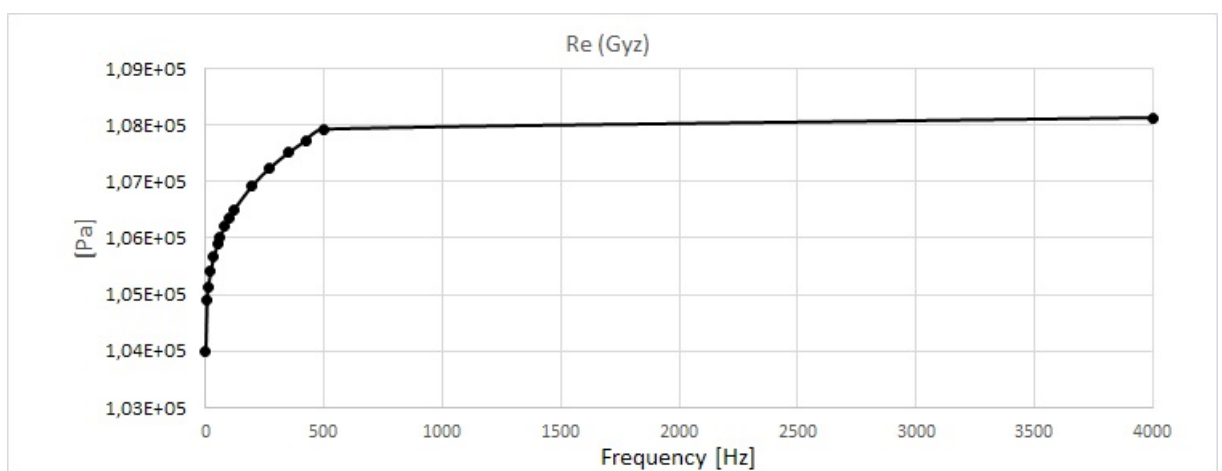


FIGURE 5.3: Melamine Foam Properties: $Im(E_x)$

FIGURE 5.4: Melamine Foam Properties: $Re(E_y)$ FIGURE 5.5: Melamine Foam Properties: $Im(E_y)$ FIGURE 5.6: Melamine Foam Properties: $Re(E_z)$

FIGURE 5.7: Melamine Foam Properties: $Im(E_z)$ FIGURE 5.8: Melamine Foam Properties: $Re(G_{xy})$ FIGURE 5.9: Melamine Foam Properties: $Im(G_{xy})$

FIGURE 5.10: Melamine Foam Properties: $Re(G_{xz})$ FIGURE 5.11: Melamine Foam Properties: $Im(G_{xz})$ FIGURE 5.12: Melamine Foam Properties: $Re(G_{yz})$

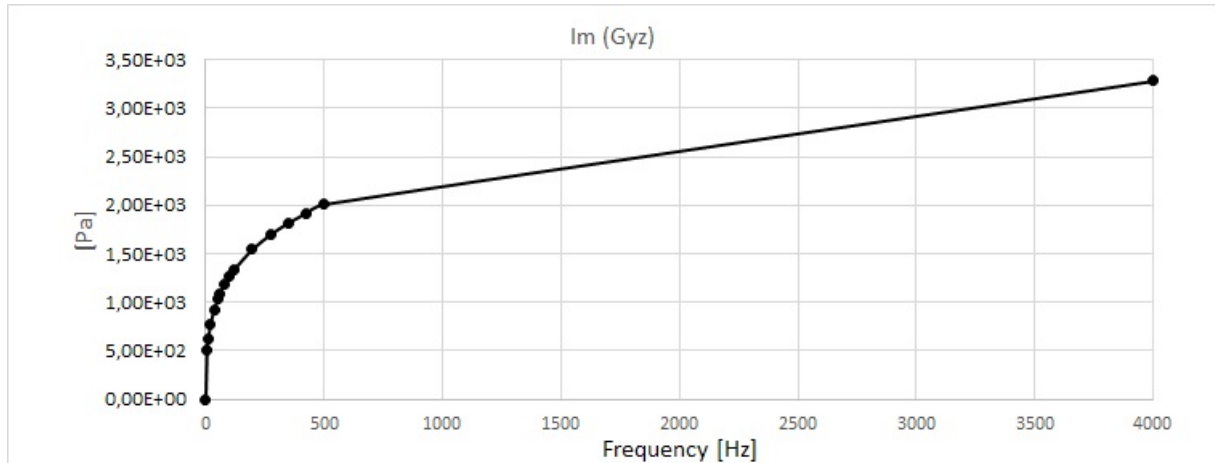


FIGURE 5.13: Melamine Foam Properties: $Im(G_{yz})$

ν_{xy}	0.445
ν_{xz}	-0.514
ν_{yz}	0.433

TABLE 5.1: Poisson ratios of Melamine Foam

5.2 Frequency-Dependent Engineering constants of Homogenized Metamaterial in Melamine Foam with Aluminum inclusions

Using the interface script, a series of metamaterial properties were created, from a volume fraction of 0.0045 to 0.03, with a 0.0015 step.

Inclusion Volume Fraction	Density [Kg/m ³]	Sample A weight (core only) [g]
0	8,00	33,60
0,0045	20,11	84,48
0,0060	24,15	101,4
0,0075	28,19	118,4
0,0090	32,23	135,4
0,0105	36,27	152,3
0,0120	40,30	169,3
0,0135	44,34	186,2
0,0150	48,38	203,2
0,0165	52,42	220,2
0,0180	56,46	237,1
0,0195	60,49	254,1
0,0210	64,53	271,0
0,0225	68,57	288,0
0,0240	72,61	305,0
0,0255	76,65	321,9
0,0270	80,68	338,9
0,0285	84,72	355,8
0,0300	88,76	372,8

TABLE 5.2: Metamaterial densities as a function of inclusions volume fraction

In order to comply the density constraint of $48 \text{ Kg}/\text{m}^3$, the selected Metamaterial have a volume fraction of inclusions equal to 0.0150, or 1.5 %.

The mechanical properties of the homogenized metamaterial in Melamine Foam with Aluminum inclusions are here described. Different inclusion volume fraction, from 0.0045 to 0.03 (respectively 0.45% and 3%) of the unit cell had been calculated. This approach doesn't point to a unique real geometry for each volume fraction: the cylinder diameter, or alternatively the distance between two adjacent ones, are free parameters. So, an homogenized plate based only on volume fraction is theoretically valid for all the cell length.

The homogenized mechanical properties are described only for 5 Vfs: 0.0045, 0.0090, 0.0150, 0.0195 and 0.03. This choice was for a better readability, due to the relatively small changes.

The effect of Vf on the real part of Young Modulus along z is higher than the x and y directions, due to the cylindrical shape along z. Also, the higher the Volume Fraction the higher are the Real Part of the Young Moduli. The opposite happen for the imaginary part: a decrease of inclusion Vf means an higher Viscoelastic material component inside the metamaterial, so an higher damping property proportional to the imaginary part moduli. The differences in damping properties along z (E_z , G_{xz} and G_{yz}) are smaller than x and y directions varying Volume Fraction.

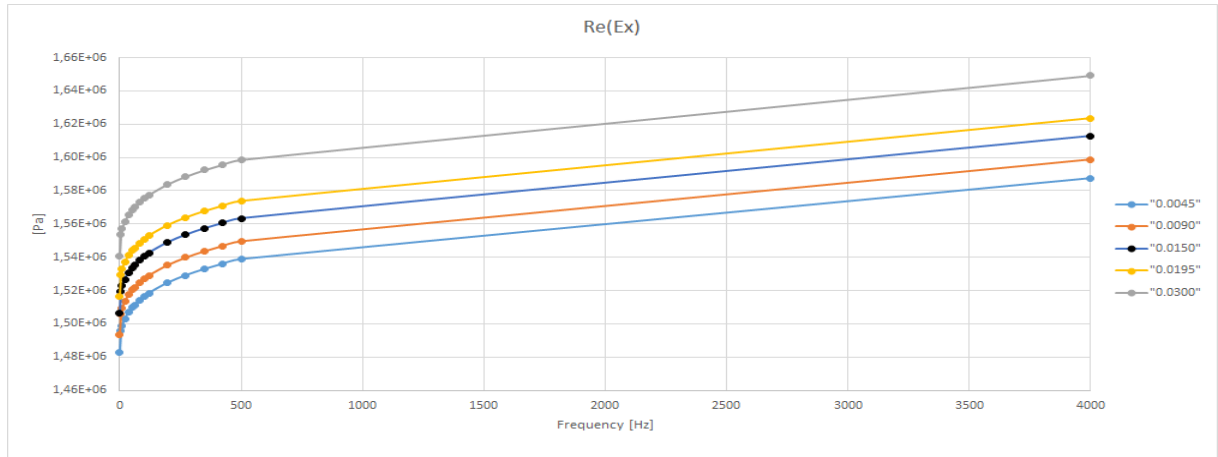


FIGURE 5.14: Homogenized Metamaterial Mechanical properties at different inclusion volume fraction: $Re(E_x)$

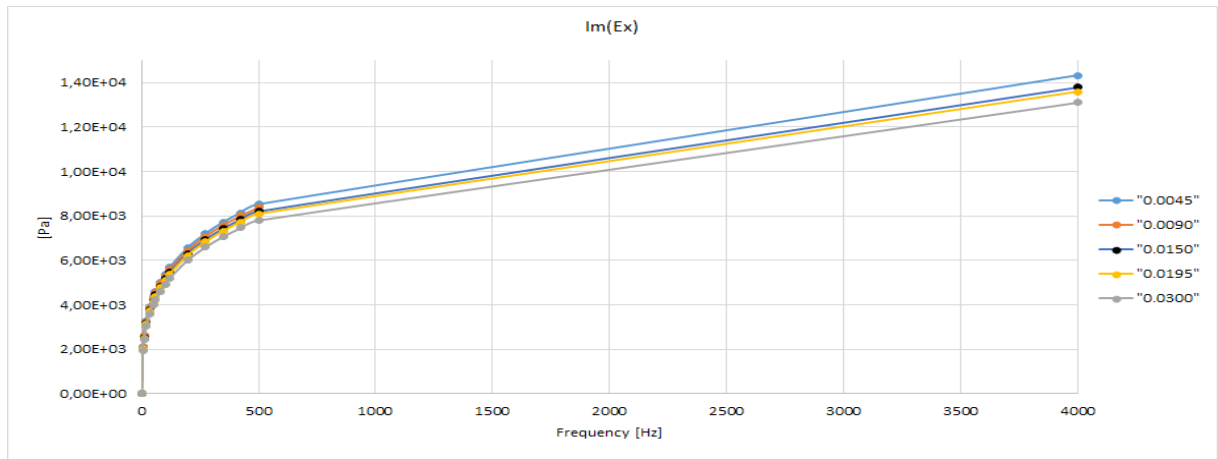


FIGURE 5.15: Homogenized Metamaterial Mechanical properties at different inclusion volume fraction: $Im(E_x)$

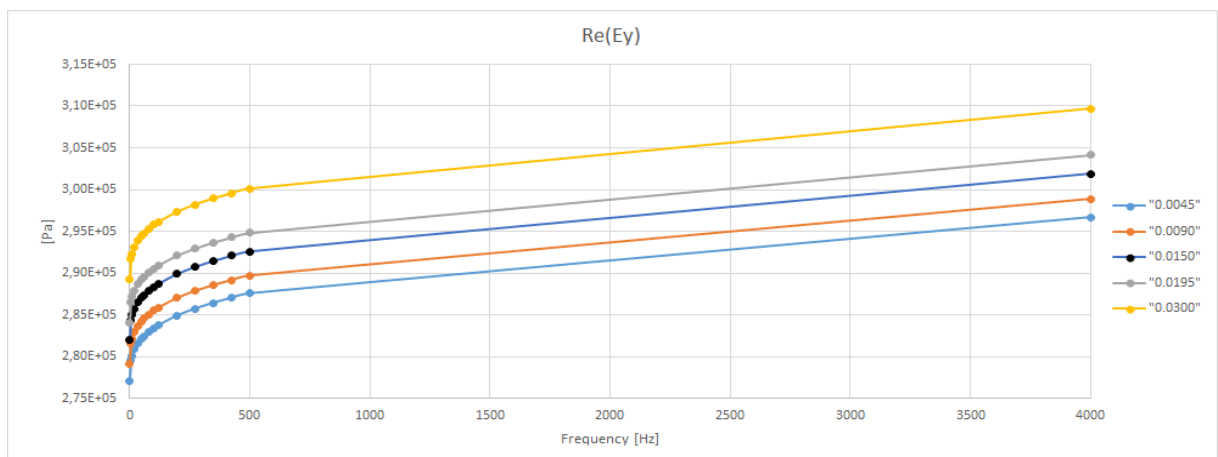


FIGURE 5.16: Homogenized Metamaterial Mechanical properties at different inclusion volume fraction: $Re(E_y)$

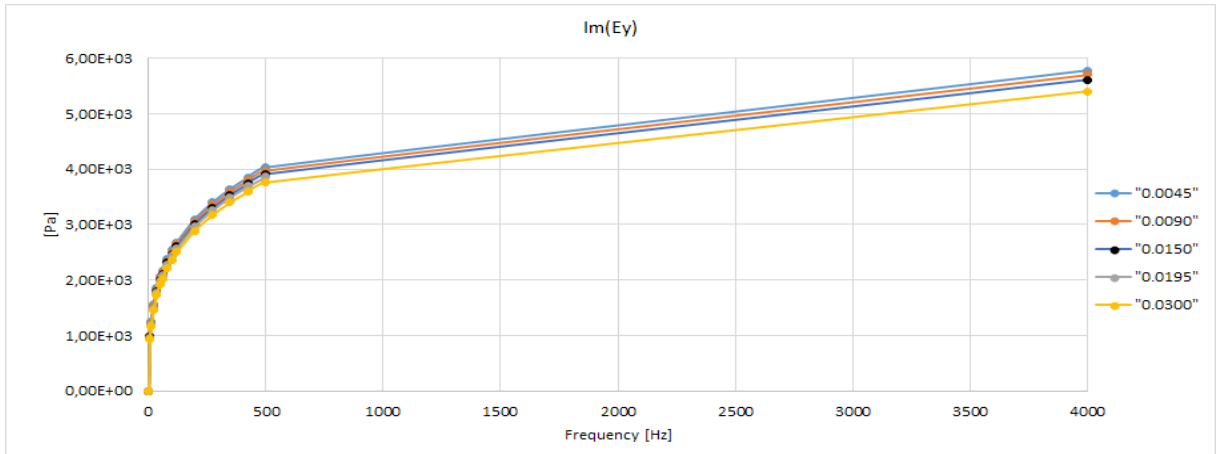


FIGURE 5.17: Homogenized Metamaterial Mechanical properties at different inclusion volume fraction: $\text{Im}(E_y)$

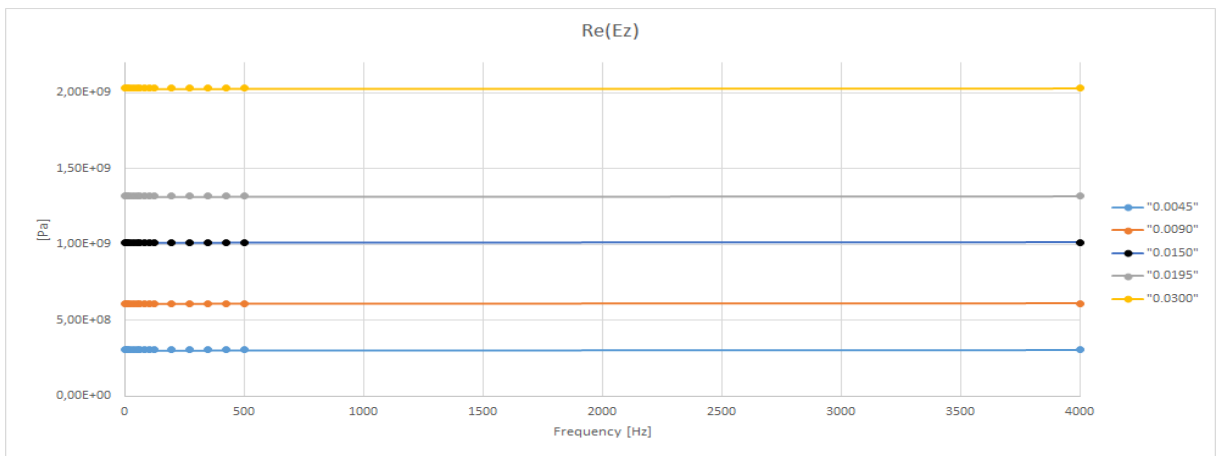


FIGURE 5.18: Homogenized Metamaterial Mechanical properties at different inclusion volume fraction: $\text{Re}(E_z)$

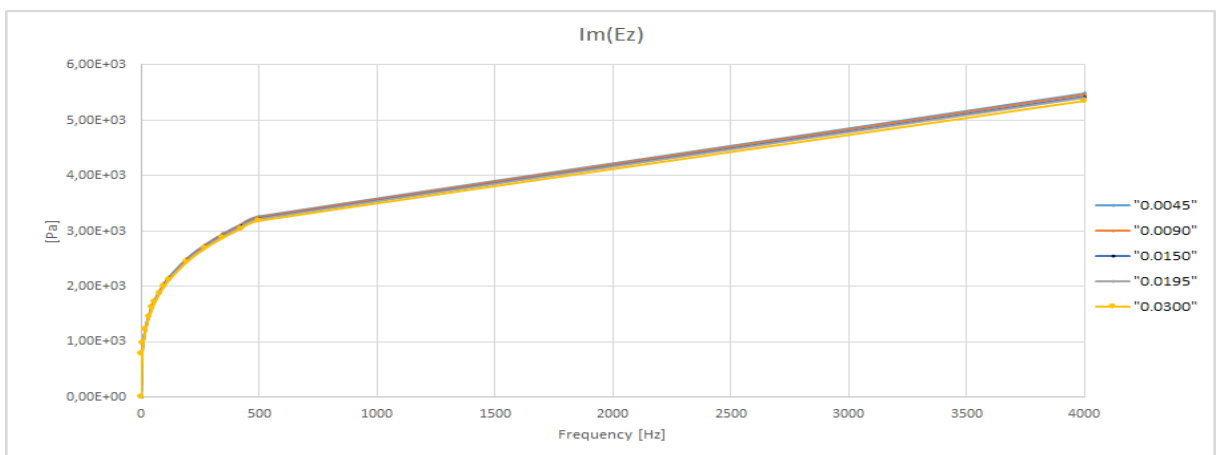


FIGURE 5.19: Homogenized Metamaterial Mechanical properties at different inclusion volume fraction: $\text{Im}(E_z)$

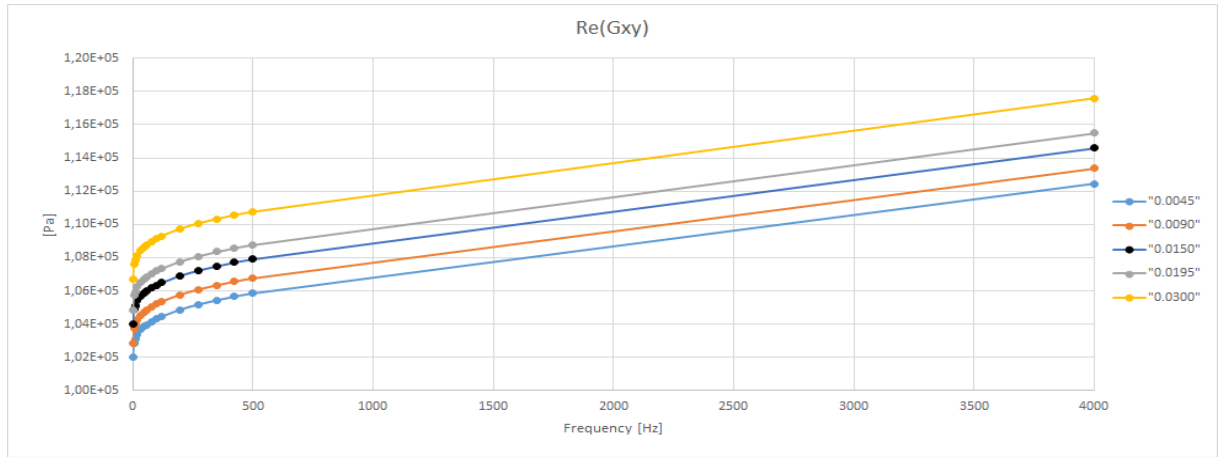


FIGURE 5.20: Homogenized Metamaterial Mechanical properties at different inclusion volume fraction: $Re(G_{xy})$

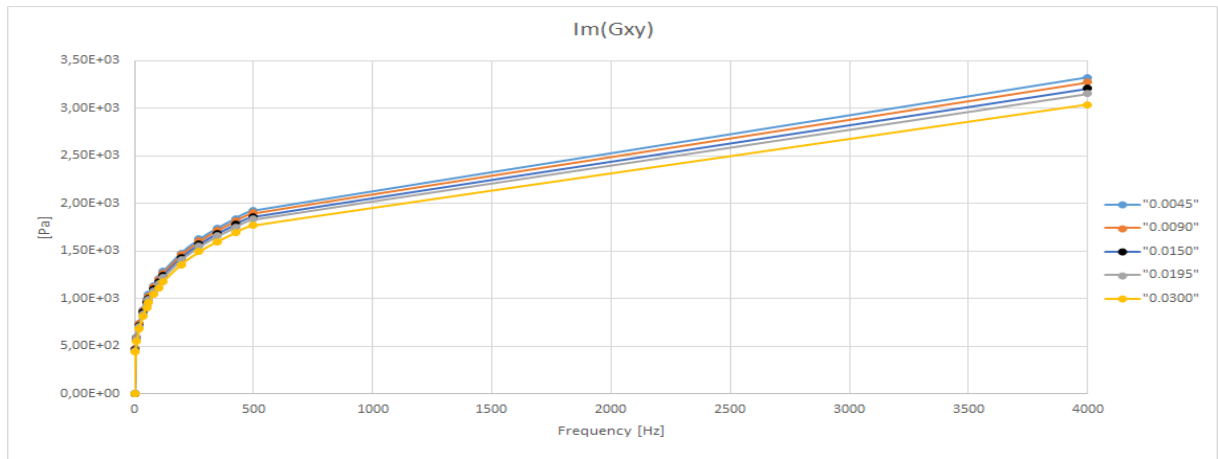


FIGURE 5.21: Homogenized Metamaterial Mechanical properties at different inclusion volume fraction: $Im(G_{xy})$

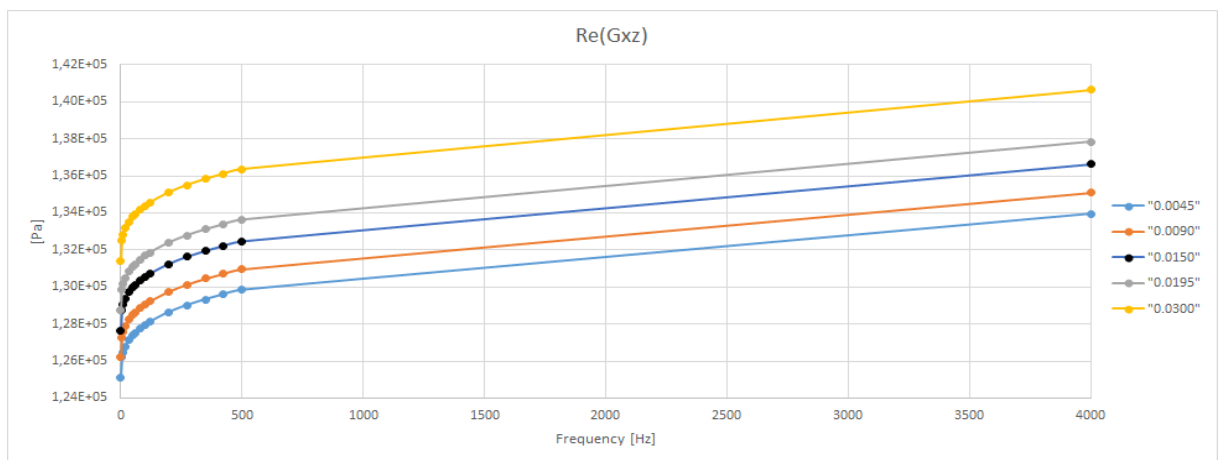


FIGURE 5.22: Homogenized Metamaterial Mechanical properties at different inclusion volume fraction: $Re(G_{xz})$

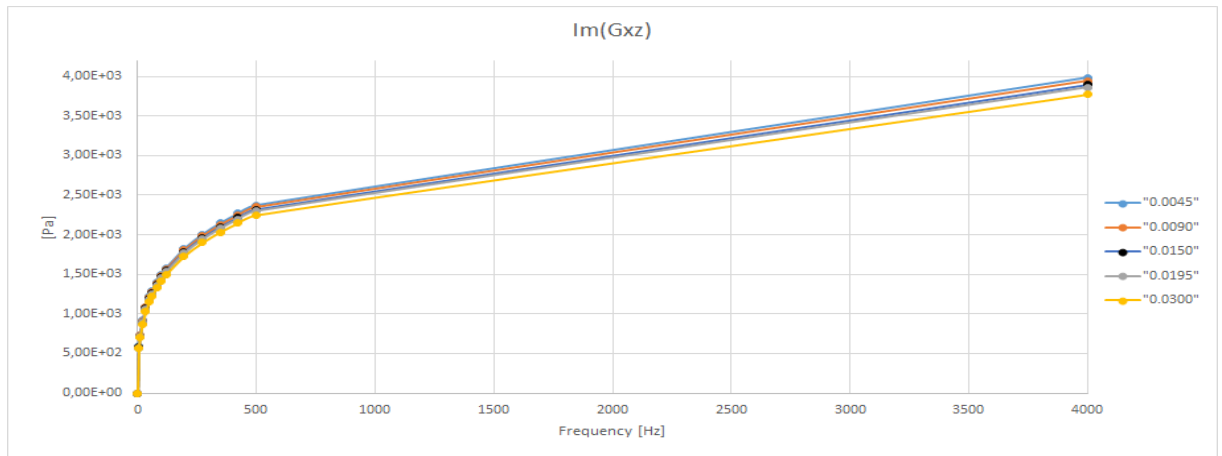


FIGURE 5.23: Homogenized Metamaterial Mechanical properties at different inclusion volume fraction: $\text{Im}(G_{xz})$

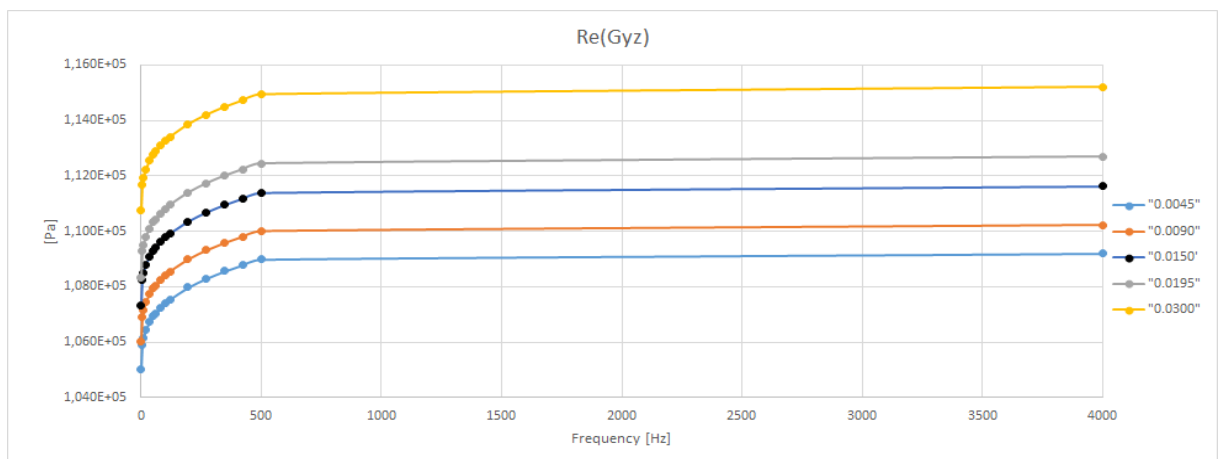


FIGURE 5.24: Homogenized Metamaterial Mechanical properties at different inclusion volume fraction: $\text{Re}(G_{yz})$

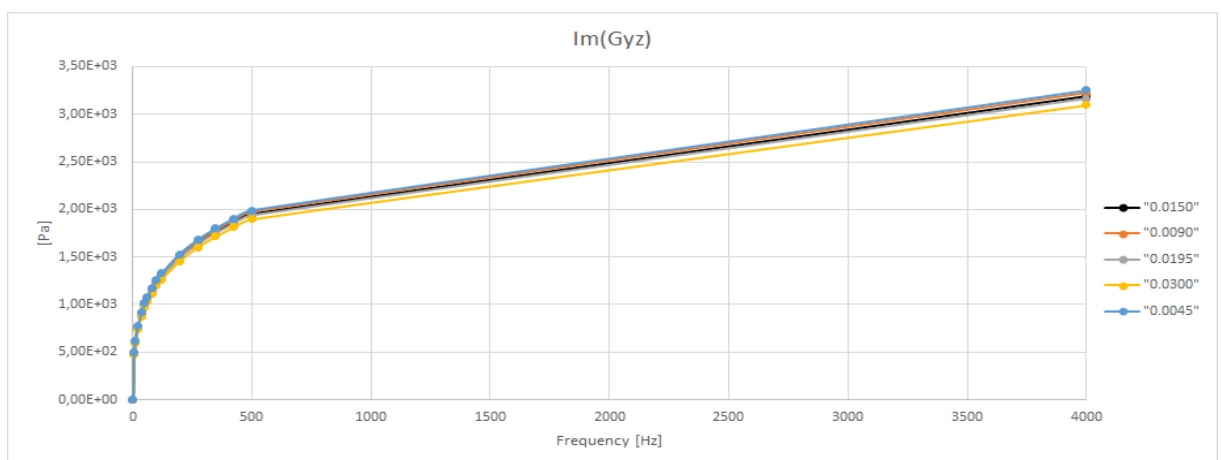


FIGURE 5.25: Homogenized Metamaterial Mechanical properties at different inclusion volume fraction: $\text{Im}(G_{yz})$

Chapter 6

Validation of homogenization method with PVC and Melamine Foam plates

As a first approach, we must achieve the resonance frequencies and make a comparison between the perforated model and the full plate made of the equivalent homogenized material.

Experimental resonance frequencies are measured using an accelerometer applied on the plates excited by a harmonic sound. The plates are 20 mm thick (z-direction), 309 mm long (x-direction) and 206 mm wide (y-direction). The hole diameter is 7 mm.

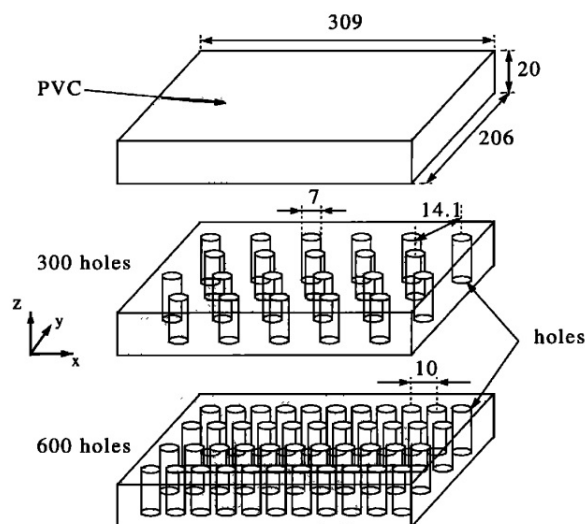


FIGURE 6.1: Schematic description of the three plates made of PVC

For more information on the modal extraction, see the ACTRAN workshop section for a plate modal extraction.

Two different plates with dimensions 309x206x20mm, free boundary condition, respectively with 300 and 600 holes are considered. The homogenized equivalent materials (300 and 600 holes) are applied to a full plate, a modal extraction is performed and the results are compared

with the experimental results obtained by Langlet et al [3] and computational results from Actran. The latter had requested the creation of the two perforated plates with SolidWorks, and a meshing process made with MSC Apex which had shown the best result for meshing around the holes. The material used is also the same (PVC) with 300 and 600 holes.

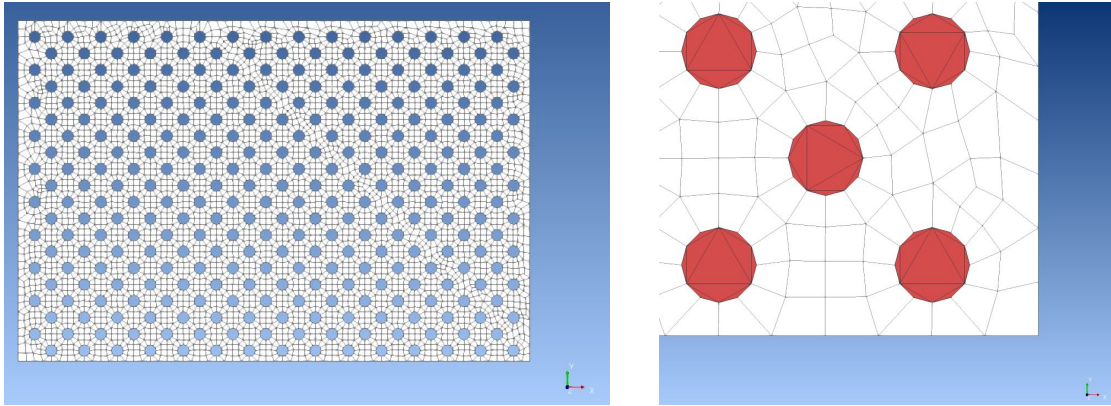


FIGURE 6.2: 300 holes Perforated Plate meshed (left). Particular of meshed holes.(right).

6.1 Mesh convergence process on a full PVC plate

In order to understand the effect of the mesh element length on the modal frequencies and to choose the best configuration, a convergence process has been carried on. Four different mesh configuration had been analyzed:

- 30x20x4 elements xyz
- 40x25x4 elements xyz
- 46x30x4 elements xyz
- 60x40x4 elements xyz

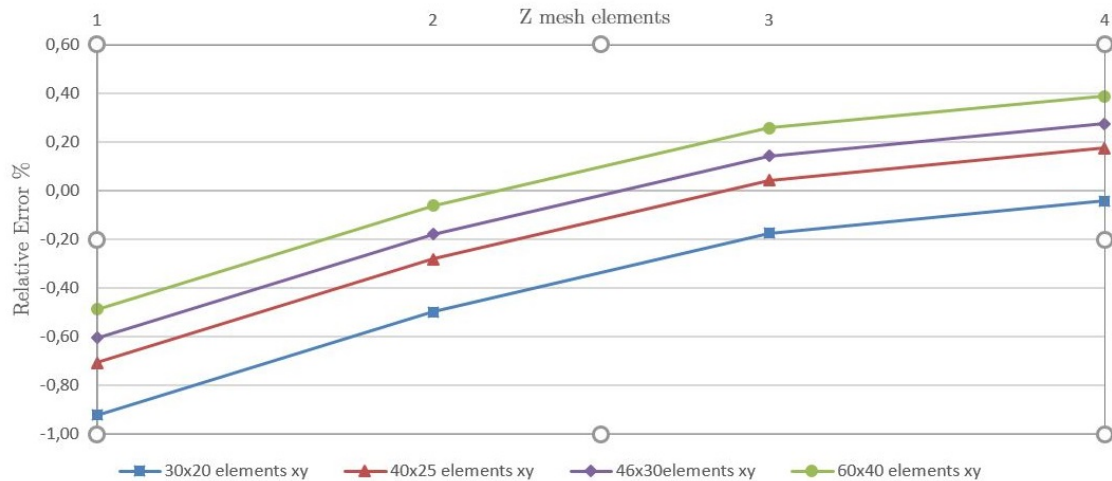


FIGURE 6.3: Actran vs experimental error (%) of a full PVC plate, as a function of mesh configuration (first mode)

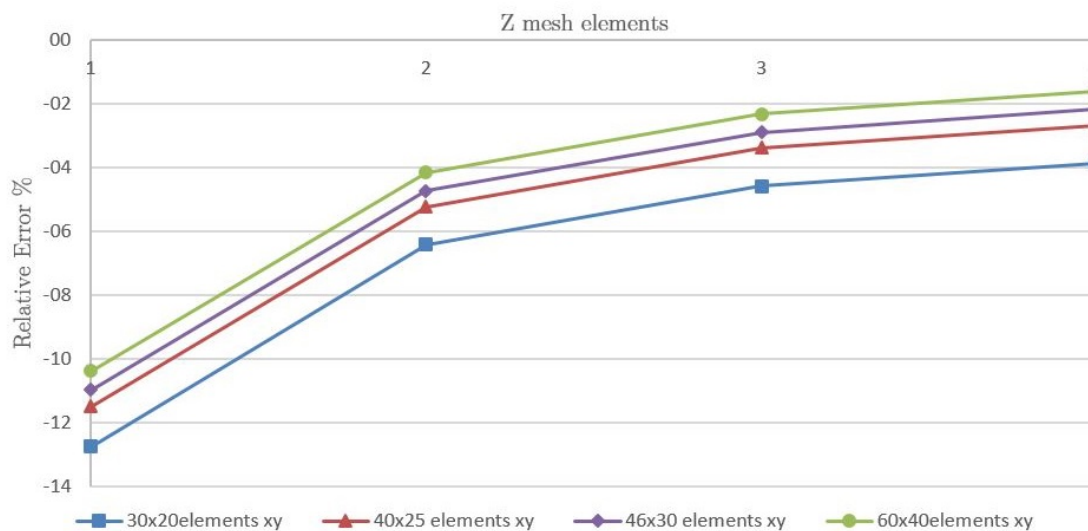


FIGURE 6.4: Actran vs experimental error (%) of a full PVC plate, as a function of mesh configuration (average of first 9 modes)

The graph in Figure 6.4 shows the mean percentage relative error of the first 9 modes compared to experimental results. It's clear that, increasing the number of elements in the three directions, the error asymptotically decrease until a further mesh refining is not necessary. The effect of z elements (along the thickness) seems to be more effective than other directions.

6.2 Modal Frequencies Results

After the mesh convergence process we are able to choose an appropriate mesh structure, and 40 x 25 x 4 elements along xyz were chosen. It

combine faster computation time and acceptable results.

The homogenized equivalent properties had been obtained by [31] with the CUF-MSG based code MUL2-UC (Fig6.1).

The method is take as reference the method proposed by Langlet et al. [3], which is without losses and doesn't take into account the air inside the holes.

	300 Holes	600 Holes
Density [kg/m^3]	1155.44	879.45
E_1 (GPa)	2.442544217	1.624513970
E_2 (GPa)	2.442544219	1.624513972
E_3 (GPa)	3.053097271	2.322408590
G_{12} (GPa)	0.7455780024	0.3071786601
G_{13} (GPa)	0.9143532202	0.5951974724
G_{23} (GPa)	0.9143532207	0.5951974731
ν_{12}	0.3042371111	0.1954291087
ν_{13}	0.4	0.4
ν_{23}	0.4	0.4

TABLE 6.1: Engineering constants of the homogenized materials obtained by the CUF-MSG based code. [31]

Modal frequencies results with homogenized properties from Actran and Langlet [3] are shown for 300 and 600 holes PVC plate.

Mode	f_{MUL2} Homog Hz	f_{ACTRAN} Perforated Hz	f_{FEM} [3] Reference Hz	$f_{Exp.}$ [3] Hz	Rel.Error% MUL2/Exp	Rel.Error % MUL2/FEM
1	254	284	282,2	272	-6,5	-9,9
2	317	305	288,6	289	9,8	10,0
3	599	646	634,1	621	-3,5	-5,5
4	733	719	680,2	681	7,6	7,8
5	805	793	755,6	748	7,6	6,5
6	948	962	919,4	901	5,2	3,1
7	1130	1173	1134,8	1116	1,3	-0,4
8	1262	1339	1302,9	1270	-0,6	-3,1
9	1671	1652	1577,3	1548	8,0	6,0

TABLE 6.2: Modal Frequency difference between a PVC plate with 300 holes (experimental) [3] and a full plate with the equivalent homogenized material(MUL2). FEM Reference results are from [3] and referred to homogenized effective properties. Actran is referred to a perforated plate.

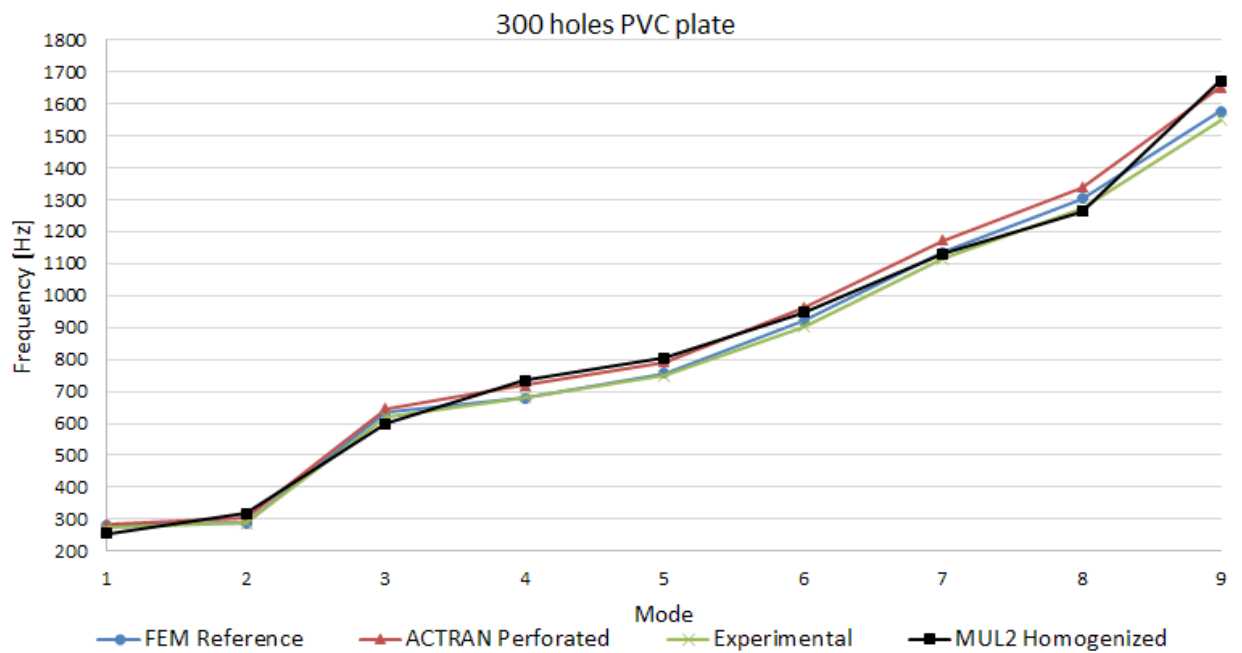


FIGURE 6.5: Modal frequencies PVC plate 300 holes

Mode	f_{MUL2} Hz	f_{ACTRAN} Perforated Hz	f_{FEM} [3] Reference Hz	$f_{Exp.}$ [3] Hz	Rel.Error% MUL2/Exp	Rel.Error % MUL2/FEM
1	190	220	192,2	180	5,7	-1,0
2	296	293	289,2	273	8,6	2,5
3	482	531	480,5	459	5,0	0,3
4	669	664	648,2	626	6,8	3,2
5	732	748	721,9	690	6,1	1,4
6	834	845	807,5	772	8,1	3,3
7	969	1025	956,1	925	4,7	1,3
8	1039	1125	1027,3	1005	3,4	1,2
9	1416	1531	1424,3	1442	-1,8	-0,6

TABLE 6.3: Modal Frequency difference between a PVC plate with 600 holes (experimental) [3] and a full plate with the equivalent homogenized material(MUL2). FEM Reference results are from [3] and referred to homogenized effective properties. Actran is referred to a perforated plate.



FIGURE 6.6: Modal frequencies PVC plate 600 holes

The results from MUL2 are all below 10% relative error respect to experimental results of Langlet.

Also, the relative error between MUL2 homogenized properties and Actran perforated plate reach a -10,4% for the first mode, and lower errors for the next 8 modes.

The curves in Fig 6.5 and 6.6 shows good agreement both for Langlet and for MUL2 with experimental results. The higher the number of holes, the more dense is the grid of unit cells, thus the closer is the homogenization to experiments on plates with holes.

Chapter 7

Sound Transmission Loss Results

7.1 PVC Perforated Plate and Homogenized material

Incident and radiated power have been calculated in order to obtain Sound Transmission Loss. A full plate made of the equivalent homogenized material of the perforated plates was modeled (See Table 6.1 with properties calculated by [31]). The plate is simply supported on its lateral surfaces.

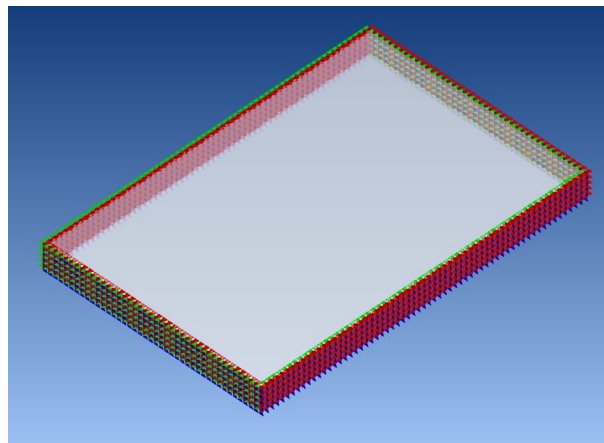


FIGURE 7.1: Boundary condition applied to lateral surfaces with zero displacement, or simply supported condition

	300 holes	600 holes	Homogenized
Elements	45348	79860	15252
Time/Frequency	5'	17'43"	1'22"
RAM	4 GB	10 GB	780 MB

TABLE 7.1: Timings and resources comparison of the PVC perforated plate

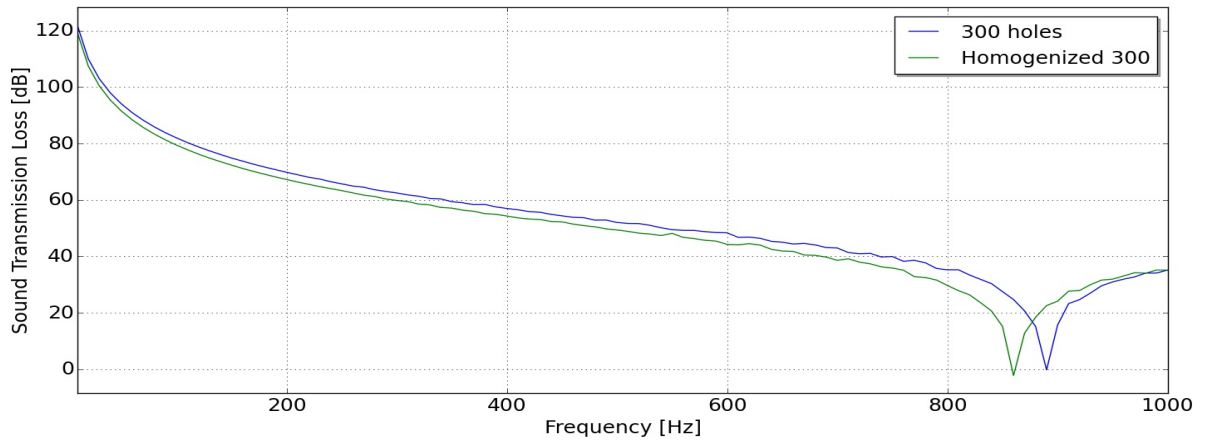


FIGURE 7.2: Transmission Loss difference between 300 holes simply supported PVC plate and a full plate made of correspondent homogenized material

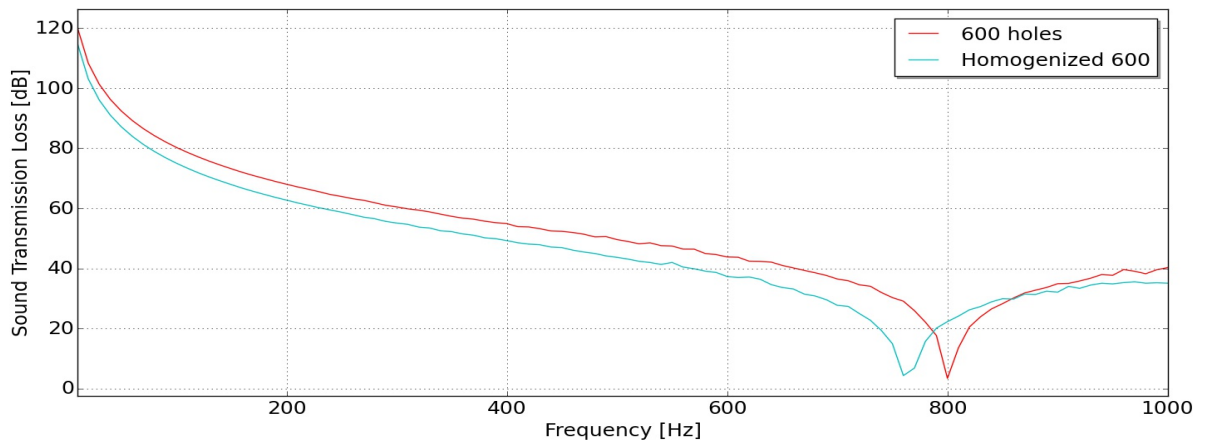


FIGURE 7.3: Transmission Loss difference between 600 holes simply supported PVC plate and a full plate made of correspondent homogenized material

Holes number	Perforated plate resonance frequency [Hz]	Homogenized plate resonance frequency [Hz]	Relative error %
300	860	890	3.49 %
600	800	760	-5.00 %

The STL curves shows good agreement thus validating the method for 3D Unit-cells also from an Acoustic point of view. Table 7.1 shows the advantage of using homogenized properties: Timings and resources performance are drastically reduced.

7.2 Melamine Foam Metamaterial with 300 and 600 Aluminum inclusions and Homogenized metamaterial

The 309x206x20mm plate is now made of Melamine Foam instead of PVC, and Aluminum instead of Air for the cylindrical inclusions. The boundary conditions are the same: applied on its four lateral surfaces (as in Fig 7.1 with zero displacement (or simply supported) condition). Sound Transmission Loss was evaluated and compared with a full plate made of the related homogenized material.

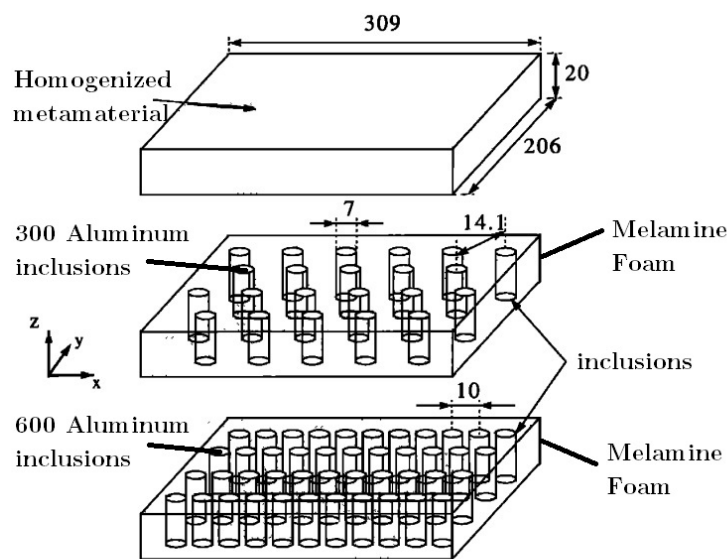


FIGURE 7.4: 309x206x20mm plate made of Melamine Foam with 300 or 600 Aluminum inclusions

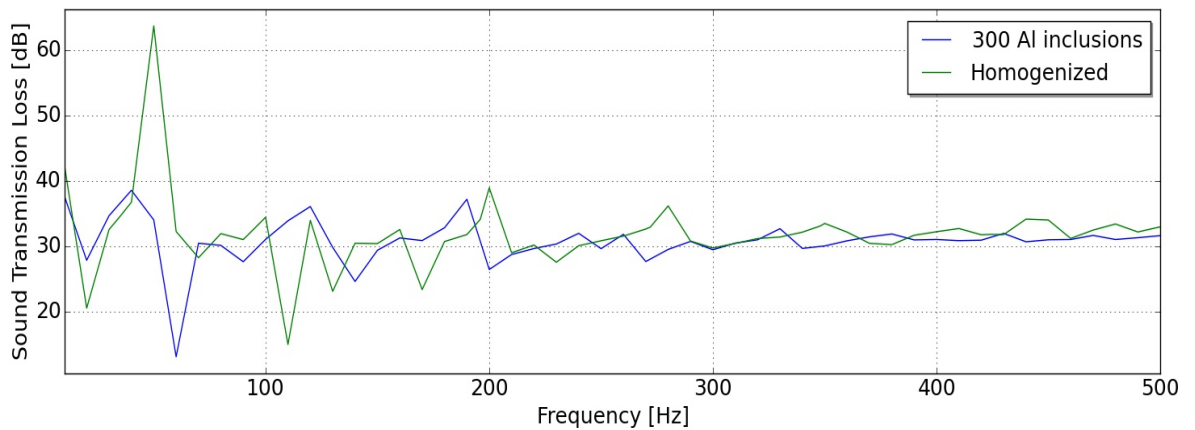


FIGURE 7.5: STL of a simply supported plate, Melamine Foam and 300 Aluminum inclusions (19.2% volume fraction): comparison with equivalent homogenized material

The results in figure 7.5 show a good agreement between 10 to 500 Hz, except for 50 Hz, which shows a 30 dB difference, while frequencies 60 and 110 Hz shows a 20 dB difference. Further investigation are needed in order to understand this results.

However, this model has a volume fraction of inclusions equal to 0.192, and according to Langlet experiment we choose inclusions with 7 mm diameter. This lead to a specific weight of about $525 \text{ Kg}/\text{m}^3$, far beyond CASTLE constraint of $48 \text{ Kg}/\text{m}^3$! Indeed, this model was a first start of the validation process.

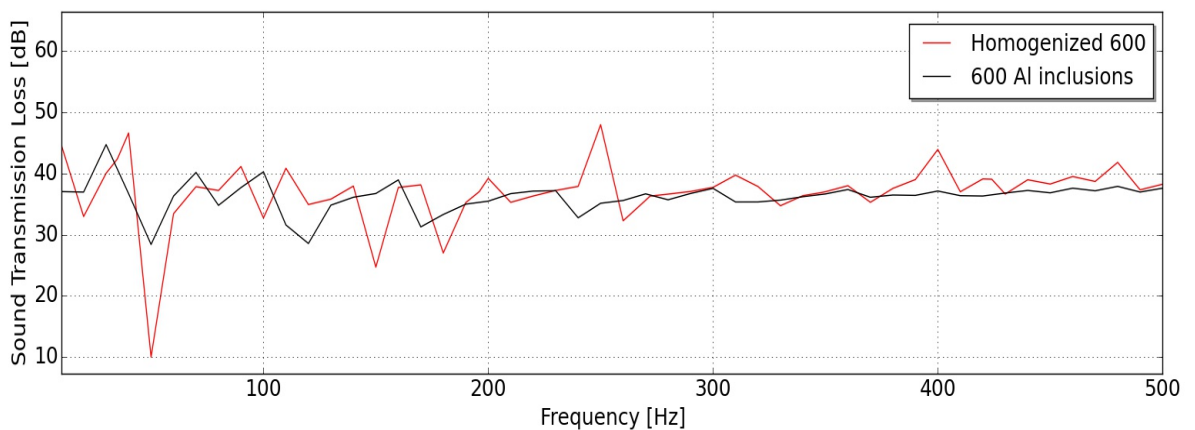


FIGURE 7.6: STL of a simply supported plate, Melamine Foam and 600 Aluminum inclusions (58.2% volume fraction) : comparison with equivalent homogenized material

The Plate with 600 inclusions shows an average good agreement along the frequencies, at 40 Hz we have the same resonance peak, even though a 20 dB difference is shown. Differences are lower at higher frequencies, and further investigation is needed to explain this behavior.

7.3 Melamine Foam Metamaterial with different Inclusions Volume Fraction

The plate is the same used for modal extraction: 309x206x20 mm, simply supported on the four lateral surfaces. For a comparison of acoustical performance and the effect of inclusions, the Sound Transmission Loss of a full Melamine Foam plate is evaluated.

Time/frequency	1 min
RAM	758 MB
Elements	15252

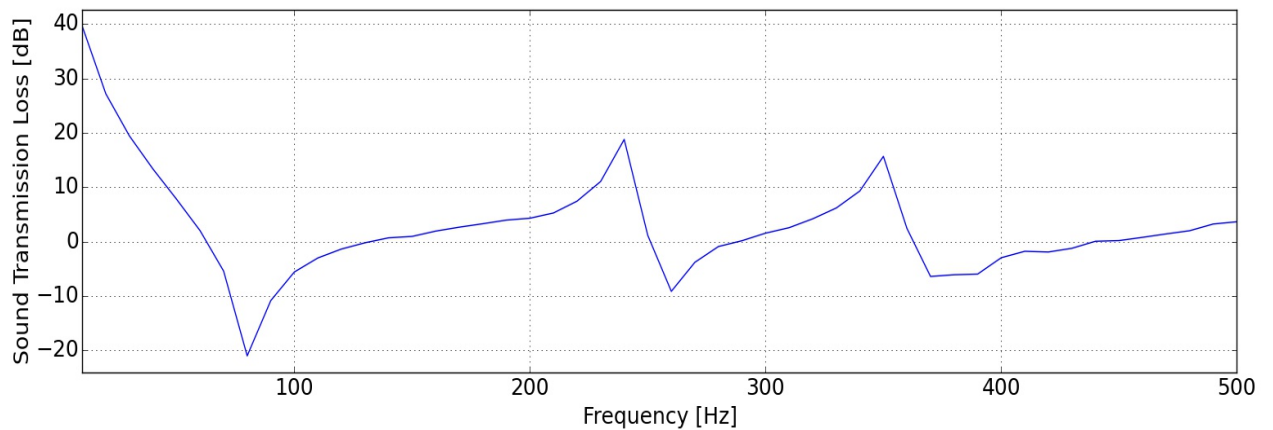


FIGURE 7.7: Sound Transmission Loss of a Melamine foam plate (simply supported)

To be clearly readable, the graphs are organized in few Volume Fractions each.

NOTE:The curves where there was no need of a fine STL evaluation are coarse and cannot often be visible the resonance peaks. This is because of the larger frequency step.

Where there's need to have a visualization of resonance peaks, a resolution of 10 Hz is used.

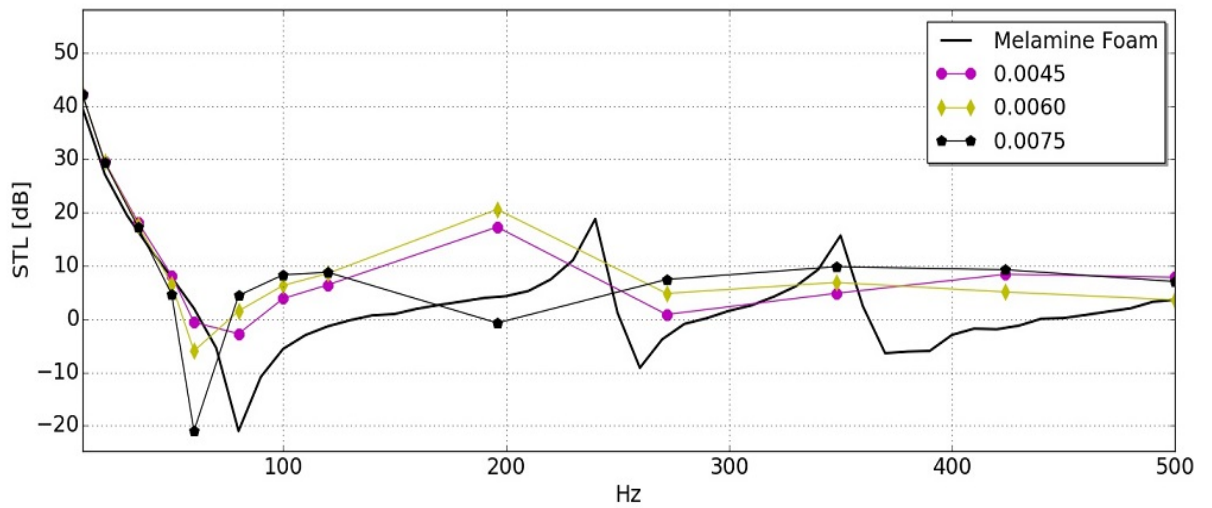


FIGURE 7.8: Sound Transmission Loss of Metamaterial plate with different volume fraction (0.0045,0.0060,0.0075) compared with Melamine Foam plate

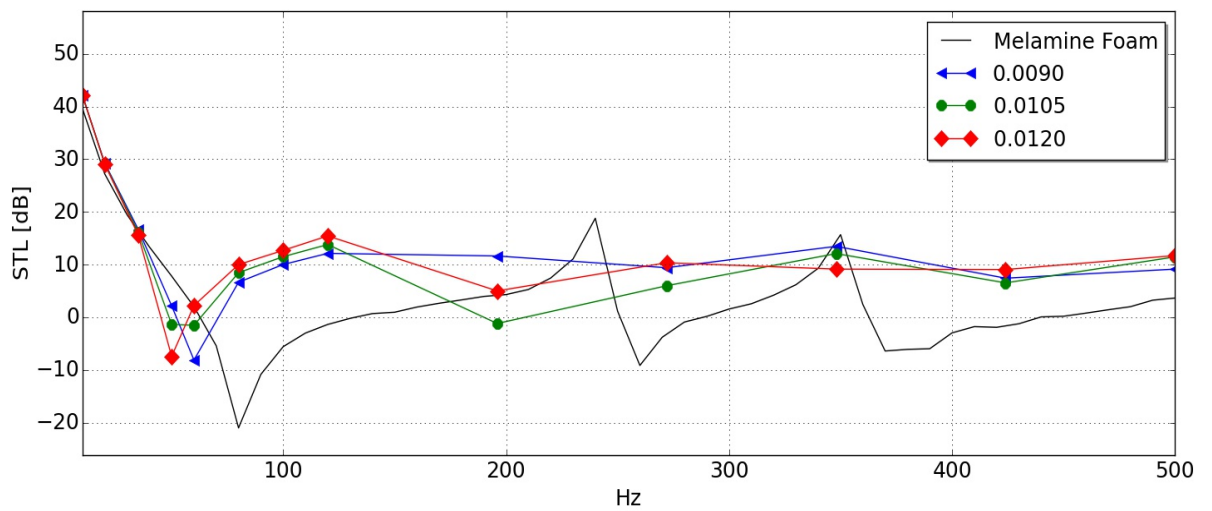


FIGURE 7.9: Sound Transmission Loss of Metamaterial plate with different volume fraction (0.0090,0.0105 and 0.0120) compared with Melamine Foam plate

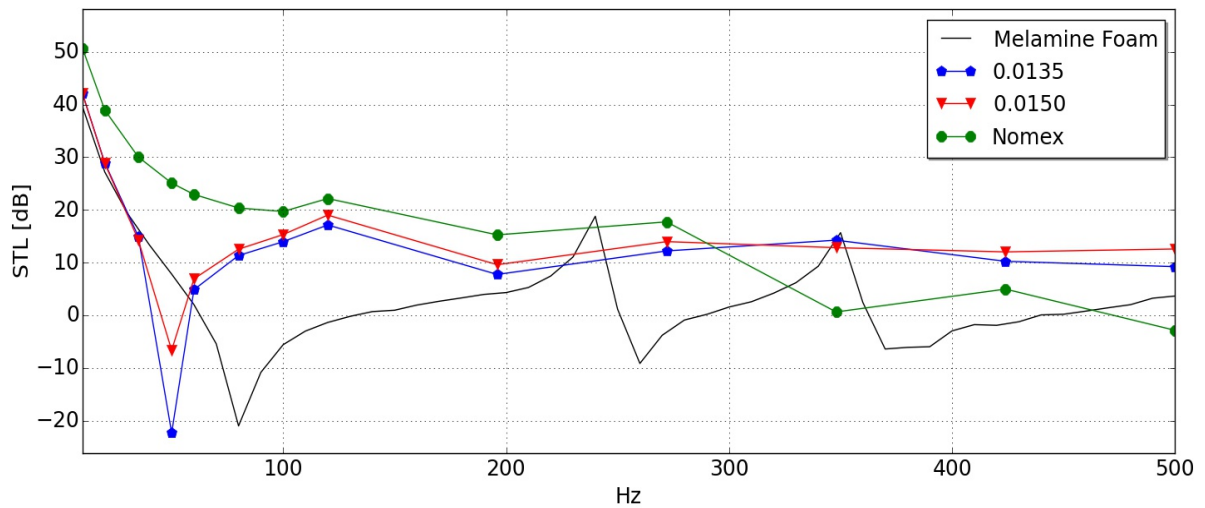
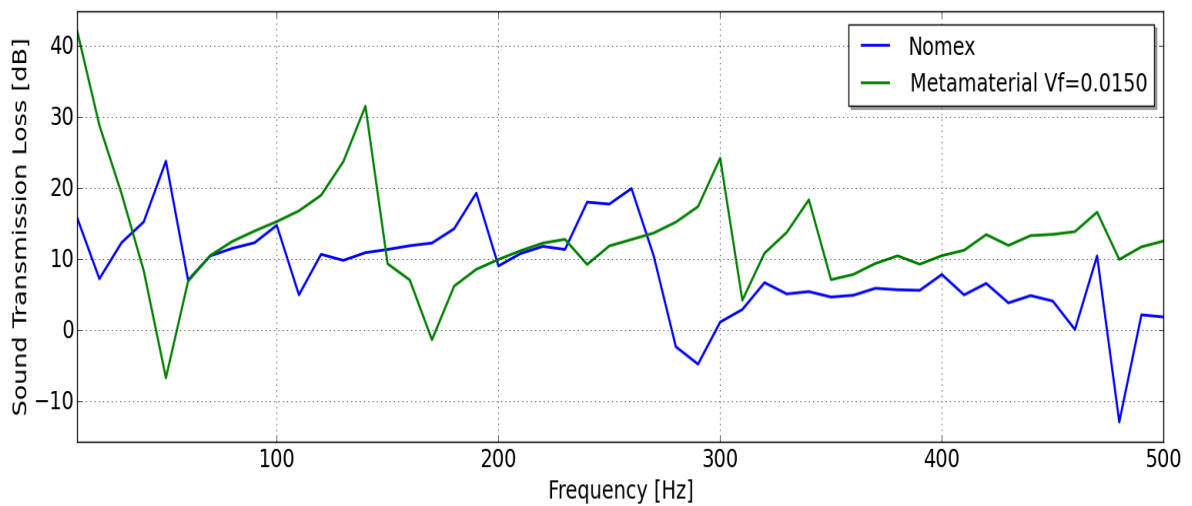


FIGURE 7.10: Sound Transmission Loss of Metamaterial plate with 0.0150 inclusions volume fraction, compared with Melamine Foam and Nomex plates

It is observed an increase in STL for high Vfs, coherently with the mass-law. The chosen metamaterial has an inclusions volume fraction of 0.0150, or 1.5%. The reason was mainly the weight constraint: the material with the same specific weight of Nomex (48 Kg/m^3) was chosen (See Table 5.2 for the other densities).



The acoustic performance difference between the selected metamaterial and Nomex is shown in the figure below:

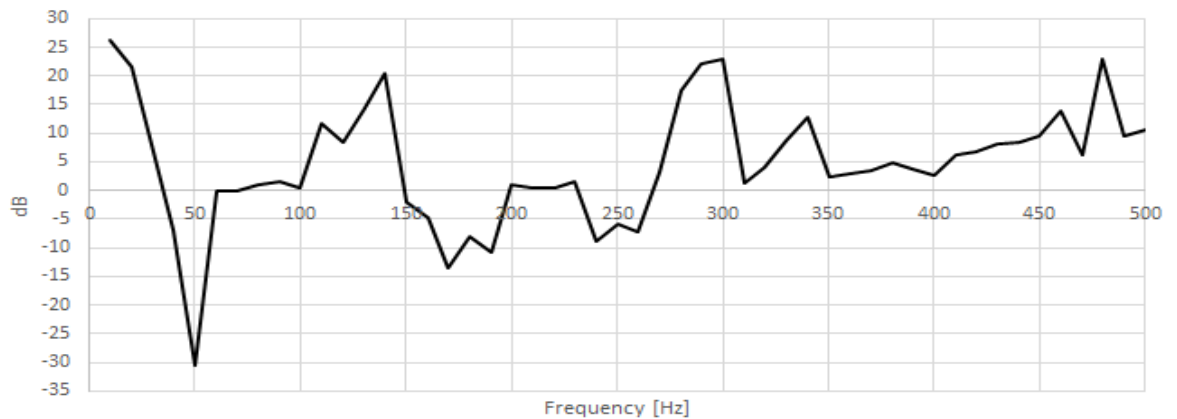


FIGURE 7.11: STL difference between Metamaterial 0.150 and Nomex, clamped plate 309x206x20mm

Nomex have an higher STL than Metamaterial with $V_f=0.0150$, up to 250 Hz. After this frequency, a minimum of 3 dB drop is seen, with a peak of 20 dB at about 300 Hz.

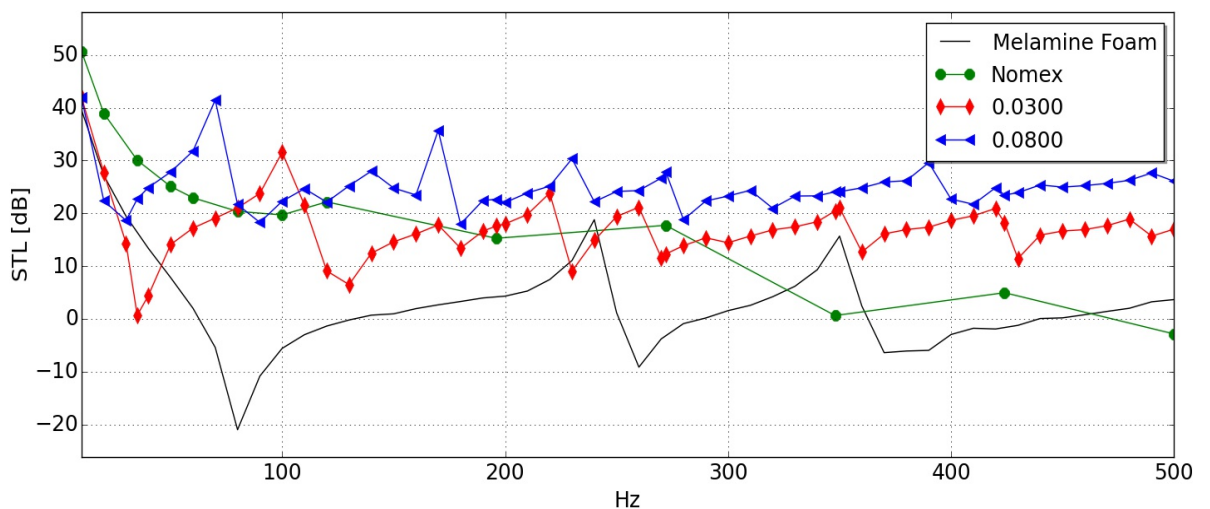


FIGURE 7.12: STL of high values inclusions volume fraction (3% and 8% respect to Nomex and Melamine Foam)

It is clear that high inclusions volume fraction lead to high Sound Transmission Loss, for the increased mass of the sample, and a compromise has to be made.

7.4 Sound Transmission Loss of Sandwich Plates

Two different Sandwich plates with same total dimension 1000x600x7mm have been considered. Their difference is due to the experiments on real

samples executed by CASTLE Partners, that suggested to update some material properties and thickness (see Tables 7.6, 7.4 and 7.5). Both plates are clamped on their lateral surfaces.

Total Plate dimensions are the same, 1000x600x7mm, with a difference in core and skins. Difference of the core are:

	Sample A	Sample B
Length x [mm]	1000	1000
Length y [mm]	600	600
Length z [mm]	6.36	6

TABLE 7.2: Samples A and B geometries

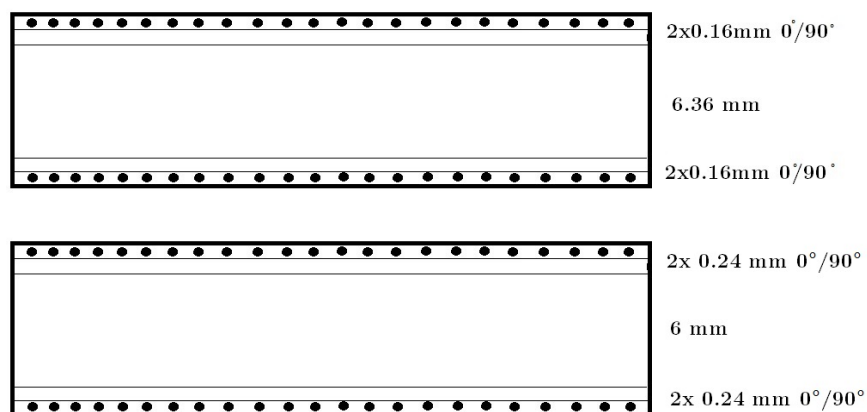


FIGURE 7.13: Sample A quotes (top) Sample B quotes (bottom).

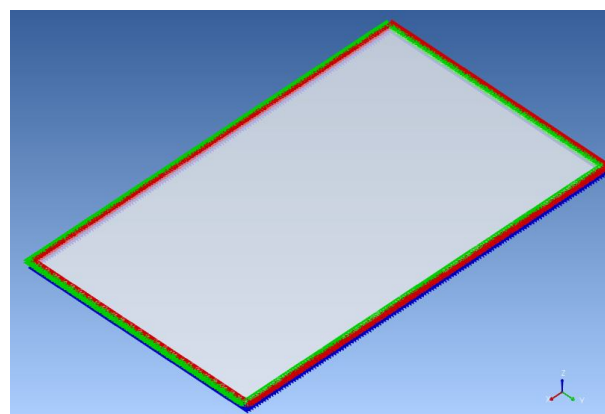


FIGURE 7.14: Sandwich plate with visible boundary conditions

The plate is clamped on its four lateral surfaces (see Fig 7.14). This dimensions were chosen together with CASTLE partners, which are proposing a Sandwich plate with Nomex as core material. The aim is to investigate the acoustic performance between Nomex and the proposed

Metamaterial, made of Melamine Foam with Aluminum cylindrical Inclusions.

In order to satisfy the minimum factor of 8 elements/wavelength, the maximum length of the element must be 4 mm (see Section 3.8 for its calculation). The mesh configuration chosen is then

	Sample A [500Hz]	Sample B [1000Hz]
Elements x	143	250
Elements y	86	150
Elements z	1	2
Total Elm	12298	75000

TABLE 7.3: Samples A and B number of mesh elements

As the shear wavelength depends on the material properties, as explained in section 3.8, this mesh configuration is fitted for Nomex and the Metamaterials at various volume fractions of inclusions, as their lowest shear moduli are quite similar (about 100000 Pa). Sample A is analyzed with a Rayleigh Surface up to 500 Hz for its high memory consumption, while Sample B use a finite fluid model and a finer mesh to reach 1000 Hz. As shown in Fig 3.16 the methods are equally reliable.

7.4.1 Nomex Core

The baseline panel for linings is constituted by a sandwich composed of woven fabric fiberglass composite skins (each skin is represented by two plies oriented at 90 degree with respect to the “L” direction of the core) and an aramid over expanded honeycomb core. The scheme of this Sandwich plate is shown in the figure below:

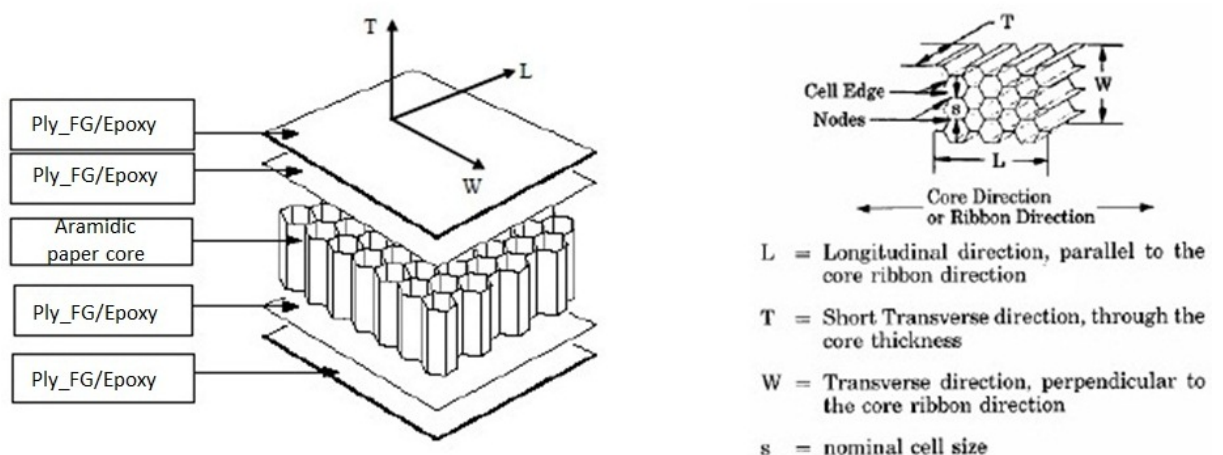


FIGURE 7.15: Scheme of the Sandwich plate [Costin-Ciprian Miglan (Cleansky)]

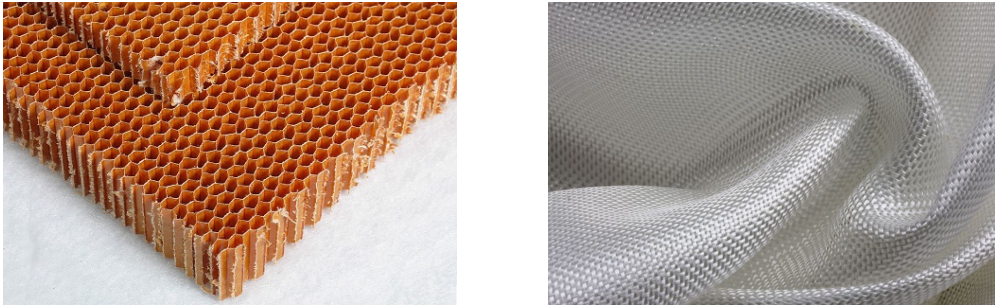


FIGURE 7.16: Example of Aramid Honeycomb (left) and Glass Fabric Pre-impregnated Epoxy Resin [27]

Skin Plies		
	Sample A	Sample B
E_x	20.7 GPa	20 GPa
E_y	20.7 GPa	20 GPa
E_z	4 GPa	3.6 GPa
G_{xy}	4 GPa	4 GPa
G_{xz}	4.3 GPa	4.3 GPa
G_{yz}	4.3 GPa	4.3 GPa
ν_{xy}	0.2	0.13
ν_{xz}	0.4	0.27
ν_{yz}	0.4	0.27
Specific Weight [Kg/m^3]	2500	1950

TABLE 7.4: Samples material properties difference: Skin plies 0/90° - Glass Fabric Pre-impregnated Epoxy Resin

Core		
	Sample A	Sample B
E_x	0.1 MPa	0.1 MPa
E_y	0.1 MPa	0.1 MPa
E_z	90 MPa	90 MPa
G_{xy}	0.1 MPa	0.1 MPa
G_{xz}	15 MPa	15 MPa
G_{yz}	31 MPa	31 MPa
ν_{xy}	0.99	0.99
ν_{xz}	0.25	2E-04
ν_{yz}	0.25	2E-04
Specific Weight [Kg/m^3]	48	48

TABLE 7.5: Samples A and B material properties difference: Core - Nomex Aramid honeycomb

	Sample A	Sample B
Core thickness [mm]	6.36	6
Ply thickness [mm]	0.16	0.24

TABLE 7.6: Samples A and B geometry differences

Weight [g]	Sample A	Sample B	Sample A	Sample B
	Nomex core		Metamaterial 0.0150	
Single skin	960		1123,2	
Core	183,17	172,80	184,6	174,2
Total sample	1143,2	1296	1144,6	1297,4

TABLE 7.7: Weight of Sandwich plates

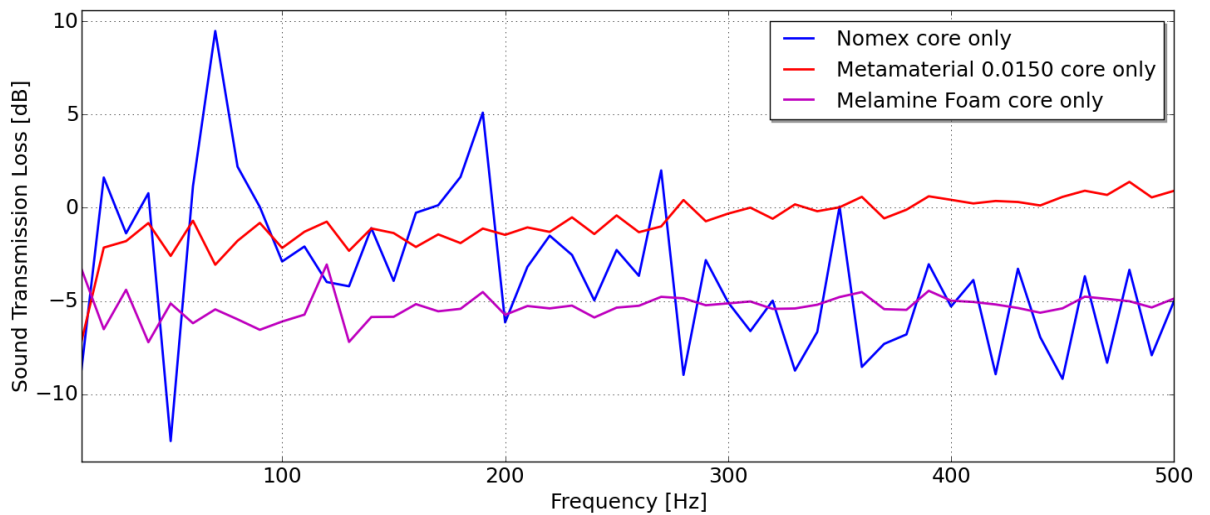


FIGURE 7.17: STL comparison between Nomex, Melamine Foam and Metamaterial 0.0150: Sample A (core only) clamped plate

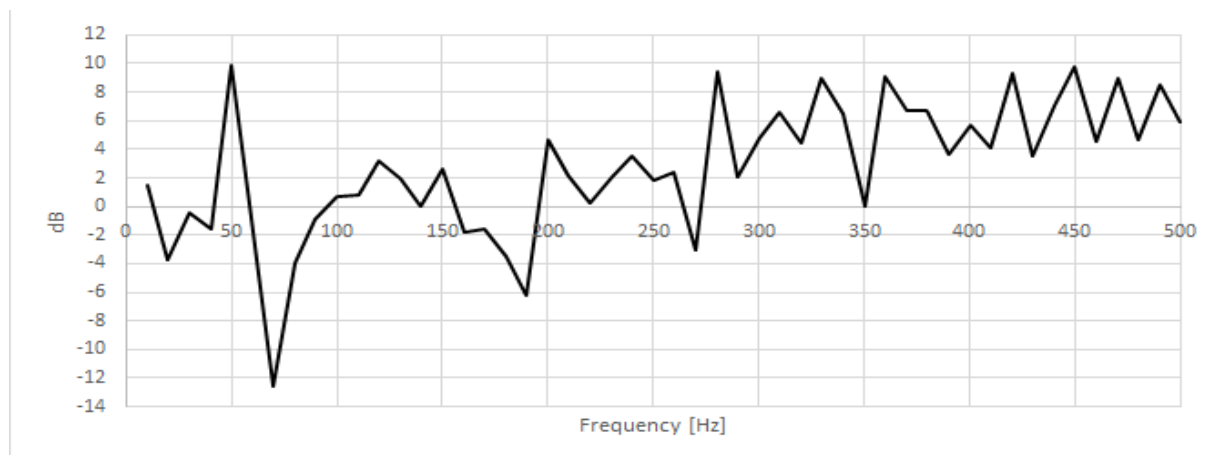


FIGURE 7.18: STL difference between Metamaterial 0.0150 and Nomex: Sample A (core only) clamped plate

STL comparison shows a rather poor acoustic performance, about -5 dB for pure Melamine Foam while Nomex shows better performance up to 300 Hz, and an average STL after this frequency similar to Melamine Foam. Metamaterial 0.0150 shows higher STL at about 280 Hz, as we can see in Fig 7.18. It is argued that the low thickness, together with lack of skins, are the main responsible of low STL. We will see a significant increase in STL adding skins, forming a Sandwich plate. (Section 7.4, in particular Fig 7.19)

7.4.2 Effect of skin in Sound Transmission Loss

The Effect of the skins are here described: Metamaterial with Volume Fraction 0.0150 and Nomex are analyzed with and without skins. The results shows an average of 11 dB gain in STL respect to core-only model, which demonstrate the importance of their presence.

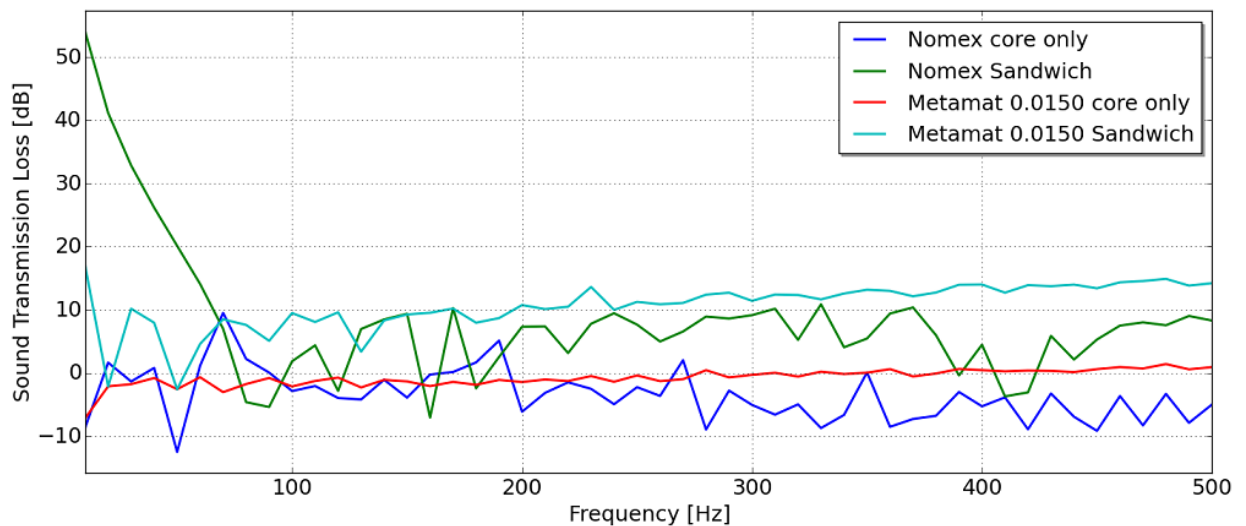


FIGURE 7.19: Effect of skin on a Melamine foam matrix with Aluminum inclusions. (Sample A, homogenized properties)

7.4.3 Sandwich STL Results

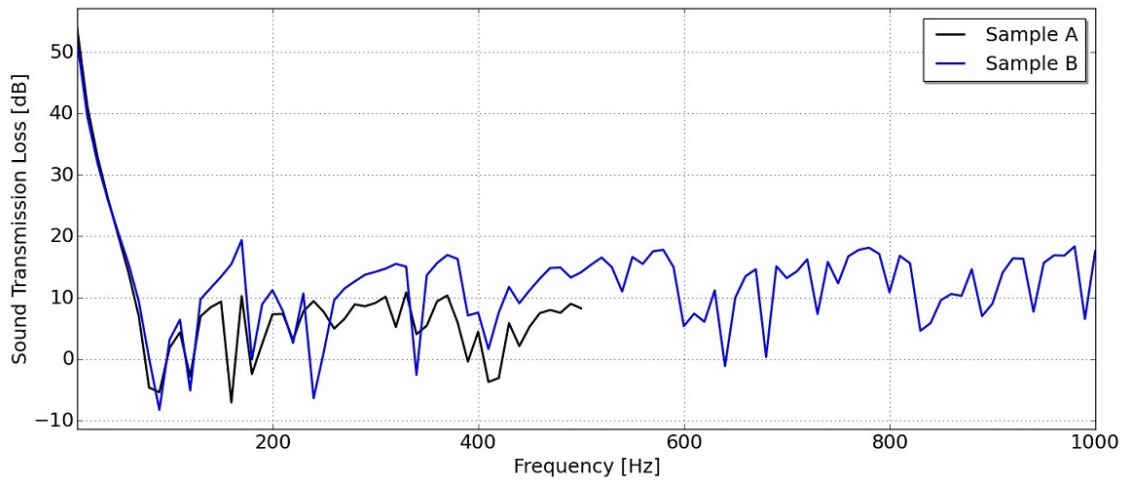


FIGURE 7.20: Transmission Loss of sandwich plate with core in Nomex: comparison Sample A and B

Sample B STL is evaluated up to an higher frequency, 1000 Hz, because was the last updated model requested by CASTLE partners, and was used the new finite fluid model, less memory-demanding and capable to reach this frequency. The increased STL is justified by the higher thickness of the Fiberglass plies.

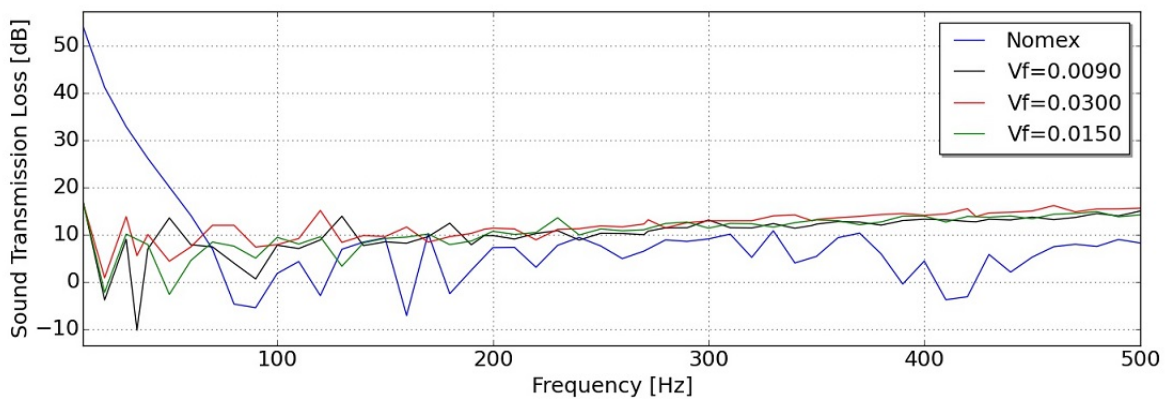


FIGURE 7.21: Effect of inclusion volume fraction. Transmission Loss of sandwich plates with 2+2 plies 0/90 in Fiberglass/Epoxy resin (Sample A)

As we can see, the higher the inclusion volume fraction the higher is the Sound Transmission Loss, and is reasonably true that this Metamaterial will have the best performance even in different geometries. Once selected the Volume Fraction 0.0150 with the same density of Nomex, we compare their Sound Transmission Loss for Sample A and B.

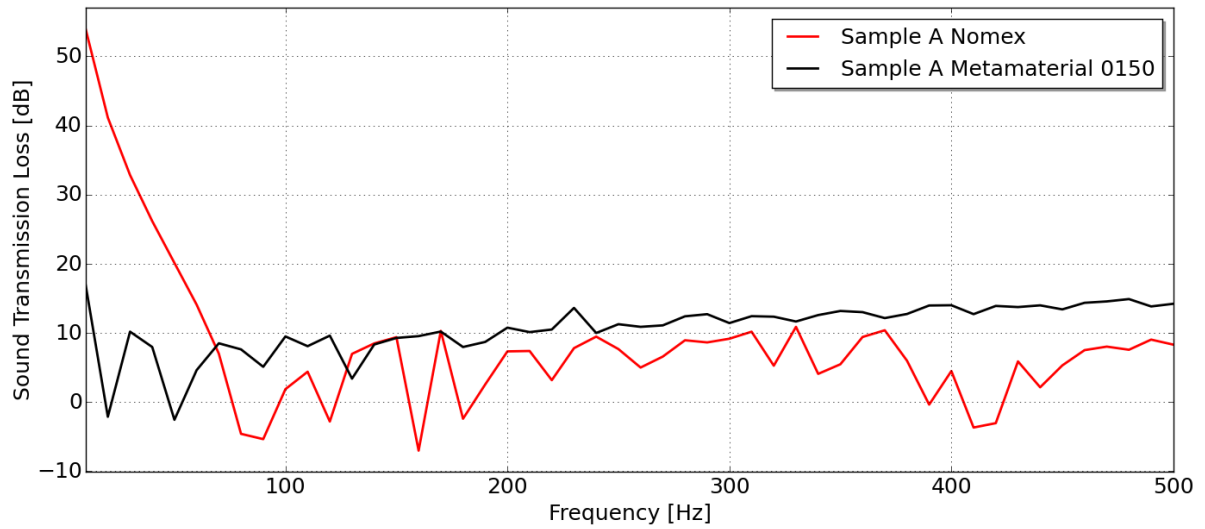


FIGURE 7.22: Sound Transmission Loss of a Sandwich plate with different core material (Sample A)

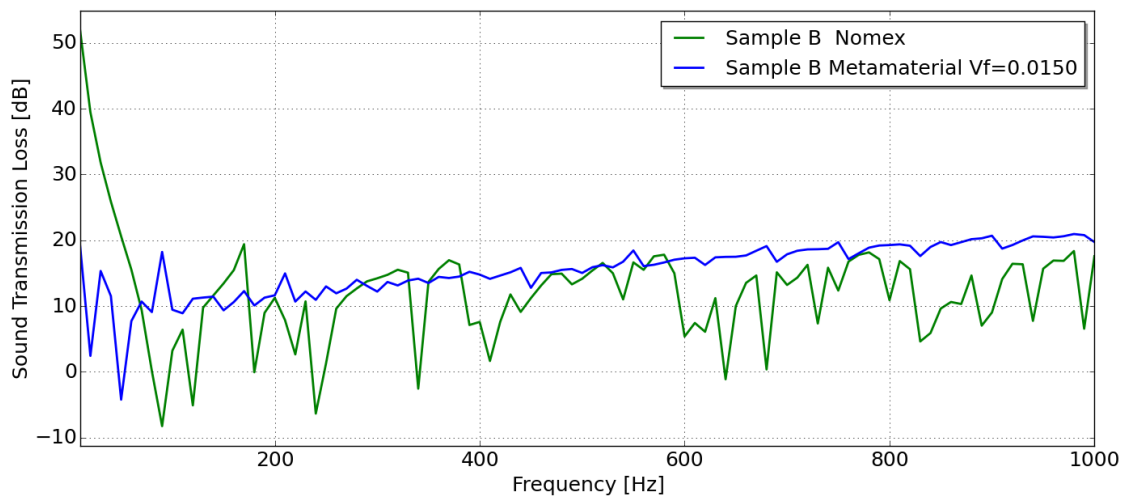


FIGURE 7.23: Sound Transmission Loss of a Sandwich plate with different core material (Sample B)

In both Samples the Metamaterial 0150 shows an higher STL than Nomex after 70 Hz, as we can see in figures below:

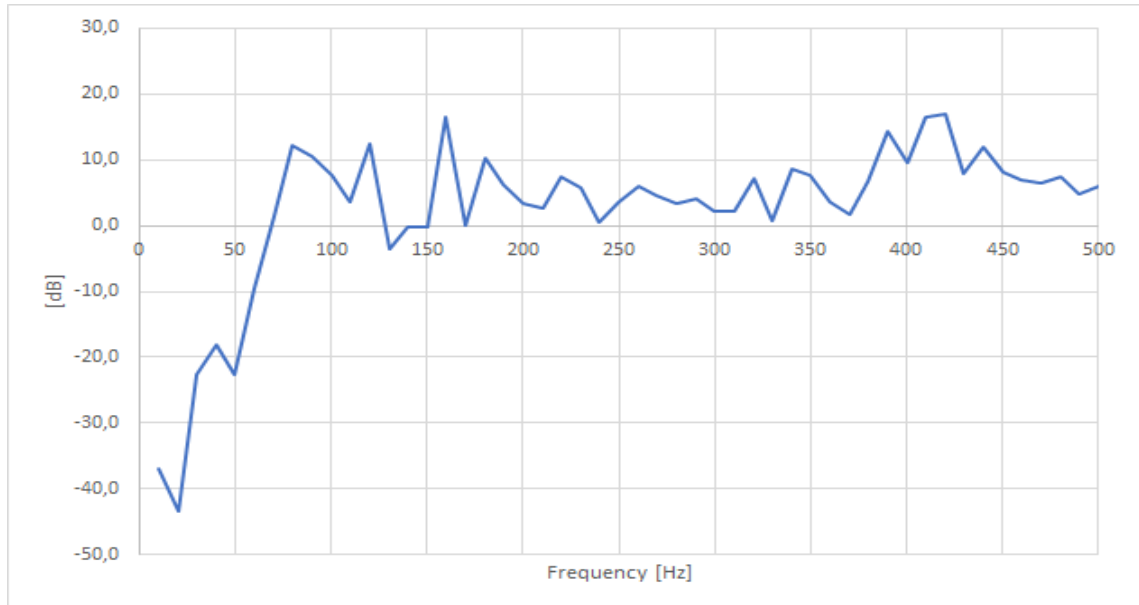


FIGURE 7.24: STL difference between Metamaterial 0.0150 and Nomex (Sample A)

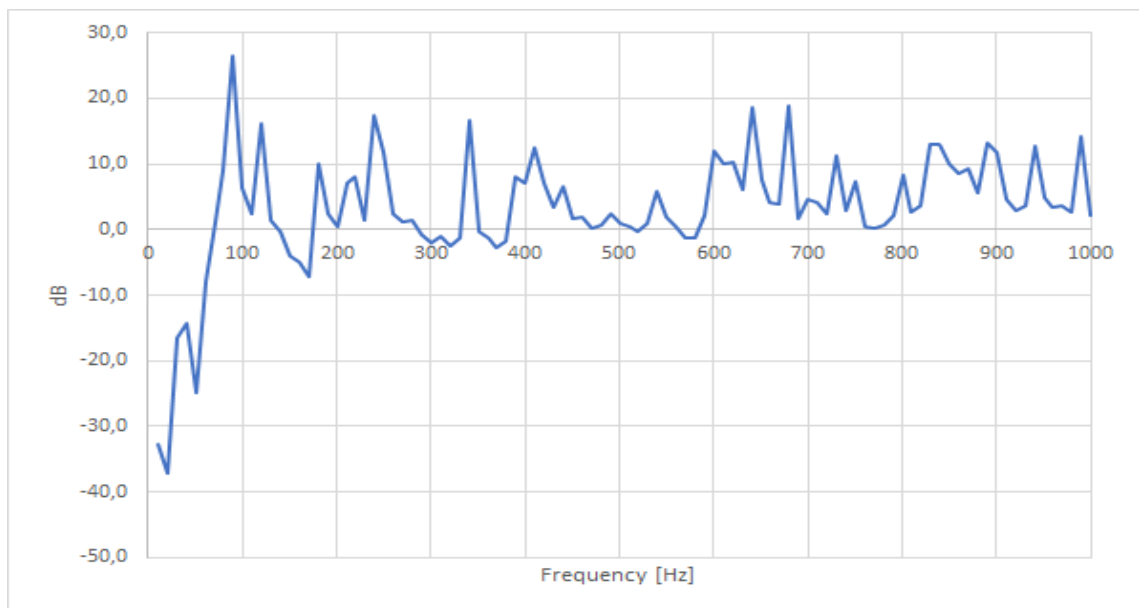


FIGURE 7.25: STL difference between Metamaterial 0.0150 and Nomex (Sample B)

Chapter 8

Conclusions

The acoustic analysis of advanced lining materials for aircraft fuselage soundproofing has been considered in this thesis. In particular, sound transmission loss evaluation of passive Metamaterial plates and sandwich plates have been performed. The results have been organized in four main parts:

1. A Modal extraction of two 300 and 600 holes PVC plates compared with homogenized properties to validate the homogenization method;
2. A Sound Transmission Loss evaluation and comparison of the previous models;
3. A Sound Transmission Loss of the same plate made of Melamine Foam with 300 and 600 Aluminum cylindrical inclusions;
4. A Sound Transmission Loss evaluation of two Sandwich plates with different core materials: Nomex, proposed by CASTLE partners, and a Melamine Foam Metamaterial in a configuration that have the same weight of Nomex.
 - The perforated plates proposed by Langlet et al have been chosen as a reference to validate the CUF-MSG-based homogenization method and comparing the first 9 modal frequencies, showing its potentiality on reducing computational time and resources, together with good agreement with Langlet experiments, thus validating the method for 3D Unit-cells.
 - The same perforated plates has been the first models being analyzed for Sound Transmission Loss, showing a 3.49% (300 holes PVC plate) and 5% (600 holes PVC plate) difference in the first resonance peak using a full plate with Homogenized properties Metamaterial.
 - Melamine foam with 300 and 600 inclusions, using the same geometry of the previous plate, had been analyzed. Different considerations have to be made in this case, because of the more complexes STL curves which shows some difference respect to full plates with equivalent homogenized properties at very low frequencies, and better agreement over 100 Hz. This incongruence remain to be investigated or supported by other experiments.

- The Sandwich plates presented in this work are the result of tests and directives of the CASTLE partners, which suggest us the Fiberglass/Epoxy resin and Nomex properties with updates due to their experimental results, together with the dimensions of the plies. These two samples, called for simplicity A and B, have been analyzed: the Metamaterial core proposed here was compared with Nomex, a material suggested by our partners, and the tests shows promising acoustical performance of the Metamaterial, with an overall dB gain respect to Nomex over 70Hz.

The STL is a characteristics that indicates the soundproofing level of a panel in that configurations, reproducing in the best possible way an acoustic test chamber. These results have sense in experimental environment, complying Acoustical Standards constraints. However the real panel will be curved and connected with other components of the fuselage, so a precise estimation of the Noise Reduction is not straightforward, without a realistic CAD model and an experimental campaign. The reason behind this work is to optimize the resources reducing the number of expensive real tests (which are yet required during airworthiness standard compliance), selecting fewer best configuration sustained by data researches. It is commonly agreed that an high STL value, especially in critical frequencies generated by a Turbo-propeller or a Turbulent Boundary Layer, will probably lead to an high soundproofing effect on the incident waves.

Once we have chosen the Inclusions Volume Fraction, we will choose the final configuration (or few bests) taking to account the number of inclusions (or, alternatively, the distance between them). Indeed, one can have several inclusions with a small diameter, or few big ones. However, we have to consider that the smaller is the unit cell dimension respect to the plate, the better is the homogenization result. An experimental campaign could give us a better understanding of the acoustic behavior of the metamaterials, and a baseline to evaluate our results.

The necessity of an interface script between MUL2-UC and Actran for the several iteration needed to explore the Acoustical soundproofing at different Volume fraction of Aluminum inclusions, was a good opportunity to increase my knowledge on MATLAB environment, writing an *ad-hoc* script.

One of the main challenges during this work was the creation of the model using a Finite fluid component and an interface. Several attempts and problem-solving work has to be made to obtain meaningful results. The lack of a Trouble Shooting section on Actran manuals was compensated by the Technical Support help. The finite fluid model, which use coupling surfaces and mesh interfaces, had requested about 40 GB of RAM, against the over 64 GB requested from a Rayleigh component model, not enough for the current capacity of the available server.

8.1 Outlooks

The first objective of the future work will be the realization of real samples made of Metamaterial, by creating a model of a perforated plate to send to a supplier that will use a CNC machine to realize the semi-finished specimen in Melamine Foam. The model specification, particularly the inclusions diameter should be compatible to the supplier stock capability and standard dimensions (for example, a 2.31mm diameter of Aluminum inclusions is not so easy to find) respecting in the same time the Volume fraction chosen, an appropriate unit cell length is a more tunable parameter.

The main outlook of this work is the enhancement of the acoustical comfort of airline passengers and crew members, especially for Turbo-prop Regional Airliner, going forward with studying the characteristics of passive Metamaterials as component of a new generation of lining panels in aircraft fuselages.

Bibliography

- [1] Erasmo Carrera, Maria Cinefra, Marco Petrolo, and Enrico Zappino. Finite element analysis of structures through unified formulation. John Wiley & Sons, 2014.
- [2] Alberto Garcia De Miguel, Alfonso Pagani, W Yu, and Erasmo Carrera. Micromechanics of periodically heterogeneous materials using higher-order beam theories and the mechanics of structure genome. Submitted.
- [3] Philippe Langlet, Anne-Christine Hladky-Hennion, and Jean-Noël Decarpigny. Analysis of the propagation of plane acoustic waves in passive periodic materials using the finite element method, The Journal of the Acoustical Society of America 98, 2792 (1995).
- [4] Anne-Christine, Hladky-Hennion and Jean Noël Decarpigny. Analysis of the scattering of a plane acoustic wave by a periodic elastic structure using the finite element method: Application to compliant tube gratings. Journal of Acoustical Society of America 87 1990
- [5] Anne-Christine, Hladky-Hennion and Jean Noël Decarpigny. Analysis of the scattering of a plane acoustic wave by a doubly periodic structure using the finite element method: Application to Alberich anechoic coatings. Journal of Acoustical Society of America 90 1991.
- [6] Anne-Christine, Hladky-Hennion and Jean Noël Decarpigny. Finite element modeling of active periodic structures: Application to 1-3 piezo-composites. Journal of Acoustical Society of America 94, 1993.
- [7] S.A.Cummer,J.J.Christensen and A. Alu', Controlling sound with acoustic. Nature,2016
- [8] S. Zhang,L.L.Yin,N.Fang, Phys. Rev. Lett. 102, (2009)
- [9] J.S.Li, L.Fok, X.B Yin, G. Bartal, X. Zhang, Nature Materials 8 (2009)
- [10] J. Zhu, J. Christensen, J. Jung, . L. Martin-Moreno, X. Yin, L. Fok,X.Zhang,F.J.Garcia Vidal,Nature Physics 7, (2011).
- [11] S.H. Lee, C.M. Park, Y.M. Seo, C. K.Kim, Phys. Rev. B 81 (2010)
- [12] J.B. Chen, Y. Wang, B.H. Jia, T. Geng, X.P. Li, L. Feng, W. Qian, B.M. Liang, X.X. Zhang, M. Gu, S.L. Zhuang,Nature Photonics 239 p.5 (2011)
- [13] D. Torrent,J. Sanchez.-Dehesa, New J. Phys 10, (2008)
- [14] W.R. Zhu,C.L.Ding, X.P. Zhao, Appl. Phys. Lett. 97 (2010)

- [15] B.I. Popa, L. Zigoneanu, S.A. Cummer, *Phys. Rev. Lett.* 106, (2011)
- [16] Luc Jaouen, Amelie Renault, Mickael Deverge: Elastic and damping characterizations of acoustical porous materials: Available experimental methods and applications to a melamine foam. In *Applied Acoustics* 69 (2008)
- [17] Christophe Van der Kelen, Jacques Cuenca, Peter Goransson A method for the inverse estimation of the static elastic compressional moduli of anisotropic poroelastic foams - With application to a melamine foam. In *Polymer Testing* 43 (2015)
- [18] MSC Actran 17 User's Guide - Volume 1
- [19] MSC Actran 17 User's Guide - Volume 2: EDAT Input File Syntax
- [20] José Sánchez-Dehesa, "Review on acoustic metamaterials", Wave Phenomena Group, Universitat Politècnica de València.
- [21] Alfonso Climente, Daniel Torrent, and José Sanchez-Dehesa, "Omnidirectional broadband acoustic absorber based on metamaterials", Wave Phenomena Group, Universitat Politecnica de Valencia, Spain (2012)
- [22] Qian Shi, "Civil aircraft cabin noise resource acoustic characteristic and transmission path analysis", *The Journal of the Acoustical Society of America* 131, 3390 (2012); <https://doi.org/10.1121/1.4708789>
- [23] Catherines, John J; and Mayes, William. H. "Interior noise levels of two propeller-driven light aircraft" - NASA-TM-X-72716, 1975
- [24] McGary, Michael C. : NASA Technical Report 2046, 1982 "Noise Transmission Loss of Aircraft Panels Using Acoustic Intensity Method"
- [25] "Lightweight yet sound-proof honeycomb acoustic metamaterial" Ni Sui, Xiang Yan, Tai-Yun Huang, Jun Xu, Fuh-Gwo Yuan, and Yun Jing. <http://dx.doi.org/10.1063/1.4919235>
- [26] L. E. Kinsler, A. R. Frey, A. B. Coppens, and J. V. Sanders, *Fundamentals of Acoustics*, 4th ed. (Wiley-VCH, New York, NY, 1999).
- [27] http://www.sea-cubed-composites.com/composite_materials.html Checked Feb 2018
- [28] <https://www.carthrottle.com/post/what-is-an-anechoic-chamber-and-why-are-they-so-important-to-the-car-industry/> Checked Feb 2018
- [29] Membrane-type Acoustic Metamaterial with negative dynamic density, Z. Yang, Jun Mei, Min Yang, N. H. Chan, and Ping Sheng
- [30] Dark acoustic metamaterials as super absorbers for low-frequency sound, Jun mei, Guancong Ma, Min Yang, Zhiyu Yang, Weijia Wen and Ping Sheng, *Nature* Jul 2011 DOI: 10.1038/ncomms1758
- [31] Homogenization of perforated plates with cylindrical pores using Carrera Unified Formulation and Mechanics of Structure Genome, July 2017.

-
- [32] Acoustic lesson 3, Steve Vanlanduit, Vrije Universiteit Brussel, http://mech.vub.ac.be/avrg/Courses/Acoustics/Acoustics_lesson_3.pdf (checked Feb2018)
- [33] <http://www.animations.physics.unsw.edu.au/jw/sound-impedance-intensity.htm> Checked Feb2018
- [34] D. W. Robinson and R. S. Dadson, "A redetermination of the equal-loudness relations for pure tones" in Br. J. Appl. Phys. 7, 166-181 (1956).
- [35] Harvey Fletcher and Wilden A. Munson, "Loudness, its definition, measurement and calculation", Journal of the Acoustic Society of America, 1933.